
UNIVERSITÀ DEGLI STUDI DI PADOVA

SCUOLA DI SCIENZE

Dipartimento di Geoscienze
Direttore: Prof.ssa Cristina Stefani

CORSO DI LAUREA MAGISTRALE
IN
GEOLOGIA E GEOLOGIA TECNICA


# *LATE QUATERNARY INCISION RATES IN THE HIGH TINÉE CATCHMENT (FRANCE): USE OF NUMERICAL MODELLING AND $^{10}$Be TCN DATING*

## Stima dell'erosione fluviale nel bacino dell'alta Tinée (Francia) nel tardo Quaternario: utilizzo di modelli numerici e datazione TCN al $^{10}$Be


*Relatore:*

*Prof. Nicola Surian, Dipartimento di Geoscienze, Università di Padova*

*Correlatori:*

*Prof. Yann Rolland, Laboratoire Géoazur, Université de Nice*

*Prof.ssa Carole Petit, Laboratoire Géoazur, Université de Nice*

*Prof.ssa Marianne Saillard, Laboratoire Géoazur, Université de Nice*

*Laureando: Davide Cassol*



ANNO ACCADEMICO 2015/2016


UNIVERSITÀ DEGLI STUDI DI PADOVA

SCUOLA DI SCIENZE

Dipartimento di Geoscienze
Direttore: Prof.ssa Cristina Stefani

CORSO DI LAUREA MAGISTRALE
IN
GEOLOGIA E GEOLOGIA TECNICA


# *LATE QUATERNARY INCISION RATES IN THE HIGH TINÉE CATCHMENT (FRANCE): USE OF NUMERICAL MODELLING AND $^{10}$Be TCN DATING*

# Stima dell'erosione fluviale nel bacino dell'alta Tinée (Francia) nel tardo Quaternario: utilizzo di modelli numerici e datazione TCN al $^{10}$Be


*Relatore:*
*Prof. Nicola Surian, Dipartimento di Geoscienze, Università di Padova*
*Correlatori:*
*Prof. Yann Rolland, Laboratoire Géoazur, Université de Nice*
*Prof.ssa Carole Petit, Laboratoire Géoazur, Université de Nice*
*Prof.ssa Marianne Saillard, Laboratoire Géoazur, Université de Nice*

*Laureando: Davide Cassol*



ANNO ACCADEMICO 2015/2016

# *Late Quaternary incision rates in the High Tinée catchment (France): use of numerical modelling and $^{10}$Be TCN dating*


## *Abstract*

With this study we try to decipher the message hidden in the longitudinal profiles of the High Tinée and of its main tributaries coupling numerical modelling and $^{10}$Be Terrestrial Cosmogenic Nuclides dating. In order to understand the respective influence of active tectonic and climate on the fluvial erosion, we have applied, the inversion code developed by Goren et al. (2014) over the last 120 kyr. The results indicate climate as the parameter driving the Tinée incision process highlighting the large effect of the post LGM deglaciation on the fluvial dynamic. However in the model signal is present a background noise, that is likely due to the regional uplift interesting the area. The TCN dating confirms the importance of the post LGM deglaciation. With it we have estimate a mean incision rate of 2 mm/yr that is in accordance with the value obtained in the neighbouring valley of the Vesubie River and with the local uplift rate. Further, there are two evident periods of rapid incision around 15 and 4,5 kyr B.P. The two periods correspond to favourable fluvial incision conditions given by a rapid deglaciation, the first one and by more abundant rainfall the second one.

# *Stima dell'erosione fluviale nel bacino dell'alta Tinée (Francia) nel tardo Quaternario: utilizzo di modelli numerici e datazione TCN al $^{10}$Be*


## *Abstract*

Il presente studio tenta di carpire le informazioni nascoste nei profili longitudinali dell'alta Tinée e dei suoi principali affluenti. Per fare ciò sono state utilizzate tecniche di modellazione numerica e la datazione TCN al $^{10}$Be di 11 campioni prelevati da una superficie d'erosione fluviale in granito.

Al fine di distinguere le rispettive influenze di clima e tettonica attiva sui profili longitudinali fluviali, si è applicato, a tutto il post "MIS 5e", il modello sviluppato da Goren et al., (2014) basato sull'inversione della "stream power law". Dai risultati ottenuti si evince che il clima è il fattore che più influisce sulle dinamiche d'incisione fluviale e che queste hanno fortemente risentito della regressione glaciale post LGM. In tutti i profili di "tasso d'incisione fluviale" ottenuti, è però costantemente presente un rumore di fondo; tale segnale è verosimilmente legato al sollevamento tettonico che interessa l'intera area di studio.

La datazione ad isotopi cosmogenetici di $^{10}$Be ha sostanzialmente confermato e raffinato i risultati ottenuti nella fase di modellazione numerica. Si è infatti ottenuta conferma dell'importanza rivestita dallo scioglimento glaciale post LGM nell'attività d'incisione della Tinée e si è potuto quantificare, con accettabile precisione, un incisione media di circa 2mm/a per gli ultimi 20'000 anni. Tale valore concorda col tasso d'incisione noto per la Valle della Vesubie e con la velocità di "uplift" regionale. Infine la datazione TCN ha evidenziato il carattere impulsivo dell'incisione fluviale della Tinée, denunciando la presenza di due momenti erosivi relativamente recenti e temporalmente localizzati. Il primo, riscontrato a circa 15'000 anni da oggi, in piena regressione glaciale post LGM ed il secondo, posto a circa 4'500 a B.P, in corrispondenza d'un aumento delle precipitazioni rilevato in tutta la regione.

*CONTENTS*

## Introduction

River incision drives the evolution of much of the earth surface topography, shaping its morphology. The relative roles played on river erosion processes by external factors (climate), and internal factors (tectonics or isostatic uplift) is a subject of debate and ongoing research (e.g., Adams, 1985; Molnar and England, 1990; Isacks, 1992; Raymo and Ruddiman, 1992). Water runoff variations, base level change, glaciers melting, internal adjustment of river dynamics are processes working simultaneously, and causing changes of incision rate through time. The river runoff path and incision rates therefore carry out a complex signal that, once decrypted, can help the understanding of several phenomena interacting to shape the Earth's surface.

Determining river incision rates can be useful in many applications, from short term issues as nutrient flux variation or soil denudation, to larger time scale, as climate change estimates (e.g., Ferrier et al., 2013 and references therein). The study of incision rate variations is also a cornerstone of tectonic geomorphology, and may help understanding uplift patterns in active mountain ranges (e.g., Wobus et al., 2006; Kirby and Whipple, 2012; Baotian et al., 2013).

All the aforementioned factors found a direct expression in the river longitudinal profiles and in their modelling with the Stream power law (e.g. Howard and Kerby,1983; Seidl and Dietrich, 1992; Seidl et al., 1994).

Longitudinal river profiles may provide information about the relative uplift rate across a fluvial terrain (Snyder et al., 2000; Kirby and Whipple, 2001; Snyder et al., 2003; Whittaker and Boulton, 2012; Kirby and Whipple, 2012). This possibility becomes really useful in areas with low active tectonics, where the classical methods of uplift rate measuring (e.g. GPS), may not have the necessary sensibility, such as the Alps. The studies of river profiles could then lead to the comprehension of tectonic forcing and climate regime of a certain area. However, to decipher these natural features remains a problem, because of the contemporaneous influence of these factors on longitudinal river profiles. The influence of climate on river longitudinal profiles is indeed still not precisely

known. Several studies aimed at quantifying its role in the valley shaping process (e.g. Ferrier et al., 2013). However, the effects of the recent climate change on these profiles are still unconstrained.

Starting from some studies evidencing a vertical movement of the whole Alpine chain by GPS data (e.g. Serpelloni et al. 2013; Walpersdorf et al., 2015), and from the work of Saillard et al. (2014) which showed that it is possible to study the incision rate and erosion dynamics on preserved polished river surface profiles, in the Vesubie Valley (Maritime Alps, SW Alps), it was decided to investigate the longitudinal profiles of the High Tinée tributaries.

The Tinée valley is located in the Mercantour-Argentera massif, a region undergoing a low intensity but constant seismic activity, and an uplift rate of the order of 1-3 mm/yr (Sanchez et al., 2010b; Walpersdorf et al., 2015). In particular the attention has been focused on a small area encompassing the highest stem of Tinée River. This area has been chosen because it shows relatively simple catchment geometries with an almost linear main stem (the Tinée River). Moreover, the steep hill slopes are prone to large landslides, which suggests recent and fast river incision (Bouissou et al., 2012; Darnault, 2012). Working on a limited area (only one watershed) gives also the possibility to neglect spatial variations of rainfall in the given mountain range.

The present study was carried out during a 6 months “Erasmus intership” in Nice (from March 1$^{st}$ to August 31$^{th}$ 2015), at the University of Sophia Antipolis, Géoazur Laboratory. The work was supervised by Prof. Yann Rolland (geological and geomorphological interpretation), Prof. Carole Petite (numerical modelling), and Prof. Marianne Saillard (TCN dating). The work is organised in two main sections:

(i) a first one, based on the Goren-Willet-Fox model (2014) and a (ii) second one, consisting of a $^{10}$Be Terrestrial Cosmogenic Nuclides (TCN) direct dating of the river polished surfaces.

- (i) The model has been used to produce an "incision rate – time" history for all Tinée's tributaries of the study area, obtaining so, for each of them,

the base level fluctuation, i.e. the incision rate of the Tinée itself . The obtained profiles have then been interpreted with the help of some previous works (Ferrier et al, 2013; Perron and Royden, 2013;Leith. et al, still unpublished). The modelling results interpretation has been coupled with a field geomorphological study.

- (ii) To constrain the information provided by the model, a TCN dating was performed on 11 samples drawn from a 41m high river cliff located within a gorge cut by the Tinée River. The cosmogenic nuclide dating technique, measuring the in situ-produced cosmogenic nuclide concentration, provides an accurate determination of the duration of the exposure to cosmic rays of a given rock surface, for instance of a river gorge polished surface. In this way, we have quantified the Tinée incision rates over the last 18 kyr.

Lastly, combining the numerical modelling interpretation with geomorphological and geochronological quantitative evidences, and in light of the geodynamic and climatic contexts of the Southern French Alps, a possible interpretation of the river profiles and corresponding incision history is suggested.

## I Numerical models and Terrestrial Cosmogenic Nuclides dating to estimate Quaternary incision rates: a brief review

The relatively recent recognition of potential global-scale interactions between climate tectonics and surfaces processes (e.g., Adams, 1985; Molnar and England, 1990, Isacks, 1992), has sparked the field of tectonic geomorphology. Since then, the dynamics of bedrock channel fluvial system has became one of the theoretical geomorphology most studied subject. Starting from the 1980s, significant progresses have been made in developing numerical models for the simulation of bedrock channel system dynamics (Howard and Kerby, 1983; Seidl and Dietrich, 1992; Anderson, 1994; Howard, 1994; Howard et al., 1994; Kooi and Beaumont, 1994; Rosenbloom and Anderson, 1994; Seidl et al., 1994; Goldrick and Bishop, 1996; Stock, 1996; Tucker and Slingerland, 1996; Stock and Montgomery, 1999; Whipple and Tucker, 1999; Whipple, 2001; Perron and Royden, 2013; Goren et al., 2014). Among all the proposed models, the most applied and used is the stream-power model, based on the Stream Power Law: $E = Ks^nA^{m.}$ Indeed, it is cast directly in term of the physics of the erosion (Howard and Kerby, 1983). The Stream Power Law states that river incision rate is given by the product of drainage area and channel slope respectively raised to the power exponents "m" and "n":

$$E = Ks^nA^m$$

where E is the erosion rate, K the erodibility, S the river slope and A the drainage area of the river.

Ferrier et al.(2013) have applied the Stream Power Law to a series of river in the Hawaiian island of Kawa, where one of Earth's steepest rainfall gradient has been registered. The study has shown, through a time-averaged analysis and numerical modelling, that river incision efficiency is positively correlated with the upstream-averaged mean annual precipitation rates. Its results provide empirical evidence for the correlation between climate and river incision. Leith et al. (submitted) applied the Stream Power model to 18 tributaries of the Rhone River (Switzerland). Using high-resolution LIDAR data and integral long-profile

analysis, the authors attempted to predict the location of common knick points across the studied region and simulated approximately 800m of regional uplift, river incision, and hill-slope erosion in the lower half of each catchment over the last 0.7 Myr.

In the Argentera-Mercantour area, a study on the river incision dynamics, coupling a Stream Power Law modelling approach with a TCN dating, has been conducted by Saillard et al. (2014) in the Vesubie Valley. The work studies the evolution of the Vesubie River longitudinal profile over a time period of 2 Myr, varying, on the stream power law, the erodibility coefficient through time. The results of this study suggest a long-term uplift rate lower than 2 mm/yr, with an increase in erodibility coefficient during the last 16 kyr. The Vesubie River is a Var tributary, joining this one just downstream the Tinée River.

The present study applies, indeed, a similar analysis to the Tinée River. However our approach is indirect, and instead of trying to obtain a modelled profile as similar as possible to the topographic one, changing the model parameters, we try to infer these parameters starting from the topographic river profile. Further, we worked with a temporally-invariant erosion coefficient, fact that increase the incision-rate variations along time, but that may represent a possible simplification in model utilization and gives the possibility to study the model dependence to a more limited number of parameters. A $^{36}$Cl TCN dating has also been performed, in Saillard et al. (2014), in order to estimate the incision rate of the Vesubie River over the last 15 kyr. The analysis suggests two main incision phases at 4-5 and 11-12 kyr B.P.. These variations seem to indicate a predominance of climate influence on the short-term incision dynamics, but do not exclude a possible role of tectonic uplift.

The Tinée Valley itself has been object of incision rate estimation through terrestrial cosmogenic nuclides dating (Darnault et al., submitted). The obtained incision rates underline an acceleration of river incision after the LGM and especially around 5 kyr B.P. with incision rates higher than 1 cm/yr.

Finally the TCN dating technique has been applied, in the Tinée Valley, to date some glacier polished surface (Darnault et al., 2012). The obtained exposure ages

highlight three stages of glacial retreat. The dating has confirmed the three-step deglaciation previously dated in other sectors of the Alps (Kelly et al., 2004, 2006; Ivy-Ochs et al., 2009; Cossart et al., 2010; Ivy-Ochs, 2015).

## II General Setting

The Tinée River is the main tributary of the Var river located into the Mercantour-Argentera massif, in the "Alpes du Sud". The latter, constituting the south western end of the Alpine chain (*Figure 3*).

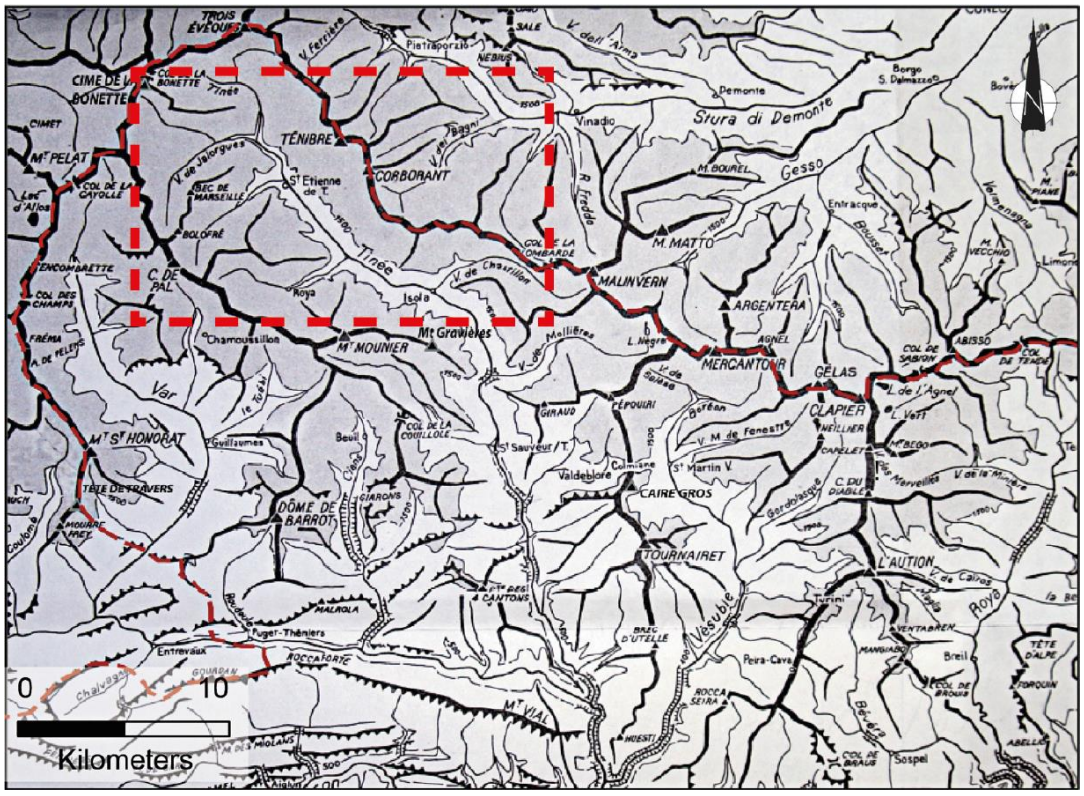


*Figure 1: map of the main north valleys of the Argentera-Mercantour massif. In the red dotted box is possible to see the area interested by this job (GPS coordinates N: 44,16 - 44,35; E: 6,78 – 7,03) and containing high stem of the Tinée River and 8 of its tributaries (modified from the morphological map of Maurice Julian, 1980).*

found instead the basin of the Vesubie River, an other tributary of the Var, while the west side of Tinée's catchment area is in direct contact with the high part of the Var basin itself.

The valley bottom elevation varies between the 900 m a.s.l. of the village of Isola, to the 2300 m a.s.l. of "camp des fourches". The ridges defining the Tinée Basin culminate above 2600 m a.s.l. with some peaks reaching altitudes of over 3000 m (Mont Ténibres 3041m a.s.l. is the highest peak).

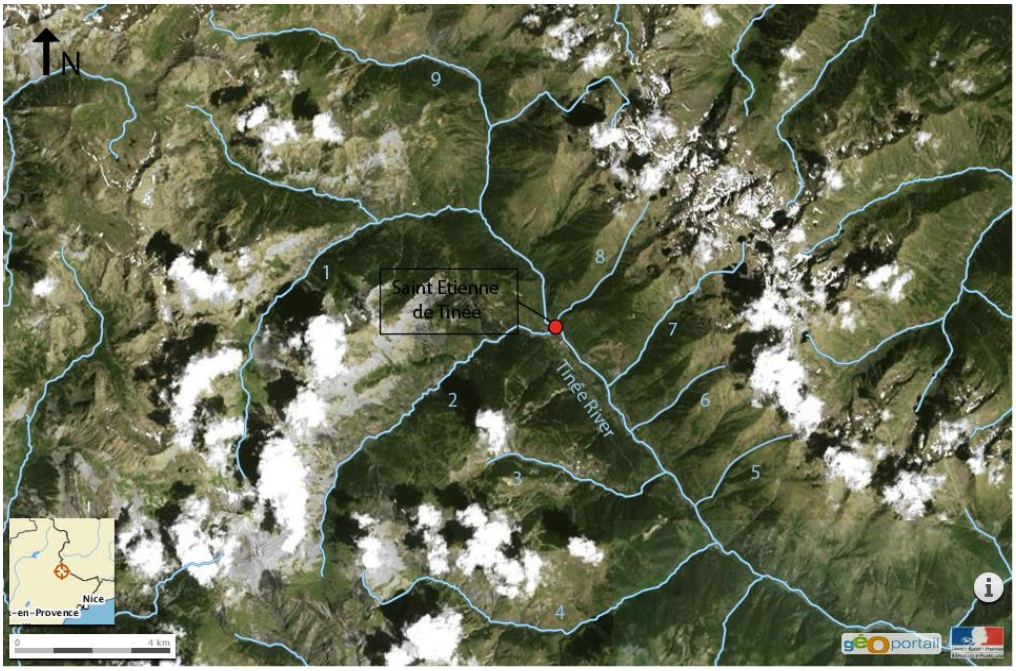


*Figure 2: the studied area with the Tinée river and its main tributaries; the numbered ones are those that have been analysed in this work. In order: 1)Giarlogue 2) Ardon 3) Auron 4)Roya 5)Douans 6)Asueros 7)Rabuons 8)Ténibres 9)The highest part of the Tinée itself.*

## *II. 1*

### *Geological and geomorphological setting*

The Mercantour-Argentera massif represents the most south-western part of the Alpine Chain and is located at the junction between the Western Alps and the Ligurian basin (Larroque, et al., 2001) into the external Alpine Domain (*Figure 3*).

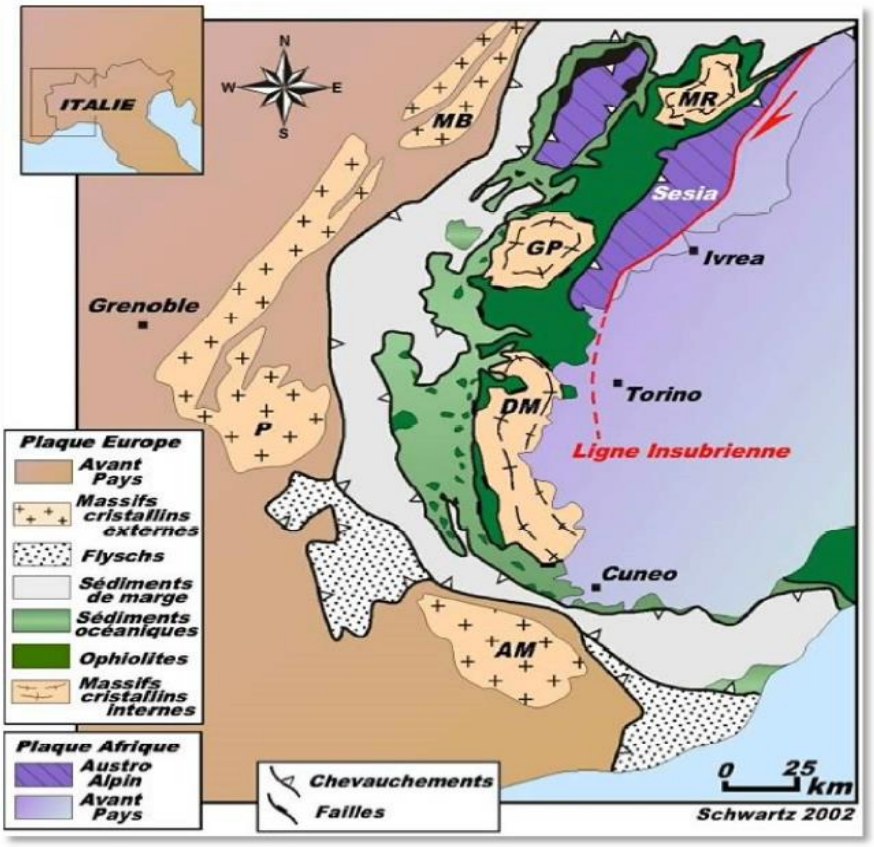


*Figure 3: Simplified structural map of Western Alps, by Schwartz (2002).* ***AM:*** *Argentera-Mercantour Massif;* ***MB:*** *Mont Blanc Massif;* ***DM:*** *Dora Maira Massif;* ***GP:*** *Grand Paradis Massif;* ***MR:*** *Mont Rose Massif.*

### *II.1.1 The Argentera-Mercantour Massif and his "tégument"*

#### II.1.1.1 The European continental crust

The Varisic basement of the Argentera-Mercantour is made of metamorphic units structured during the Varisican orogeny (Faure-Muret, 1955). It is composed by three principal units (*Figure 4 and 5*) outcropping in the left side of the High Tinée, and so defined:

- Tinée western unit (Faure-Muret, 1955), consisting in three lithological set

and one intrusion:

  - The Varelois set, composed of plagioclase gneiss with biotite and sillimanite.
  - The Anelle set, composed of two micas gneiss and migmatite.
  - The Rabuons set, characterised by a two micas augen gneiss.
  - The Iglière intrusion, made of a quartz diorite also named as "Argentera Granit". The intrusion rocks have been dated of 293+/-10 Ma (Upper Carboniferous – Lower Permian; Faure-Muret, 1969).

- The eastern unit: (Faure-Muret, 1955) composed of anatectic gneiss with biotites and anphiboles, associated to the Argentera two micas granites (Malinvern-Argentera complex).
- Valetta Molière mylonitic unit: consists in the fault zone separating the two previous units.

In discordance on the metamorphic units lie, on the south and east side of the massif, the carboniferous sequences. These units dating to the Westphalian and Stephanian stages (315-295 Myr) are composed of black schist, arkose and conglomerate made of basement pebbles and can be easily found stuck into the fault zone also within the massif.

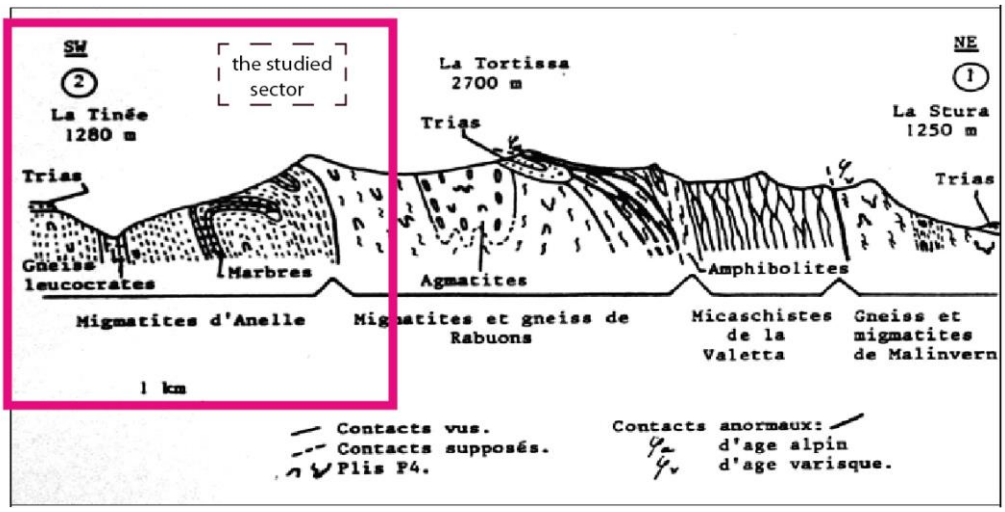


*Figure 4: cross section through the metamorphic basement of Argentera (Bognadof, 1986)*

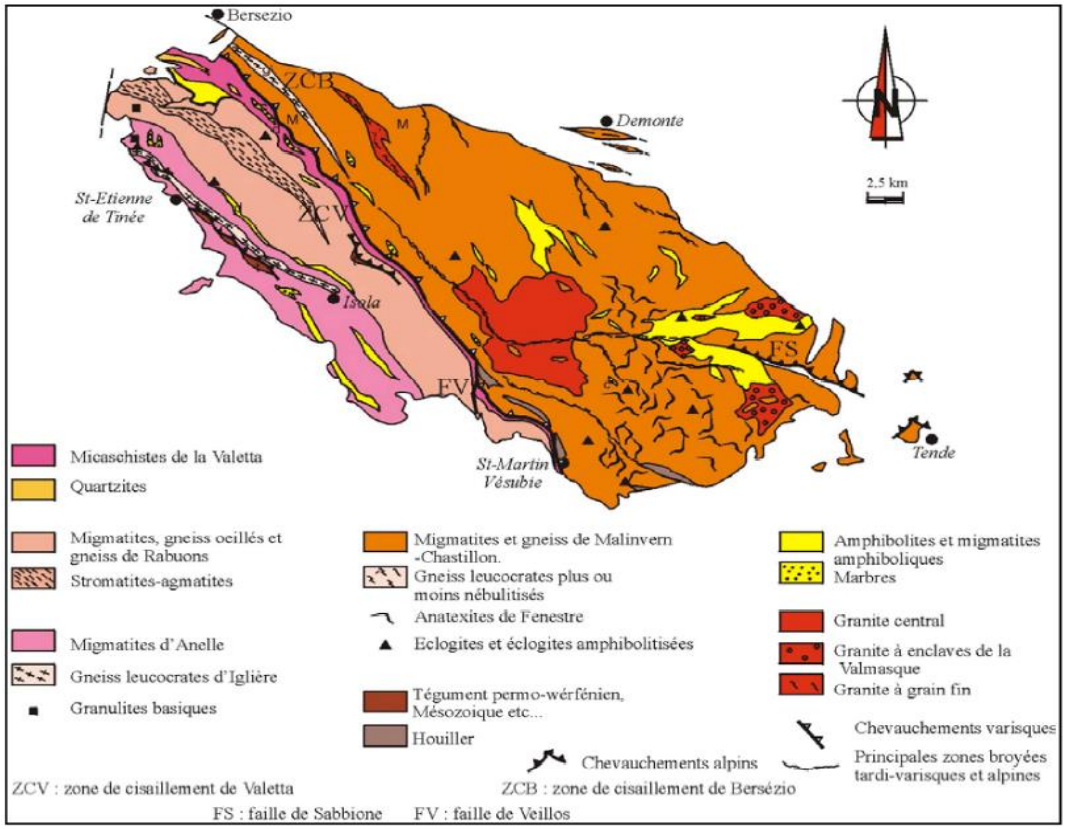


*Figure 5: geologic map of Argentera-Mercantour massif illustrating the main lithologies of the crystalline massif (after Bogdanoff, 1986*

### *II.1.1.2 The Permo-triassic "tégument"*

The Covers in direct contact with the crystalline basement date from Permian to Early Triassic (Werfen) and form the "tégument". During the Alpine Orogeny these layers remained structurally coupled to the basement and are now outcropping all around the massif and in the Dome du Barrot area.

The Permian units are composed by detritic sediment: red pelites, sandstones, green red or grey conglomerates, and overlie in discordance the carboniferous

sequence or, otherwise, are in direct contact with the basement as in the Tanneron Massif.

*II.1.2 The sedimentary cover: the foreland*

II.1.2.1 The Mesozoic sequence (Upper Triassic – Jurassic – Cretaceous)

Overlying "tégument" and basement there are, in unconformity contact, secondary sedimentary covers with an average estimated thickness of 2300m and 3000m. These younger covers are basically made of Jurassic – Cretaceous limestone and marls suggesting a depositional paleoenvironment of continental shelf type (Campredon, 1977). The Jurassic sedimentary pile is represented by thick (600 m) calcareous deposits and is generally thought to be mechanically decoupled from the Lower Triassic by a detachment level in gypsum and cellular dolomites of the Upper Triassic (Keuper). The Cretaceous is marked by marls and calcareous marls with large thickness variations (600m to 1000m), which are principally controlled by the activity of normal faults during the Lower Cretaceous.

II.1.2.2 The Paleogene

The tertiary sequence of the external zone records a complete sedimentary cycle started after an emersion period of the foreland and of the Argentera-Mercantour massif during the Upper Cretaceous. This sequence is characterized by several unconformities on the Cretaceous strata, but also on the Jurassic and sometimes on the Triassic too.
The Paleogenic sequence is made by units of marls and limestone (Nummulites limestone) at the bottom, overlapped by detritic units with increasing granulometry, from flysch to sandstone, toward the top. This trend is the evidence of a progressive emersion of the European platform.

II.1.2.3 The Perialpine Neogenic basins

The Neogenic basins are made of a sedimentary sequences going from the Upper Miocene to the beginning of the Quaternary. The bottom of this one consists in deltaic molassic formations, made of fluvial conglomerates composed by pebbles, results of alpine erosion. Above we found molasses with a sandstone-conglomeratic structure rich in Miocenic littoral fauna and at the top the chaotic Pliocenic sequence, made of marls and conglomerates enclosing sometimes Paleogenic and Neogenic blocks.

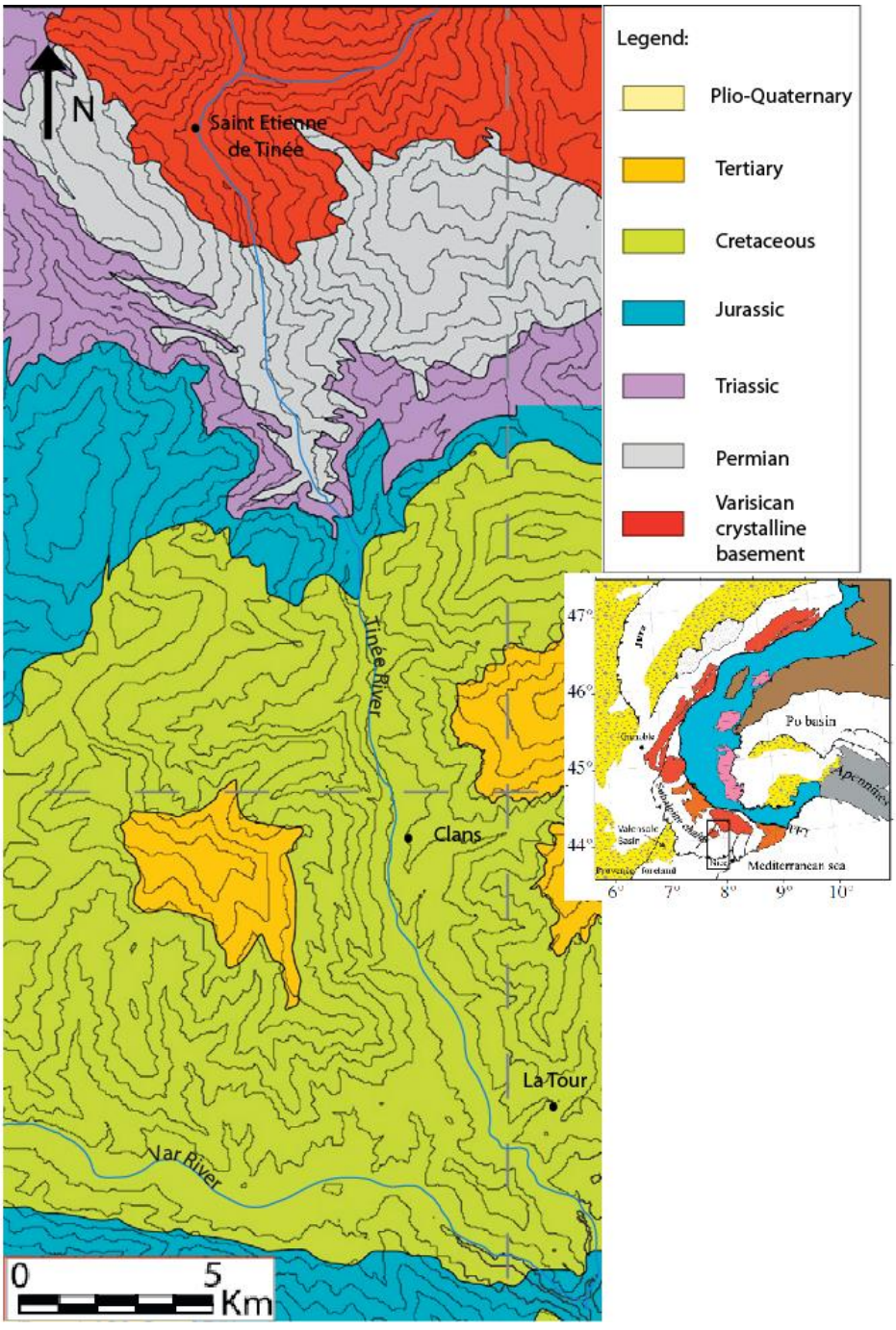

*Figure 6: geologic setting of the Tinée and Var catchment areas. Southern French Alps (after Jourdon et al., 2014). Inset shows the tectonic setting of the study area in the framework of the western Alps.*

### *II.1.3 Deformation and tectonic*

The deformations that is possible to find within the crystalline massif of Argentera-Mercantour are the result of a superimposition of the effects linked to the Varisican and Alpine orogenesis. Five phases of Varisican deformation have been recognised and considered as giving rise to the global structure of the massif (Bogdanoff, 1986; Corsini et al. 2004).

The structures appearing in the Argentera-Mercantour crystalline massif and in its

"tégument", suggest an N-S shortening that caused, through a transpressive regime, strike-slip and transpressional faults (Valetta-Mollières), folds of the basement and folds affecting the permo-trias covers (Dome du Barrot, Cime du Diable, Mont Bégo).

II.1.3.1 Seismicity and active tectonic:

The Western Alps are considered as an area of low to medium seismicity (Giardini et al., 1999), nevertheless the western Alps system can be considered as a potentially destructive complex (Thouvenot et al.,1990), especially if considering events as the Lambesc earthquake of 1909 or other historical phenomena with intensities overcoming the value 6 in the MSK scale (corresponding to V in MCS scale). Particularly the areas of Briançon, Piemonte and Nice region can be considered submitted to a more important seismicity.
Starting from the Forties the developing of seismic instruments has enabled to define two main seismic arcs, the Briançon one and the Piemonte one (Rothé, 1941). The knowledge about the subject has progressively developed following the technological increment. During the years has been so possible to define 3 important tectonic systems:

- An extensional regime localised into the internal zones (Briançon and Piemonte Areas) and locally in the external zones N-W from the Argentera-Mercantour massif. (Sue, 1998; Sue et al.,2000; Delacou et al., 2004; Bethoux et al., 2007; Larroque et al., 2009;)
- A compressive regime localised in external zones, in the areas of Jura front, of Belledonne, of Provence, of the Ligurain Margin and of Po plain (Bethoux et al., 1992; Sue 1998; Barroux et al., 2001; Larroque et al, 2001).
- A strike-slip tectonic observed in the whole chain without internal/external distinction. It defines regions with transpressive behaviour and others with trans-extensif behaviour:
    - In the external domain the shortening compressive axes are fanned out,

radially to the Alpine Arc (Eva&Solarino, 1998; Sue et al., 1999; Baroux et al., 2001; Kyrstrup et al., 2004) going from a NNW – SSE direction in the eastern Suisse area, to a NE-SW direction in the South France.

- In the internal domain these strike-slips structures are compatible with the extensive regional directions, N-S south of Vallais and from E-W to NE-SW in the Briançon and Argentera-Mercantour areas.

The Southern French Alps are so submitted to an active transcurrent deformation that is active at least since the Holocene period and that is accommodated mainly by a N140° dextral segmented active fault system (JTF-STF), a conjugate N20 sinistral fault (MDF GV-PFEF) and minor conjugate N20 sinistral (RF, VF, PLF) and N-S extensional (HDF) or dextral faults (DF, BAF, BF, SF) (Sanchez et al., 2010b; *Figure 7 and 8*). The active character of the tectonics in the "Alps du Sud" has also been confirmed by geodetic studies (Walpersdorf et al., 2015) showing, in addition to a 0.5 mm/yr E – W extension, and an average uplift of 0.4 +/- 1.4 mm/yr. This result has been obtained on data acquired during an only five years monitoring campaign, but are corroborate by the results of the two long standing permanent stations CHTL and MODA, situated just north of the network and attesting respectively uplift of 2.2+/-0.3 mm/yr and of 1.8+/-0.4 mm/yr.

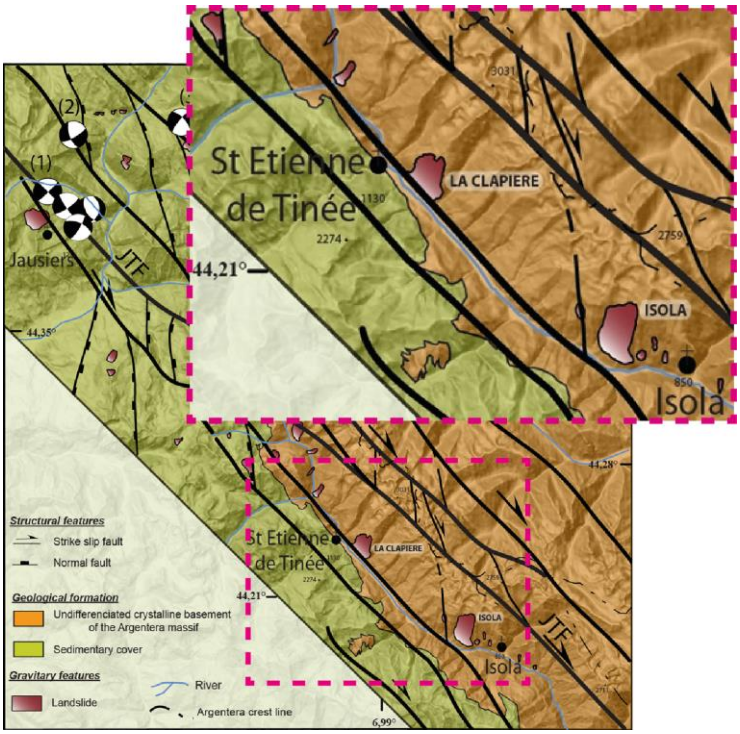


*Figure 7: Simplified structural map with a zoom on the studied area (modified from Sanchez et al., 2010b). To note the same orientation of the Tinée valley and the strike-slip fault system N140. This correspondence is also more marked in the studied part of the Tinée stem where a stirke-slip fault run along the river bed.*

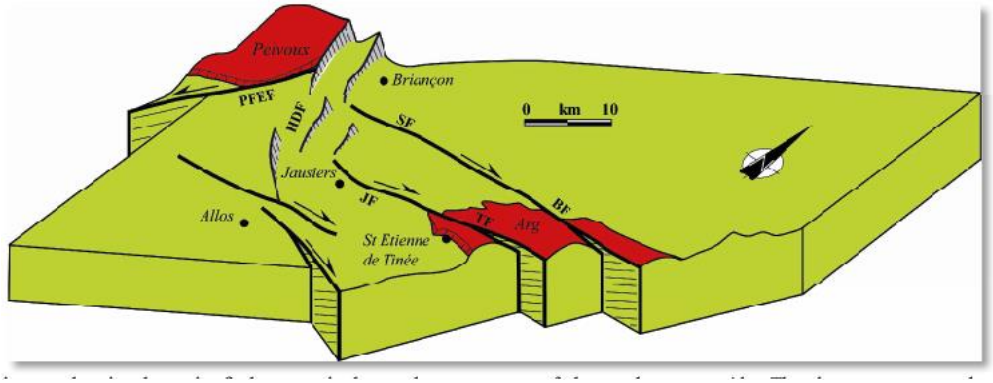


*Figure 8: block diagram showing the active fault system in the north-western part of the south-western Alps. The picture represents the pull-apart system with the two major dextral Jausier-Tinée fault and Serennes-Bersézio*

.

### II.1.4 Geomorphological context of the Tinée Valley

From the beginning of Pliocene (5,3 Myr) the Argentera-Mercantour Massif is a mountainous region with altitude ranges from 400m to 3143m (Mt Gélas) (Fauquette et al., 1999).

The Tinée Valley is the result of the combined action of fluvial and glacial processes. Unfortunately don't really exist recent geomorphological data concerning the valley and its glacial history. The last study concerning the subject dates up to the Eighties (Julian,1980), and still, only a chapter of it, is dedicated to the Tinée Valley. In his Phd thesis Romain Darnault (2012) has dated with the 10-Beryllium TCN method some glacial polished surfaces located in the Vens and Fer valleys, secondary valleys of the Tinée basin. The obtained data attest, in accordance with other studies effectuated along the Alpine Arch (Ivy-Ochs et al., 2006, 2008 and 2009; Böhlert et al., 2011; Federici et al., 2008;), three post LGM deglaciation phases: an oldest one around 15 kyr B.P, a second one around 11 kyr B.P. and the youngest one dating around 8,5 kyr B.P. Is anyway important to

remark that these data have been recollected above 2000m of altitude, while for lower valley doesn't exist any kind of chronological information. However what is evident is the change in section shape shortly upstream the village of Isola. If downstream the valley has the classical "V" shape, consequence of river incision, further upstream the fluvial features get lost or hidden by the opening of the valley, showing now some characteristics testifying a possible glacial origin; or at least a more important glacial contribution of the local geomorphology.

An other evident characteristic of the valley is its amount of active landslides, first and foremost the "Clapiere" landslide. Probably, at the origin of this unstable situation, there is the combined activity of glacial and fluvial phenomena. The glacial retreat has indeed caused a distension in the steep sides of the valley, while the constant river incision keep digging the valley bottom undermining slopes stability (Darnault et al. 2012).

### II.1.4.1 *Landslides and fluvial erosion:*

Numerous studies pointed out that since the LGM mass-wasting events may be correlated to climate changes in European mountain areas (e.g. Mattews et al., 1997; Borgatti and Soldati, 2002; Soldati et al., 2004; Cossart et al., 2008; Sanchez et al., 2010a; Darnault et al., 2012). The climate is directly linked to deglaciation and to rainfall rate, two of the most influential factors in terms of landslide triggering. The Tinée valley is indeed littered of landslides of all sizes (Darnault , 2012) (*Figure 7 and 9*). The valley indeed creates optimal condition for slope instability with mobilized volumes ranging from $5 \times 10^6$ to $60 \times 10^6$ $m^3$ (Jomard, 2006; Sanchez et al., 2010a; El Bedouiet al., 2011). The major Tinée valley landslides, "La Clapiére" and "Le Pra", have largely been studied and investigated (Bigot-Cormier et al., 2005; EL bedoui et al., 2009; Sanchez et al., 2010a; Bouissou et al., 2012; Danault et.al., 2012). A third large landslide but less studied, is present in the valley: the "Isola" landslide.

*Figure 9:one of the several active landslide present in the Tinée valley. The one in the photo is situated just downstream of the Roya and Tinée junction and is emblematic of the role played by river activity in landslides triggering.*

### *II. 2 Climatic setting*

Once defined the geological setting, there is another essential constraints that must be considered if we have as aim the study of rivers longitudinal profiles and their possible geological and climatic meaning (Koppes et al., 2009): the glacial and interglacial phases. Starting from the Riss (MIS 6), all the most important glacial and interglacial phases can be found in the studied area. Obviously, to know the glacial phases is necessary to have data about the thermal fluctuations (*Figure 10*).

#### *II.2.1 Upper Pleistocene and Holocene glacial and interglacial phases*

- The MIS6 stadial:

The end of Middle Pleistocene (250000 – 122000 years B.P.) is marked in the Alps by a cold and dry period during which the glaciers reached their maximal extension; e.g. the Rhone Glacier was stretched until the actual town of Lyon, and its altitude was over 1400 m. (Campy, 1982). It is during the MSI6 that the Argentera-Mercantour valleys got carved.

- The MIS5 stadials and interstadials:

The Upper Pleistocene (128000 – 11700 years B.P.) starts with a warming period (MSI5e) that caused the retreat of Alpine Glaciers. The MIS 5 (129000 – 72000 years B.P. ) (Drysdale et al., 2005) (Corresponding to the previously called Riss – Wurm Interglacial) saw during its warm and humid first 13000 years (Eemian, MIS 5e), the glaciers melting. This period ends with a progressive oscillating cooling trend.

- The MIS4, 3 and 2

In the global scale the so called “Wurm glaciation” begin 72000 year B.P., and is subdivided it into three internal stages:

  - MIS4 stadial, (c.a. 72000 – 60000 years B.P.), cold and humid at the beginning, cold and dry after.

- MIS3 interstadial, (c.a. 60000 – 25000 years B.P.), cold and dry.
- MIS2 stadial, (25000 – 17000 ), marked by very low temperature (Guiot et al., 1989).

Stadials MIS4 and 2 were, in the Alps, less important than MIS6 stadial in terms of glacier extension. – For instance the Rhone Glacier remained upstream of "Les Echets"(Miribel, Ain, Rhone Alpes) and presented a maximal elevation of 1200 m.

In Sylvain Coutterand Phd thesis (2010) is possible to find a well synthesized LGM (Last Glacial Maximum) history, explaining that there are two main currents about the LGM dating, one considering it previous to 28000 years B.P. and an other fixing it between 21000 and 17000 years B.P.. A different explanation for the multiple LGM dating is given by Jorda et al. (2000); they explain that is possible to have different precipitation regimes fact that could cause different climatic condition and so different dating of the LGM inside the Alpine Chain.

The MIS2 advanced occurred between 22000 and 20000 years B.P. (Cossart et al. 2010). In the "Alpes du Sud" the LGM is estimated to be around 21500 years B.P. (Jorda et al., 2000) with a maximum glacial thickness varying between 600 and 1000 m, and covering an area going from the 3000m peak of the Argentera-Mercantour massif, to the 600m m a.s.l. of the low valley (Cossart et al., 2008).

- The post-glacial period

The Tardiglacial period following the LGM (end of MIS2and beginning of MIS1: 17600 – 11300 years B.P) is marked by a fluctuating warming trend (Heuberger, 1966 and 1968; Patzel, 1972; Kerschner, 1986). During this period two minor phases of glacial advance have been dated through several different methods (pollen, $^{14}C$, $^{10}Be$):

- The Oldest Dryas, covers the period from 18-17 to 14,7 kyr (Maisch, 1992; Maisch et al., 1999; Ivy-Ochs et al., 2008). During this period hundreds meters thick glaciers re-descended to altitudes around 1000m a.s.l. (Cossart et al., 2010) and also after 15kyr little glaciers persisted

around the peaks. In the “Alpes du Sud” has been detected a juniper expansion dating around 15-14,7 kyr B.P., fact that attest rapid warming and deglaciation linked to the xeric condition of the area (Jord and Rosique, 1994). The same authors underline also the fact that this rapid melting of the glaciers caused a decompression on the flanks valley and a sudden rapid erosion breaking the previous balance and trigging movements in the valley slopes.

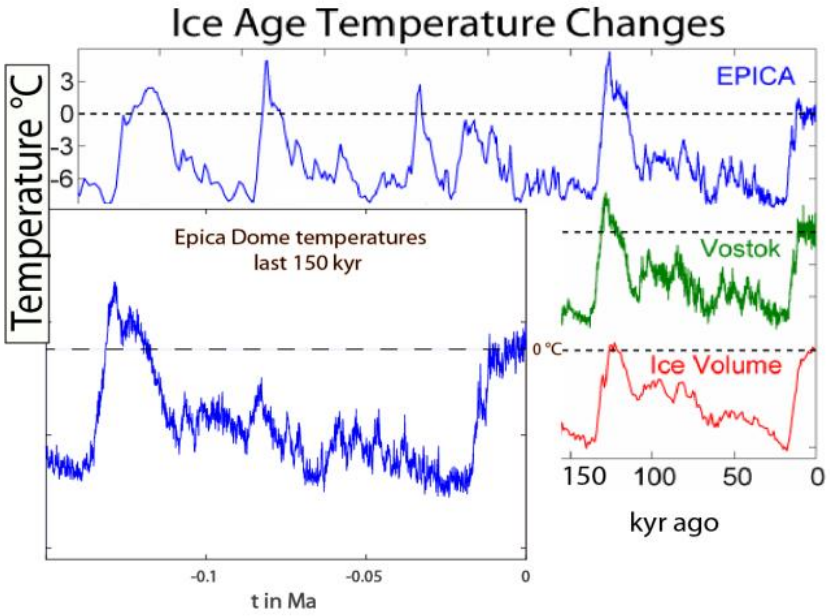


*Figure 10: graphic reporting the temperature fluctuation 450 kyr with a zoom on the last 150 ("Ice Age Temperature". Licensed under CC BY-SA 3.0 via Wikimedia Commons - https://en.wiki2.org/wiki/File:Ice_Age_Temperature.png#/media/File:Ice_Age_Temperature.png)*

- The Younger Dryas, dating from 12,6 to 11 kyr (Mangerud et al., 1974; Maisch et al., 1999; Ivy-Ochs et al., 2008; Ortu et al., 2008). This cold period results to be followed by a warm period between 11,6 and 9,0 kyr (Warner et al., 2008). In the “Alpes du Sud” after Jorda et Rosique

(1994) this period caused less developed glaciers than the Oldest Dryas. The same authors estimate for this period an annual average lowering of several degree in less than a century. The end of the Younger Dryas, i.e. of the cold period, marks the beginning of the Holocene.

These two post LGM glacial phases seem, in first approximation, in accordance with the $\delta^{18}O$ record of the North GRIP core (North GRIP members, 2004).

## II Methods

With the purpose of better understanding the behaviour of fluvial incision in response to active tectonics and climate changes, the present study has employed two main techniques: numerical modelling and TCN dating.

### *II. 1 Inversion of river longitudinal profiles*

#### *II.1.1 The Goren, Willet and Fox model*

The model used for this study is based on the code developed by Goren, Willet and Fox (Goren et al., 2014) that proposes a formal linear inversion scheme for the stream power law, with the aim of translating topography features into uplift rate information (Appendix 2 for mathematical detail). Basically, environmental variations like tectonic forcing and climatic regime cause changes in the river incision rate through time. The river long-profile records the result of these variations. Indeed, climatic and tectonic changes influence the altitude of the base level of the river, so that the channel is forced to adapt and tries to reach a new equilibrium profile. Because of regressive erosion, the new equilibrium profile is first reached downstream and the environmental change information propagates upstream to modify the longitudinal profile accordingly until a new equilibrium profile is reached all along the channel, if possible. Understanding how temporal variations in the erosion rate are propagate upstream is fundamental for the interpretation of river long-profiles, and is what the Goren-Willet-Fox model aims to do. This code uses the non-dimensionaliation of the stream power law proposed by Perron and Royden (2013). The latter approach allows transformation of river concave-up profiles (*Figure 11*) into straight lines in non-dimensional chi-elevation profiles where $\chi$ [-] is a non-linear distance coordinate (Appendix 2). This process reduced the problem to four variables: space, time, uplift rate and elevation, in a non-dimensional space coordinate $\chi$ (Perron et al., 2013 ).

Using these parameters, Goren's work (2014) shows how the linear inverse problem, produced by Royden and Perron's normalization, can be used to determine a continuous record of the relative uplift rate and how is possible to reintroduce natural units calibrating them with external data and geological constrains.

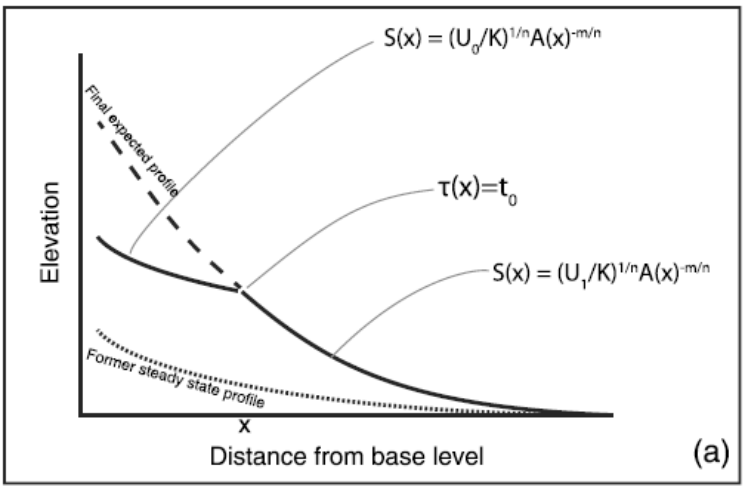


*Figure 11: schematic representation of a river long-profile evolution consequent to a changing in uplift rate U at time $t_0$ before present. The equation $S(x) = (U/K)^{1/n}A(x)^{m/n}$ is just the stream power law expressed in function of slope considering a topographic equilibrium state (after Goren et al., 2014).*

Tectonic forcing can change in time and in space, but in the study area we consider it as spatially homogeneous, so the analysis performed here has been based on the "Block Uplift Conditions" where Goren parametrization considers the uplift as space invariant.

*II.1.2 The Matlab code and how it works*

The Matlab inversion code developed by Liran Goren (Pers. Comm.) works as follows:

- it reads topographic and hydrographic data extracted from DEM analysis as input grids in ASCII format (Appendix 1, Code 1).
- it calculates a best-fitting concavity index (m/n) using the chi-plot method by computing the lowest residual between the actual river profile and a given number of linear segments, for different values of m (Appendix 1, Code 2).
- it uses the pre-defined m value to linearise the river profile into a polyline composed by as many segments as required by the user (Appendix 1, Code 3).
- it applies the inversion scheme and outputs the continuous signal of uplift rate in function of time (Appendix 1, Code 4).

II.1.2.1 Topographic data production with free-software GIS WhiteBox (https://whiteboxgeospatial.wordpress.com/ )

The Matlab inversion scheme needs, as input, topographic and hydrographic data. These data have been produced using the free-software GIS WhiteBox, and are: the topography, the flow direction of every single cell of the DEM, the flow-path length from every single cell within the watershed, the Horton-Strahler order of the streams, a watershed index, the drainage area and the main stem for each watershed.. We used the Aster satellite DEM with a 30 m resolution.

The Whitebox tools used for our study are as follows:

- WB-tool "Fill Depressions": DEM correction of artificial DEM depressions; this step eliminates local topographic minima that would invalidate the computing of the drainage pattern.
- WB-tool “D8 Flow Pointer”: an “8-direction” (D8) method that considers the 8 cells surrounding the working cell of the DEM grid, as the only 8 possible directions for the flow (*Figure 12*). The topography is the only input parameter used by this modelling tool, and the flow direction will point toward the cell

located in the direction of the steepest slope. It is important to note that water is not partitioned between multiple neighbour cells depending on their slope, as for instance in the D-infinity algorithm.

- WB-tool "D8 and Rho8 Flow Accumulation": this tool allows to identify the spatial coverage of up slope (or down slope) nodes draining to each pixel of the DEM. The Flow-Accumulation process registers the number of "incoming-cells" for each cell; obviously, the cells with the highest number of "incoming cells" will be defined as the river bed. The river outlet has a flow accumulation value equal to the drainage area.
- WB-tool "Extract Streams": it extracts raster cells in which flow accumulation exceeds a threshold value, given by the user, hence extracting the river beds from the flow accumulation grid.
- WB-tool "Horton-Strahler Stream Order": it calculates the H.S. order of each stream.
- WB-tool "Down slope Flowpath Length": it calculates the distance of each cell of the catchment area from the outlet cell of the main stem.

| | | |
|---|---|---|
| 64 | 128 | 1 |
| 32 | 64 | 2 |
| 16 | 8 | 4 |

*Figure 12: Whitebox GAT stores D8 pointers as binary numbers; in the figure a possible representation of the flow direction for the yellow cell. Each code corresponds to the flow direction, e.g., 64 means that water will be routed north-west from the "working cell".*

- WB-tool "Create Blank Outlet Raster": it creates a raster grid of zeros that can be modified changing by hand the value of each pixel. The pixels placed at the junction between main Tinée stem and each tributary have been given different indices.
- WB-tool "Watershed": it selects all the cells "pointing" to the "output cell" with

a given index; this operation allows to put different indices on the catchments.
- WB-tool "Find Main Stem": it identifies the main channel of every network.

II.1.2.2 Goren-Willet-Fox inversion code in "Block Uplift Conditions".

The Matlab inversion scheme in "Block Uplift Conditions" depends on the parameters n, m and K. These parameters have been chosen through a geological, geomorphological, geographical, and bibliographical analysis.

The χ value defined as $\chi = \int_{xb}^{x} \left( \frac{A_0}{A(x)} \right)^{m/n} dx$ (Perron and Royden, 2013), represents space in a non-dimensional system and depends on the m/n exponent, called "concavity index". The parameters "n" and "m", are, in the stream power law, respectively the exponent of slope and catchment area. In Goren's inversion scheme, a fundamental assumption is the linear dependency between the local slope "S" ad the erosion rate "E" in the stream power erosion model; that is to say, it assumes that n = 1.

The n value found in the literature, when estimated with stream power modelling purposes, varies between n = 0,7 n = 1 and n = 1,05 – 1,45 (Howard and Kerby, 1983; Tucker and Slingerland, 1997; Seidl and Dietrich, 1992; Whipple and Tucker, 1999; Attal et al., 2008). Mathematical analyses show different migration rates for different slope-patches of different slopes (Perron and Royden, 2013), which means that river reaches are consumed or created along slope breaks. The main problem is that field estimations are hard to obtain, and anyway the cannibalization between slope patches is not expected to leave traces along river longitudinal profiles. Estimations of n from large data sets, suggest a value of n = 1 for the Siwalik Hills, Nepal, and for Hawaii (Wobus et al., 2006; Ferrier et al., 2013). Another evidence suggesting that the "n = 1" assumption is acceptable, comes from the results of several finite difference and non linear inversion methods (Roberts and White, 2010; Roberts et al., 2012a; Roberts et al.,2012b). In the afore-mentioned works it is also reported that n > 1 is, in threshold-independent model, the way for modelling incision events that take place only

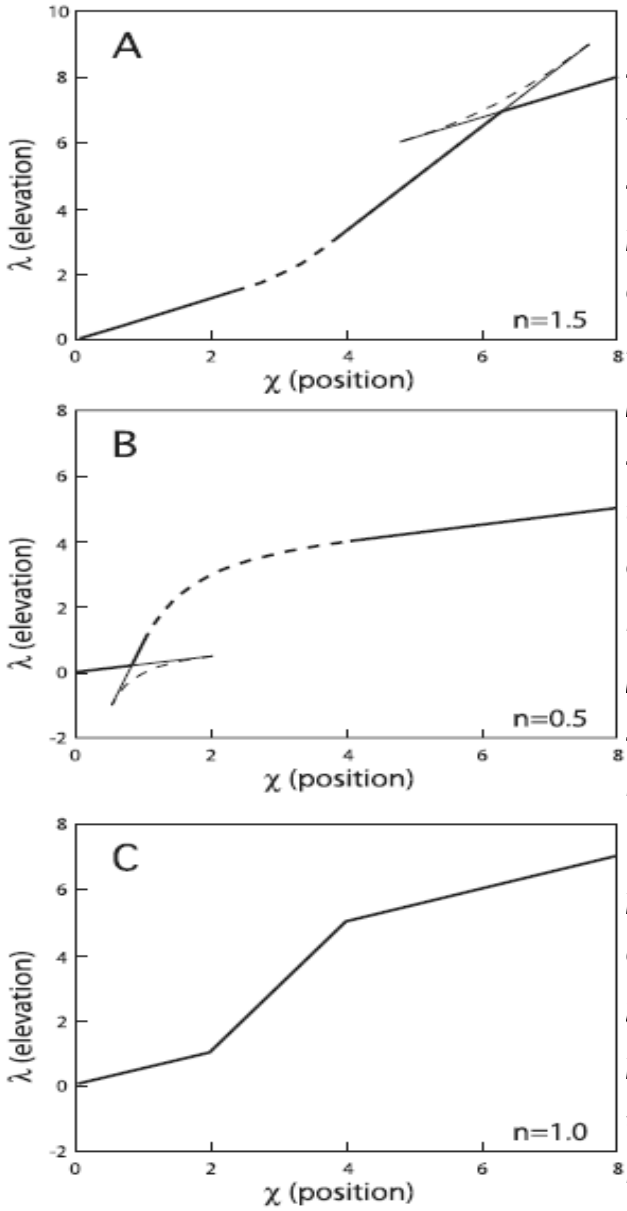


*Figure 13: Behaviour of the slope patches for different n values. If n < 1, the less steep segments migrate upstream faster than the steeper ones and only concave-up migrating knick points persist. Conversely, if n > 1 steeper segments are faster than less steep ones, and only concave-down migrating knick points are preserved. If n = 1, the segment have all the same horizontal migration rate. The displayed profiles are formed by two instantaneous changes in uplift rate, first from υ =0.5 to υ =2.0, followed by a change from υ=2.0 to υ =0.5, for (A) n=1.5, (B) n=0.5, (C) n=1.0. The straight, solid line segments consist of slope patches formed at base level during the periods of constant uplift rate. The curved, dashed sections formed during the moment of instantaneous change in uplift rate; for n=1 these curved sections are collapsed to a single point. Heavy solid and dashed lines are physically realized portions of the river profile; light solid and dashed lines are not physically realized but are still part of the slope patch solution"(cit. Perron and Royden 2013; figure taken from the same author).*

whene the stream energy overcomes a given threshold. Considering that the rivers studied in this work, have in four cases a mean slope above 25% and in the other five a mean slope above 7%, it is acceptable with respect to the long-term fluvial landscape evolution, to neglect the threshold behaviour. Finally, looking at the sharpness of the knick points present in the analysed streams it is possible to exclude the case of n < 1, situation that would have preserved only the concave-up knick points (Perron and Royden, 2013) and would have led to a smoothing of the river topographical profiles (Tucker and Whipple, 2002).

For all these reasons we have used an n=1 value for the High Tinée basin.

Assumed n = 1, the concavity index m/n becomes automatically function of the only m parameter.

To estimate the "m" value, the Goren code plots the $\chi$ – z linearised profiles. Starting from a $\chi(0) = 0$ value for the outlet pixel of each river, it computes the $\chi$ value in the following way: $\chi_{xi} = \chi_{xj} + \frac{x_i - x_j}{A_{xi}^m}$, where $x_j$ is the receiver of $x_i$, whose $\chi$ value has already been updated. Varying "m" between 0 and 1, since $\chi$ depends form m, it calculates the m minimizing the scatter between each m-dependent profile and the measured one. For the evaluation of the scatter, the $\chi$ space is divided into several bins (elementary segments) and the scatter is defined as the mean over the standard deviation of z in each segment. In this study the number of bins has been fixed to 20. This number is chosen arbitrarily, as a too low number of bins will result in a low number of linear segments that will not fit observations, while a too large number will result basically in fitting the noise (*Table 1*). With the same purpose also the number of time intervals has been ascribed a value of 40. To reduce the incision rate change between two time intervals, the code uses a damping coefficient. For the present analysis it has been fixed to a value of 100. The performed tests have demonstrated that the damping coefficient has a real effect upon the incision-rate-profile only for values of a $10^2$ order. Increasing the damping coefficient leads to a smoother incision rate time history, but degrades the fit between modelled and observed river profiles.

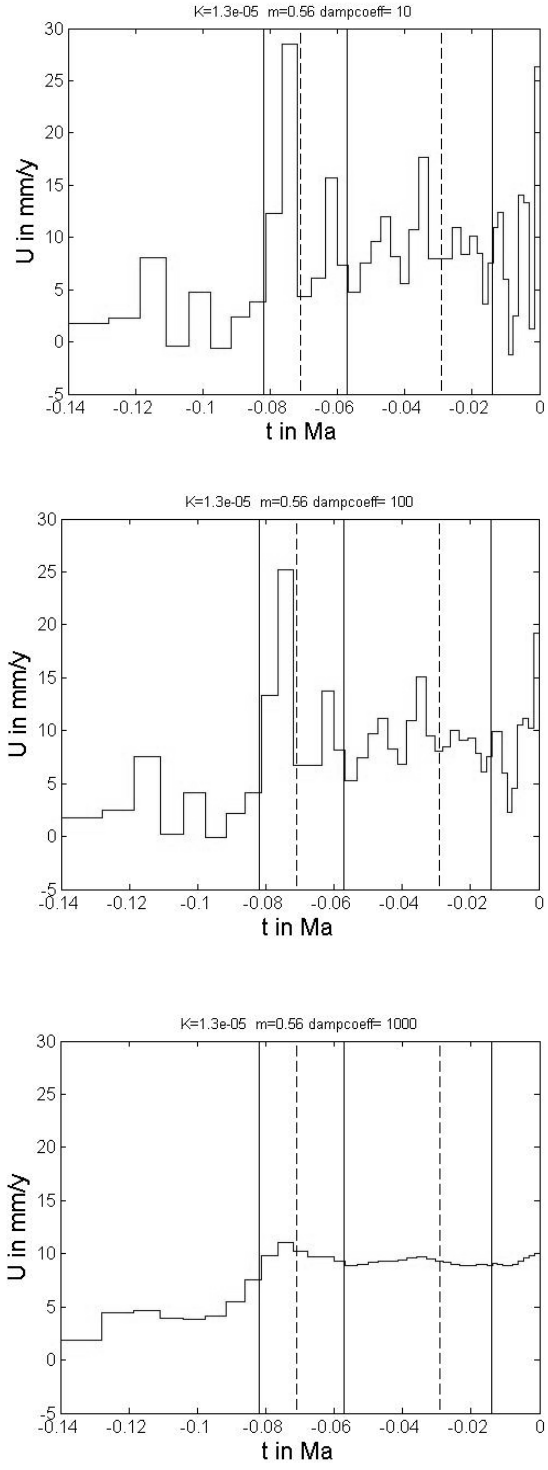


*Figure 14: Effects of damping coefficient on the Tributary 1 incision-rate-profile. From left d.c. of 10, of 100 and of 1000. The other parameters remain the same: K = 1.3 $10^{-5}$, m = 0.56. Note how the maximum incision rate values change of only 3 mm/yr also with a d.c. of 100.*

In our analysis, however, regression fit for the χ-plot and the linearisation of the river profile did not give a satisfying result for m. Most of the time the "m" values were neither univocal neither contained in a bibliography-acceptable range. Furthermore, the calculated residuals were quite elevated and did not variate much across the [0 – 1] range of m. We have therefore decided to fix the m value at 0,5 ·and gradually modify it inside the range [0.4 - 0,6], in order to obtain the m – K couple giving the most "environmentally" logical U – t profiles.

| Scatter of "Goren m" | Scatter of choosen m |
|---|---|
| 2,04 | 2,25 |
| 2,30 | 2,34 |
| 6,56 | 6,56 |
| 5,29 | 5,68 |
| 14,31 | 15,65 |
| 13,66 | 15,57 |
| 9,41 | 10,28 |
| 11,76 | 12,07 |
| 3,13 | 3,40 |

*Table 1: scatters between topographic profiles and mathematical ones induced by the m minimizing them and by the m chosen for our modelling.*

To choose the "m" and "K" parameters leading to the most realistic results, we need to calibrate the model. The linearisation and the inversion of the stream power law indeed give a non-dimensional uplift rate $U^* = \frac{U}{KA_0^m}$, that has to be converted into a dimensional (space-time) variable with appropriate m and K values. During the model calibration we have noticed a good synchronization between the incision peaks of each rivers, and a very interesting concordance between incision peaks and post MIS5e world temperature fluctuations; i.e., there

may be a strong climatic control on the valleys erosion and gorge shaping by global climatic changes. The model has then been calibrated based on the hypothesis that in a small area as the studied one (c.a. 270 $km^2$) there must be a synchronization in the incision peaks of the different streams since they respond to similar climatic conditions. A second constrain imposed to the incision peaks, also linked to the climatic control assumption, has been the temporal concomitance between the peaks and lows of the Epica-Dome C Temperature (*Figure 10*) curve and those of the incision rate signal. A third factor taken into account has been the "age" of the incision rate signal. Considering that all knick points are moving at the same horizontal speed (Perron and Royden, 2013), it is evident that shorter and steeper rivers carry with them a shorter history than the longer ones, because older information were deleted by the upstream movement of the more recent knick points. In the choice of "m" and "n" we have tried to keep a logical ratio between topographic profiles lengths and incision rate ages. The variation range of the erodibility factor K has been chosen based on the results of Saillard et al. (2014) in the Vésubie River. The erodibility factors used in this study are slightly higher than those used for the Vésubie. The strong landslide activity registered in the Tinée Valley (Sanchez et al., 2010a; Darnault et al., 2012) indicates a stronger intensity of the river incision, which supports this choice. In this study, oppositely to the one by Saillard et al. (2014) we have decided to keep the K value constant over time. The consequence is that incision rate changes are converted into uplift rate changes rather than in K-value changes, but our interpretation takes into account this fact. The practical effect of varying m and K is that increasing their values gives a shortening (i.e. a rejuvenation) of the incision-rate-profile (*Figure 15 and 16*). Obviously indeed, a higher erodibility coefficient and a higher influence of the drained surface increase the incision efficiency.

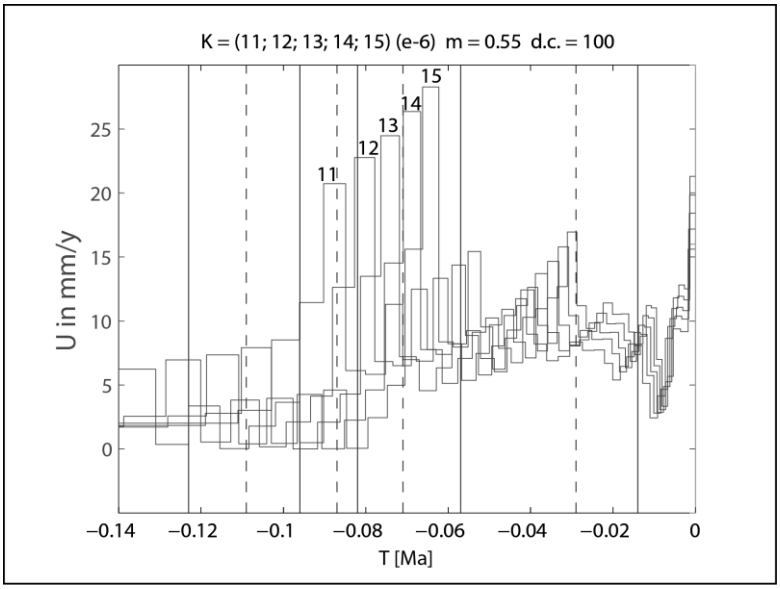


*Figure 15: K influence on incision-rate-profiles. Above each profiles is marked the relative K value divided by $10^{-6}$.*

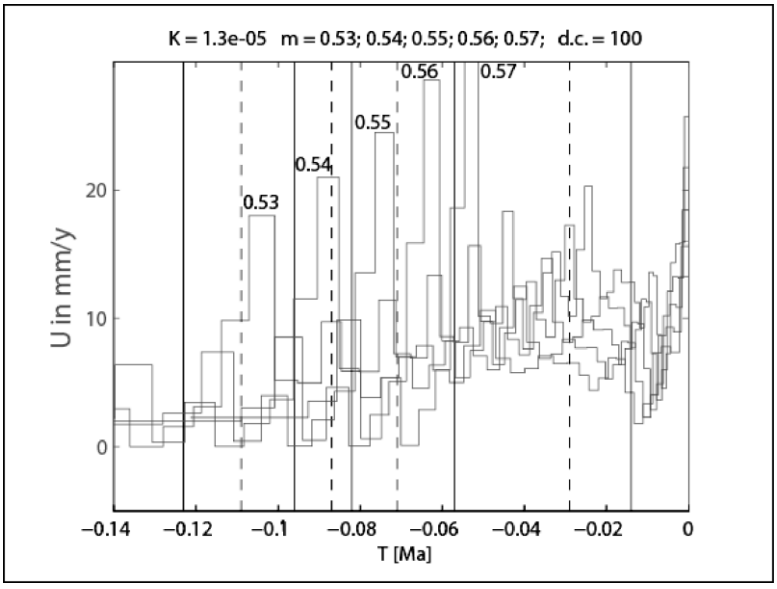


*Figure 16: m influence on incision-rate-profiles. Above each profiles is marked the relative m value.*

It is anyway important to note that this modelling has been performed not with the aim of quantifying the incision rate, but rather to better understand the "behaviour" of the incision processes during the last MIS stadials and interstadials. The understanding of the time variation of the incision rate helps to clarify the relationships existing between longitudinal river profiles, active tectonics and climate. Late Pleistocene to Holocene incision rates have been constrained by TCN dating.

### *II.2 $^{10}$Be Terrestrial cosmogenic nuclide (TCN ) analysis*

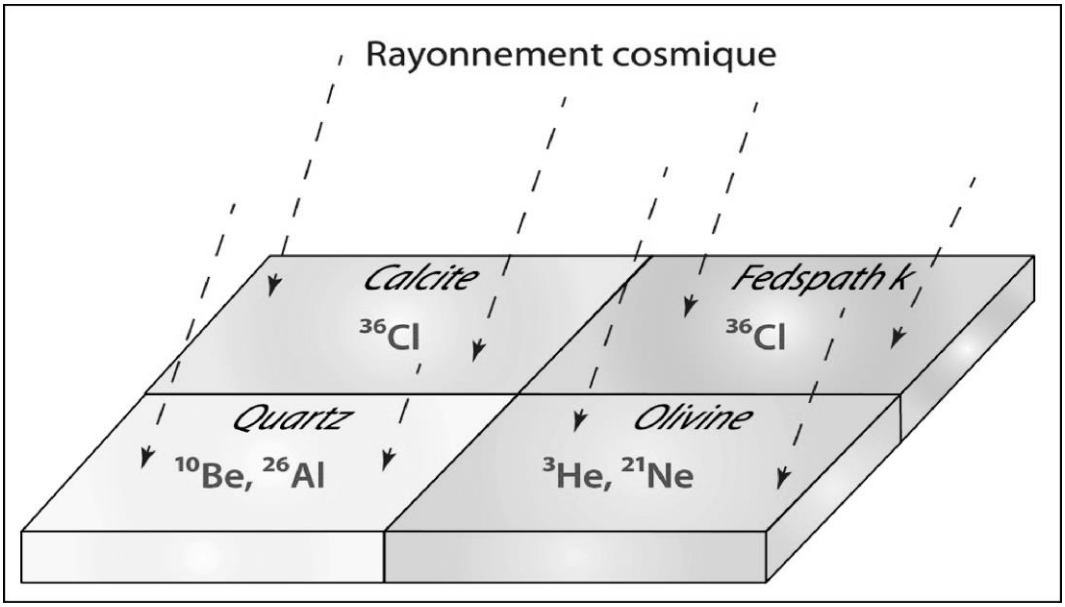


*Figure 17: Target minerals and product cosmogenic nuclides(after Darnault et al. 2012).*

*Nuclides half-lifes are given in Appendix 3.*

Cosmic rays are high-energy, charged particles that impinge on the Earth from all directions. These cosmic rays are originated by supernova explosion events that happen in our galaxy approximately once every 50 years (Dunai, 2010). Interacting with terrestrial atmosphere, primary cosmic rays (protons and α-particles) produce, mainly through the spallation phenomenon, secondary cosmic rays (neutrons, protons, α-particles, electrons and positrons, gamma ray photon, pion and muon). Because the neutrons do not suffer of ionization, as protons do, there is a gradual shifting in the cosmic ray flux composition that becomes completely neutron-dominated at the ground surface (98% of nucleonic cosmic ray flux; Masarick and Beer, 1999). Once these rays reach the terrestrial surface they penetrate more or less deeply into the rock depending on its density, and produce "cosmogenic nuclides" by their interaction with rock elements nuclei. At the earth surface, more than 98% of the cosmogenic nuclide production derives

from secondary cosmic-ray particles (neutrons and muons). The ray–rock interaction creates, mainly through a spallation process that takes the form of a cascade reaction, cosmogenic radionuclides.

In the present study we used the 10-Beryllium cosmogenic radionuclides. $^{10}$Be has not yet a univocal accepted half-life; in this study we have used the one proposed by Nishiizumi et al. (2007) of 1.36 +/- 0,07 Ma. In surface rocks $^{10}$Be is mainly produced by spallation reactions from O, with a secondary contribution of Mg, Al, Si and Ca (Dunai, 2010). The $^{10}$Be production linked to muons activity is around 3,6% at the first surface, and increases with depth (Hisingher et al. 2002a). Working with $^{10}$Be dating, it is important to remember that its atmospheric production is, on average, $10^3$ times faster than its rock one. This atmospheric 10-beryllium can precipitate and be absorbed by the rock. Fortunately it has been demonstrated (Khol and Nishiizumi, 1992) that, for quartz samples, sequential chemical dissolution can reliably remove the meteoric component.

The TCN $^{10}$Be methodology has already been used in the Tinée valley for dating polished surface of glacial and fluvial origins in Darnault's (2012) PHD thesis. In the Vesubie valley a study on the river incision rate (Saillard et al. 2014) has used the $^{36}$Cl cosmogenic nuclides.

To further constrain and discuss the modelling results we have performed a new $^{10}$Be TCN dating on eleven samples collected on a river polished surface, along a vertical section in the Tinée valley.

### *II.2.1 Sample-collection process*

The samples have been taken on a gorge surface located downstream of the village of Isola (see Chapter III). The samples have been collected abseiling from the top of the polished surface and with the help of hammer and chisel. The sampling has been made so that the distance between each sample was as constant as possible. Where possible the samples have been taken from quartz veins, which is the best target for $^{10}$Be production.

All the samples have been given a name, an altitude, a thickness; GPS coordinates

and topographic shielding are identical for all the samples. The shielding has been measured using a compass and allows us to calculate with CRONUS – earth online calculators (http://hess.ess.washington.edu )(*Figure 18*), the reduction on $^{10}$Be production due to the topographic obstruction and then the correct exposure age of the surface. Practically, twelve quadrants covering a horizon of 360° have been created (*Table 2*); to each quadrant has been associated the value corresponding to the angle between the base of the polished surface and the maximum topography within the considered quadrant.

| **Quadrant [°]** | 0 – 40 | 40 – 64 | 64 – 87 | 87 – 106 | 106 – 150 | 150 – 230 | 230 – 240 | 240 – 260 | 260 – 280 | 280 – 320 | 320 – 340 | 340 – 360 |
|---|---|---|---|---|---|---|---|---|---|---|---|---|
| **Quadrant Width [ ° ]** | 40 | 24 | 23 | 19 | 44 | 80 | 10 | 20 | 20 | 40 | 20 | 20 |
| **Altitude [ ° ]** | 20 | 25 | 16 | 50 | 70 | 70 | 16 | 19 | 38 | 45 | 47 | 40 |

*Table 2:Quadrants shielding, starting from N 190.*

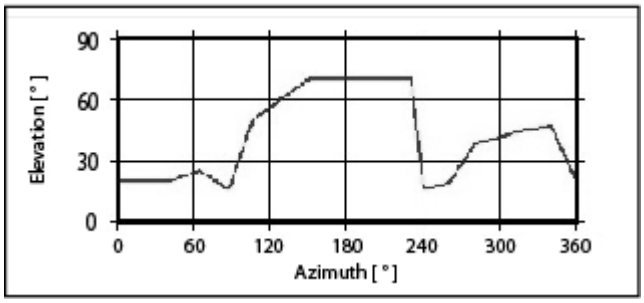


*Figure 18: Shielding profile obtained with CRONUS* – earth online calculators
( *http://hess.ess.washington.edu* )

II.2.2 S*amples preparation*

Once recollected, the samples have been prepared for the AMS-analysis through a mechanical and chemical process. The samples preparation has followed the procedure sheets provided by the CEREGE laboratory.

II.2.1.2 Mechanical preparation

The mechanical preparation of the samples is divided into three steps:

- Fine-grained fraction acquisition: the samples have been grounded and sifted in order to obtain a granulometry between 250µm and 800µm.
- Samples pre-washing: this step allows us to eliminate lighter particles (clays and finer-grained particles). After the pre-washing the samples are dried in heating plates.
- Quartz grain sorting: finally, with the use of a Frantz separator, magnetic and para-magnetic particles have been removed. By this way we have obtained samples made only of diamagnetic minerals, among which, of course, the quartz.

II.2.2.2 Chemical preparation

For chemical processing the samples have been introduced in weighted Nalgene bottles, expressly made to resist to the acid-washing.

The chemical samples preparation is made in 7 steps,

- $H_2SiF6$ + HCl dissolution: impurities dissolution through hydrofluorosilicic ($H_2SiF6$) and chloridric acid (HCl), both diluted at 50%. The Nalgene bottles containing the samples get filled with the solution and shaken for 24h. After the acid-washing the samples are rinsed with distilled water. The operation is repeated as many times as necessary to have a clear post-shaking-solution.

- HF decontamination: The HF-washing allows eliminating the atmospheric Beryllium contained into the rock and to conserve only the in-situ produced Beryllium. A series of three sequential HF-washings, dissolving 10% of the quartz mass, allows us to completely purifies the samples (Brown et al., 1991). Afterwards the samples are rinsed with distilled water, dried and weighted. Only 20 – 40 g of matter is kept for the rest of the process. The remaining is stored.

The samples are, at this point of the process, almost entirely made of pure quartz and are then ready for the Beryllium extraction.

- $^{10}Be$ / $^{9}Be$ ratio fixation: water and entrainer are added in the Nalgene bottles. The water helps to mix the entrainer with the samples, and is necessary to reduce the heating produced by the following HF addition. The entrainer, 100µl of $^{9}Be$ solution with a 3025ppm concentration, helps to fix the ratio $^{10}Be$ / $^{9}Be$. It is fundamental to weight the exact amount of entrainer inserted, because this will be finally used to measure the quantity of Beryllium. The ratio $^{10}Be$ / $^{9}Be$ of the blank will be subtracted from those obtained from the sample analysis.
- Sample dissolution: to dissolve the samples an in-excess quantity of HF is added into the bottle. The heat produced by this exothermic reaction is controlled by placing the bottle into a tray fulfilled with water. Once cooled, the samples are shaken for 24h.
- The obtained solutions are transferred in into a Teflon beaker, and the not-dissolved residual particles are recollected and weighted. Their mass will be subtracted from the effectively dissolved quartz mass. The beaker containing the samples solution is placed on heating plates, in order to evaporate the HF. The samples are now a dry dust that could anyway still be contaminated by Boron, abundant into the terrestrial environment and natural isobaric element of Beryllium. To eliminate the Boron, 5 ml of HF are added in three subsequent steps. The Boron is transformed into boron fluoride ($BF_2$) and then eliminated through evaporation (Delunel, 2010). Three following additions of 5ml of $HNO_3$, and a last one of 10 ml, with a

final evaporation allow elimination of the remaining HF. Once dried, 3ml of pure chloridric acid are added into the beaker , and the whole solution is transferred into a test tube, with the help of a dropper. The test tube containing the samples is centrifuged.

- Beryllium concentration: to concentrate and extract the Be, exchanging resins have been employed. These exchangers of ions are insoluble macromolecules bringing ionisable groups with the property of exchanging ions in a reversible way (Delunel, 2010). To concentrate and dissolve the beryllium, ammonia ($NH_4OH$) has been inserted into the test tube. The quantity of ammonia has been chosen in order to reach a pH of 8 – 9, acidity level that cause the precipitation of beryllium, but keep the Boron in solution. A centrifugation allows separation of the Be from the solution. A further solution is made by diluting the Be with 1,5ml of HCl (10,2 mol).

- First column: the first column is a cationic resin DOWEX 1×8 (100-200 mesh). It keeps the metallic cations so that the solution is free from Fe2+ and Mn2+.

- Second column: after a re-precipitation of Be with the addition of ammonia, a following centrifugation, and an addition of less concentrated HCl (1,0 mol ) the solution is filtered with a DOWEX 50Wx8 (100 – 200 mesh) resin. The resin retains the remaining Boron and the Al2+.

- Samples oxidation: The Be precipitate is washed twice with water (with pH around 8 – 9). 200µl of nitric acid ($HNO_3$) to re-dissolve the beryllium are added into the test tubes. Finally the samples are transferred into labelized crucibles, and dried at a temperature of 400°C for 10 minutes. Afterwards they are placed into a muffle furnace for 2h at 900°C. At the end of the process the samples have been reduced to BeOS.

At the end of this process, the samples are chatodized, i.e. the beryllium oxide dust is mixed with Niobium (Nb, conductive metal ). This final mix is the one that will be used for the AMS (accelerator mass spectrometry ) measurement. In this study the AMS used is the ASTER of the CEREGE laboratory (Aix en Provence ). Once the AMS has calculated the ratio $^{10}Be$ / $^{9}Be$, it is possible to obtain the

exposure age of the sample using the equation:

$$C_{\chi,\varepsilon,t} = C_0 * e^{-\lambda t} + \frac{P_{spal}}{\lambda} * e^{-\chi/\Lambda\eta}\left[1 - e^{-\lambda t}\right] + \frac{P_{\mu s}}{\lambda} * e^{-\chi/\Lambda\mu s}\left[1 - e^{-\lambda t}\right] + \frac{P_{\mu f}}{\lambda} * e^{-\chi/\Lambda\mu f}\left[1 - e^{-\lambda t}\right]$$

Where: $C_{\chi\varepsilon}$ is the $^{10}$Be concentration in function of depth $\chi$ [g·cm$^2$] and of exposition time [yr];$C_0$ is the $^{10}$Be concentration inherited before the exposition of the surface;$\Lambda_\eta$, $\Lambda_{\mu s}$, $\Lambda_{\mu f}$, are the effective attenuation factors [g /cm$^2$]of respectively neutrons, negative muons and fast muons.

$P_{spal} + P_{\mu s} + P_{\mu f}$ , are respectively the spallation production rate the negative muons production rate and the fast muons production rate.

Note that $P = P_{spal} + P_{\mu s} + P_{\mu f}$ .

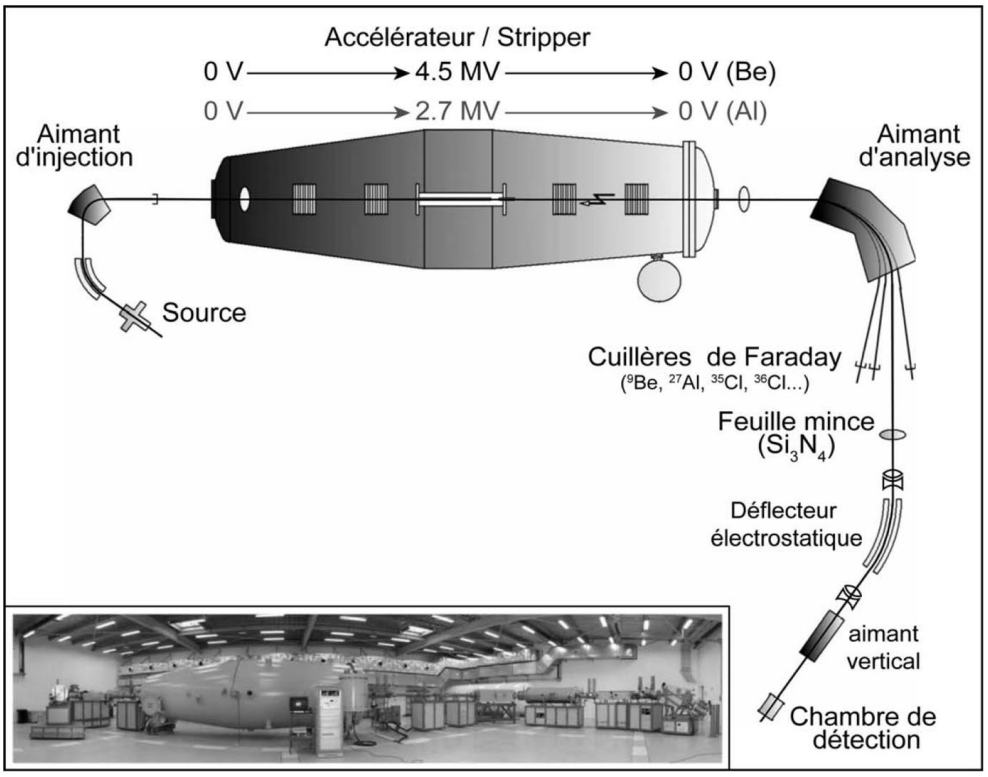


*Figure 19: Scheme mass spectrometer of ASTER accelerator located in CEREGE laboratory (Aix en Provence).*

*(from Klein et al., 2008, modified by Delunel 2010)*

*II.2.C Quantification of shielding factor and calculation of exposure ages with CRONUS – earth online calculators (http://hess.ess.washington.edu )*

With the online program "Cronus" it is possible to obtain the shielding factor correction and the exposure ages with relative spallation and muons $^{10}$Be production rates. For the shielding factor evaluation the program needs the strike and dip of the sampled surface and the altitude in degree of all objects hiding the samples from the cosmic rays.

To calculate the exposure the following parameters are needed: latitude, longitude, elevation, samples thickness, samples density, shielding correction, erosion rate, $^{10}$Be concentration, uncertainty in $^{10}$Be concentration, standardization of $^{10}$Be to use, $^{26}$Al concentration, uncertainty in $^{26}$Al concentration, standardization of $^{26}$Al to use.

# III Results

## *III.1 Incision rate profile modelling*

### *III.1.1 Parameters employed and general results*

Inverse modelling of incision rate variations in the High Tinée tributaries (*Figure 20, Table 3*) has been performed, as seen in chapter 2 , assigning the m and K parameters values, constrained by geographical and geomorphological considerations.

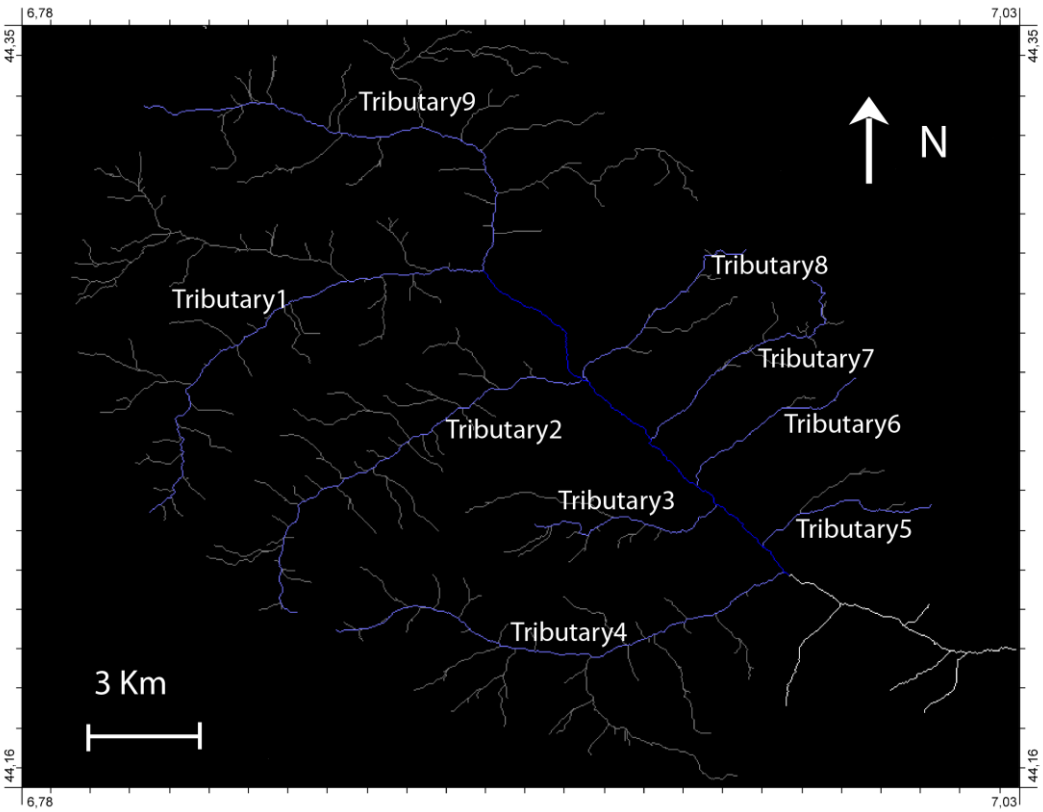


*Figure 20:hydrographic network of the High Tinée: in dark blue is the Tinée stem and in light blue the 8 tributaries.*

| River [ - ] | River code [ - ] | Length [ m ] | River altitude [ m ] | Slope % |
|---|---|---|---|---|
| Giarlogues | Tributary 1 | 15000 | 1050 | 7 |
| Ardon | Tributary 2 | 13620 | 1000 | 7 |
| Auron | Tributary 3 | 6500 | 800 | 12 |
| Roya | Tributary 4 | 15000 | 1070 | 7 |
| Douans | Tributary 5 | 5300 | 1350 | 25 |
| Asueros | Tributary 6 | 4100 | 1325 | 32 |
| Rabuons | Tributary 7 | 5000 | 1250 | 25 |
| Ténibres | Tributary 8 | 4891 | 1225 | 25 |
| Tinée | Tributary 9 | 14020 | 1050 | 7 |

*Table 3: analysed rivers; eight of the Tinée tributaries and the highest stem of the Tinée itself.*

III.1.1.1 The concavity index "m/n" and the erodibility factor "K"

Concavity index (m/n) and erodibility factor (K) have been chosen in order to obtain a similar incision signal from all the Tinée tributaries. "K" and "m" have been changed independently with the aim of reaching the best synchrony between all the incision rate profiles, and between the U* value variations ($U / (k (Ao)^m)$) and the Epica curve Temperature fluctuations.

The concavity index varies within a range going from m/n=0,54 to m/n=0,59 (*Table 4*) with a mean value of 0,55 and a standard deviation of 0,02. It is important to note that n has been considered equal to 1 such as: m/n = m.

The erodibility factor, "K", varies between $10 \cdot 10^{-6}$ $mm^{1-2m}yr^{-1}$ and $20 \cdot 10^{-6}$ $mm^{1-2m}yr^{-1}$ (*Table 5*). Rivers flowing for the main part on marls or limestone lithologies (tributaries 1, 2, 3, 4) show slightly higher k values:

- The mean k value of rivers with a crystalline substrate is $11,4 \cdot 10^{-6}$ $mm^{1-2m}yr^{-1}$ with a standard deviation of $1,5 \cdot 10^{-6}$ $mm^{1-2m}yr^{-1}$.
- The mean K value for marls or limestone lithologies is $14,7 \cdot 10^{-6}$ $mm^{1-2m}yr^{-1}$ with a standard deviation of $3,6 \cdot 10^{-6}$ $mm^{1-2m}yr^{-1}$.

| River [ - ] | m [ - ] | Scatter [ - ] |
|---|---|---|
| Tributary 1 | 0,55 | 2,25 |
| Tributary 2 | 0,54 | 2,34 |
| Tributary 3 | 0,55 | 6,56 |
| Tributary 4 | 0,54 | 5,68 |
| Tributary 5 | 0,59 | 15,65 |
| Tributary 6 | 0,56 | 15,57 |
| Tributary 7 | 0,56 | 10,28 |
| Tributary 8 | 0,56 | 12,07 |
| Tributary 9 | 0,54 | 3,40 |

*Table 4: values of the concavity index obtained for the Tinée tributaries and relative scatter. The scatter is defined as the mean over the standard deviation of chi – z in each of the 20 bins used for the linearization process (see chapter methodologies).*

| River [ - ] | K / (10^-6) [$mm^{1-2m}yr^{-1}$] |
|---|---|
| Tributary 1 | 13 |
| Tributary 2 | 20 |
| Tributary 3 | 14 |
| Tributary 4 | 12 |
| Tributary 5 | 10 |
| Tributary 6 | 11 |
| Tributary 7 | 11 |
| Tributary 8 | 11 |
| Tributary 9 | 14 |

*Table 5:values of erodibility coefficient (K [$mm^{1-2m}yr^{-1}$]) obtained for the 9 tributaries.*

III.1.1.2 Incision rate obtained for the different rivers

The calibration of the incision rate with estimated K and m values gave the following results:

| River [ - ] | Umax [mm/yr] | Umin [mm/yr] | Δ U [mm/yr] |
|---|---|---|---|
| Tributary 1 | 24,0 | 0,2 | 23,8 |
| Tributary 2 | 16,0 | 2,4 | 13,6 |
| Tributary 3 | 26,0 | 1,3 | 24,7 |
| Tributary 4 | 21,7 | 1,7 | 19,9 |
| Tributary 5 | 45,0 | 0,6 | 44,4 |
| Tributary 6 | 25,0 | 6,0 | 19,0 |
| Tributary 7 | 24,5 | 11,0 | 13,5 |
| Tributary 8 | 28,0 | 1,0 | 27,0 |
| Tributary 9 | 17,0 | 2,7 | 14,3 |
| | $U_o$ [mm/yr] | min mean [mm/yr] | integral mean [mm/yr] |
| Tributary 1 | 18,0 | 4,4 | 6,9 |
| Tributary 2 | 7,2 | 5,9 | 8,6 |
| Tributary 3 | 26,0 | 5,9 | 6,4 |
| Tributary 4 | 19,4 | 4,3 | 4,8 |
| Tributary 5 | 45,0 | 10,9 | 11,8 |
| Tributary 6 | 6,0 | 13,4 | 16,2 |
| Tributary 7 | 12,0 | 13,9 | 15,7 |
| Tributary 8 | 11,7 | 11,4 | 15,6 |
| Tributary 9 | 16,6 | 5,2 | 6,4 |

*Table 6:Umax and Umin: Highest and lowest incision rate for each tributary. ΔU: range of U fluctuations for each studied river. Uo: Current incision rate calculated for the Tinée tributaries at their outlet corresponding to the current Tinée incision rate. Min mean: Weighted mean of the minima of each incision-rate profile. Integral mean: integral mean of each incision-rate profile. It is important to know that for the tributary 5 the reported mean has been calculated between 140 1nd 14 kyr B.P. to avoid the influence of the final probably over-estimated peak. In Table 10 are reported the means obtained using the whole profile.*

The $U_o$ value represents the inferred incision rate for the lowest part of the Tinée tributaries. Being the Tinée the base level of its tributaries, if we consider its variations as the trigger for the incision rate variations along them, we can consider the Uo incision rates as an approximation of the Tinée incision rate.

It is also possible to note that the rivers joining the Tinée in approximately the same place have quite different incision rates (*Figure 21*).

-Tributaries 2 and 8: difference in rate incision of 1,9 mm/yr; weight of the difference 23,3 %.

-Tributaries 1 and 9: difference in rate incision of 1,4 mm/yr; weight of the difference 8.3 %.

This fact derive probably from the fact that the reaction dynamics of a river to an external forcing depend from several factors, among which the steepness of the river itself. Steepness is really different in the opposite sides of the Tinée Valley (*Table 3*).

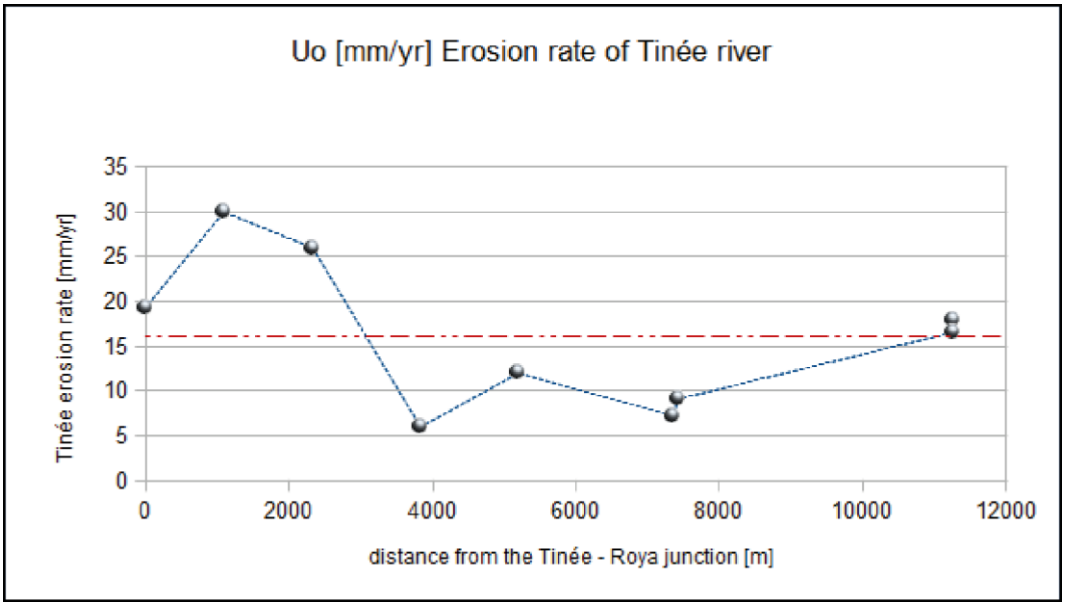


*Figure 21: incision rate at Tinée level. Each dot represents the incision rate of one tributary, calculated on his lowest linearised segment. The tributaries are ordered from the Tinée - Roya junction in upstream direction: T.4; T.5; T.3; T.6; T.7; T.2; T.8; T.9; T.1. The red dotted line represents the obtained Tinée incision-rate mean, 16,03 mm/yr. For T5 has been used the value of 30.*

### *II.1.2 Incision-rate-profiles presentation and description*

All the incision rate profiles (U – time) produced with the Goren-Willet-Fox code, show, for every tributary, an incision peak around 14000 yr B.P. (MIS 1). Other three peaks recur regularly, with more or less precision, at the ages of 38, 57 and 82 kyr B.P. It is important to note that for the quantification of m and K, necessary to calibrate the model in order to bring back the incision rate value to a dimensional system, the following criteria have been considered, in order of importance (see chapter II):

- Presence in incision-rate profile of peak A (*Table 7)*;
- Constant horizontal migration of knick points, with a consequent major loss of information in shortest and steepest rivers;
- Presence of peaks B, C, D (*Table 7*).

- Presence of any incision-rate peak synchronous to Epica curve fluctuations.
- To keep the incision rate possibly inside the range 0,8 – 25 mm/yr (values of local uplift rate and maximum erosion rate obtained in the Vesubie valley by Saillard et al, 2014).

| | Regularly recourring peaks [ yr B.P. ] |
|---|---|
| **Peak A** | 14000 |
| **Peak B** | 38000 |
| **Peak C** | 57000 |
| **Peak D** | 82000 |

*Table 7:peaks used in calibrating the profiles parameters.*

It is possible to divide the time – incision-rate profiles into three different groups characterized by common features in the incision-rate-profiles. It is worth to note that this division, made on numerical modelling data, group together rivers placed in the same zone of the studied area: tributaries 1, 2 and 9 for group 1 (North); tributaries 3, 4 and 5 for group 2 (West and South); tributaries 6, 7 and 8 (East) for group 3 (*Figure 20*). For every group of profiles has been calculated a "Mean Profile". The punctual mean profiles highlight the features common to the tributaries of a certain area, underlying the incision characteristic linked to its geographical and geomorphological peculiarities.

III.1.2.1 Group 1, with tributaries 1, 2 and 9

This group contains three homogeneous time – incision-rate profiles, that, excepted for one case (incision peak at MIS4, profile 1; *Figure 23*), do not show incision peaks exceeding significantly 15 mm/yr. The common feature of these three rivers is their length. With tributary 4, these rivers are the three longest rivers studied in this work (*Table 3*) bringing the oldest incision rate information. These three rivers are the most upstream studied tributaries.

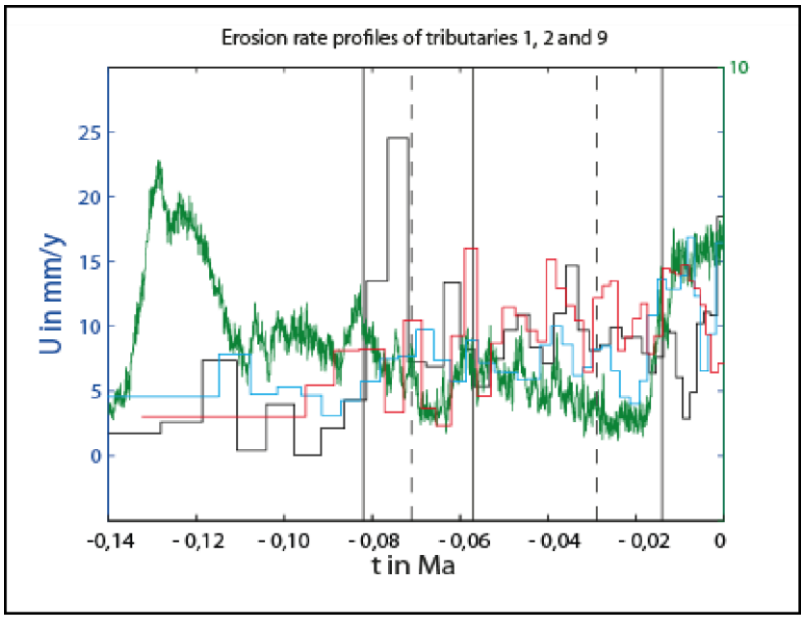


*Figure 22:comparison between incision rate profiles of Tributary 1 (black), Tributary 2 (red) and Tributary 9 (blue). The green line is the Epica Dome Temperature record for the last 140000 yr. The vertical black continuous line represents the warm MIS (from right: MIS1, MIS3, MIS5a), the black dotted lines the cold MIS (from right: MIS2, MIS4).*

- Tributary1:

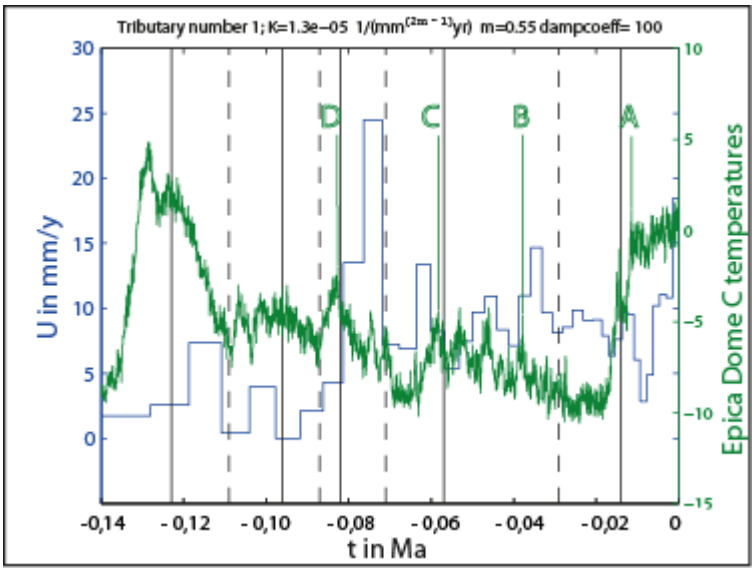


*Figure 23:incision-rate profile of Tributary 1(blue line), with the Epica curve (green line).The vertical black continuous line represents the warm MIS (from right: MIS1, MIS3, MIS5a), the black dotted lines the cold MIS (from right: MIS2, MIS4).*

Long 15040 m Tributary1 (Gialorgues) is the longest studied river and shows the longest incision-rate profile starting at 120-140 kyr. The four peaks common to all profiles (*Table 3*), are present with peak C slightly in advance if compared to the Epica peak of reference. The incision-rate profile shows also an anomalously elevated peak D, and an unexpected minimum after the MIS1. The 4 erosion peaks are visible also along the topographic profile (*Figure 24*), where is evident the elevated slope corresponding to incision-rate-peak D. It is also possible to see in *Figure 23* (*Table 8* for the values) a general augmentation in the mean erosion that starts from interstadial MIS5a.

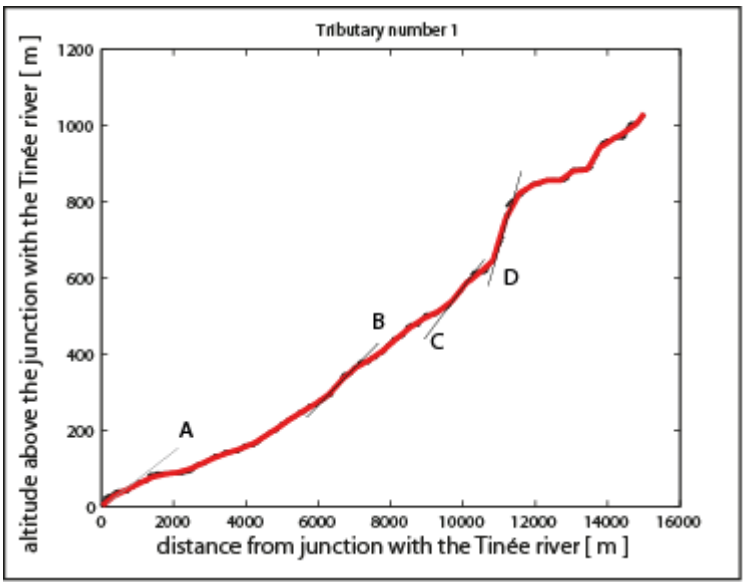


*Figure 24: topographic profile of tributary 1. The tangent segment with relative letter are the changing slope that have probably been read by the model as the incision peaks.*

| | mean [ mm/yr ] | Min mean 1st part [ mm/yr ] | Min mean 2nd part [ mm/yr ] | Min mean 1st – 2nd [ mm/yr ] |
|---|---|---|---|---|
| **Tributary 1** | 4,4 | 0,2 | 7,0 | 6,8 |
| | **mean [ mm/yr ]** | **Int. mean 1st part [ mm/yr ]** | **Int. mean 2nd part [ mm/yr ]** | **Int. mean 1st – 2nd [ mm/yr ]** |
| **Tributary 1** | 6,9 | 6,9 | 10,3 | 3,4 |

*Table 8:integral mean and incision-rate mean calculated over the minima of the profile for the whole profile, for the interval 140 – 80 kyr B.P (1st part), for the interval 80 – 0 kyr B.P. (2nd part). In the last column are reported the difference between the incision rates of the two intervals.*

- Tributary 2:

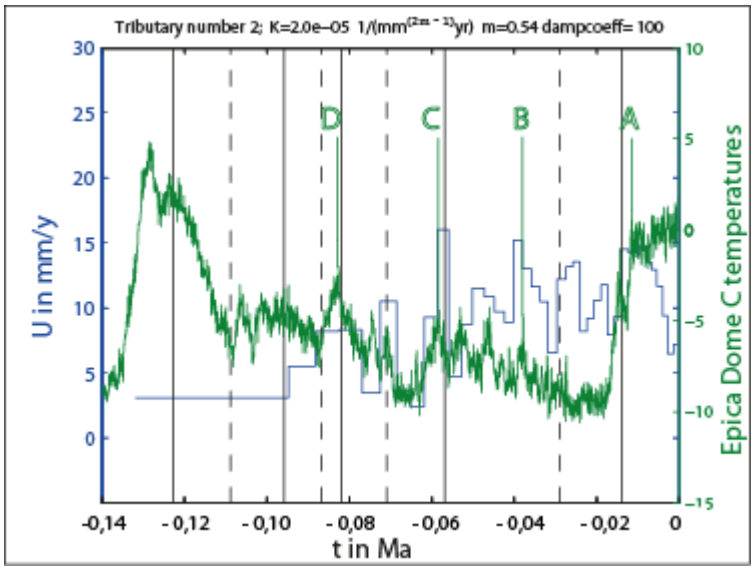


*Figure 25:incision-rate profile of Tributary 2 (blue line), with the Epica curve (green line). The vertical black continuous line represents the warm MIS (from right: MIS1, MIS3, MIS5a), the black dotted lines the cold MIS (from right: MIS2, MIS4).*

The incision-rate profile of tributary 2 (Ardon) shows a generally good synchrony between his fluctuations and those of the Epica curve. Despite the good synchrony, between the two profiles, there is not a correspondence in intensity. All the incision-rate-peaks have roughly the same values, while the Epica curve shows a marked difference between the post MIS1 temperature-peak and the previous ones. For this profile it has also been quite difficult to choose the appropriate K value. It has been indeed necessary to arise it well above the other erodibility factor (*Table 5*) to have a profile with the same age of the other river with similar length and slope (e.g. *Tributary 1, Table 3*), and to fit temperature and incision-rate-peaks. All the 4 expected peaks are present, with a well marked peak C. Two peaks, with an unexpected intensity, underline the two little fluctuations of the Epica curve in the middle of the MIS2 stadial. After peak A there is a decrease in the erosion rate. In *Figure 25* is also possible to spot an increment in the mean

erosion around 60 kyr B.P. (*Table 9* for the values).

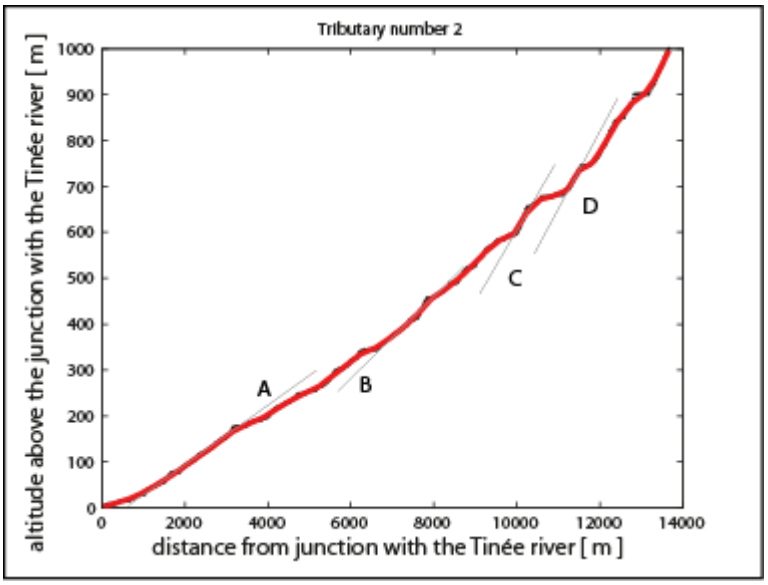


*Figure 26: topographic profile of tributary 2. The tangent segment with relative letter are the changing slope that have probably been read by the program as the incision peaks.*

| | mean [ mm/yr ] | Min mean 1st part [ mm/yr ] | Min mean 2nd part [ mm/yr ] | Min mean 1st – 2nd [ mm/yr ] |
|---|---|---|---|---|
| **Tributary 2** | 5,9 | 2,9 | 7,6 | 4,7 |
| | **mean [ mm/yr ]** | **Int. Mean 1st part [ mm/yr ]** | **Int. mean 2nd part [ mm/yr ]** | **Int. mean 1st – 2nd [ mm/yr ]** |
| **Tributary 2** | 8,6 | 6,0 | 10,8 | 4,9 |

*Table 9:integral mean and incision-rate mean calculated over the minima of the profile for the whole profile, for the interval: 140 – 60 kyr B.P (1st part), 60 – 0 kyr B.P. (2nd part). In the last column are reported the difference between the incision rates of the two intervals.*

- Tributary 9:

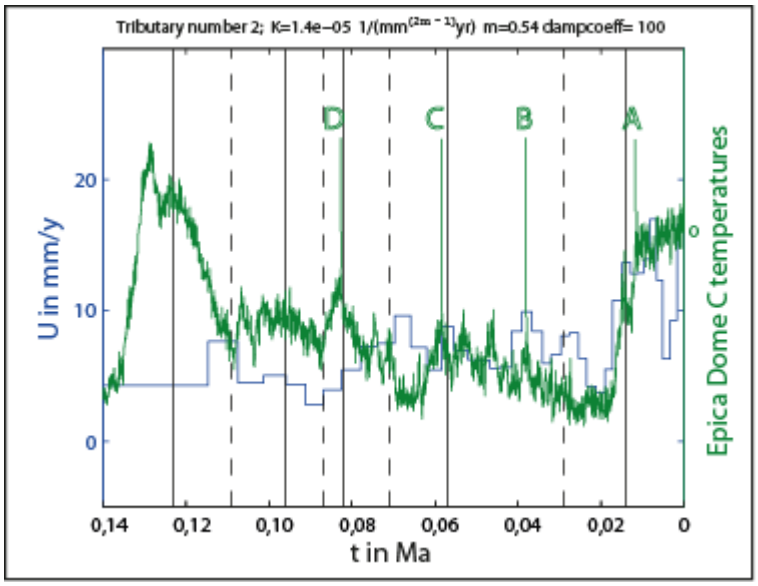


*Figure 27: incision-rate profile of Tributary 9 (blue line), with the Epica curve (green line).The vertical black continuous line represents the warm MIS (from right: MIS1, MIS3, MIS5a), the black dotted lines the cold MIS (from right: MIS2, MIS4).*

Tributary 9 is actually the highest part of the Tinée itself. To fit the whole profile with the Epica curve, changing the parameter K and m inside acceptable range ($1{,}5 \cdot 10^6$ +/-$0{,}5 \cdot 10^6$ for K; 0,5 +/-0,1 for m; see chapter II for further explication), has resulted impossible. The choice has been to keep as first bond the coincidence between peak A and MIS1. This fact has led to a mis-fit of peak C that is shifted to younger ages. The peak B fits perfectly the Epica curve. After the MIS5a the profile shows a light but general increase in the incision-rates (*Table 10*). In *Figure 28*, it is possible to see how around 1100 m from the junction of the tributary with the Tinée, there is not any change in the topographic slope, as it is instead observed in the two previous profiles (the oldest inflection present in the profile is probably linked to the 110 kyr old peak). The absence of this change in slope could be the reason for which incision-rate-profile 9 doesn't show any peak D.

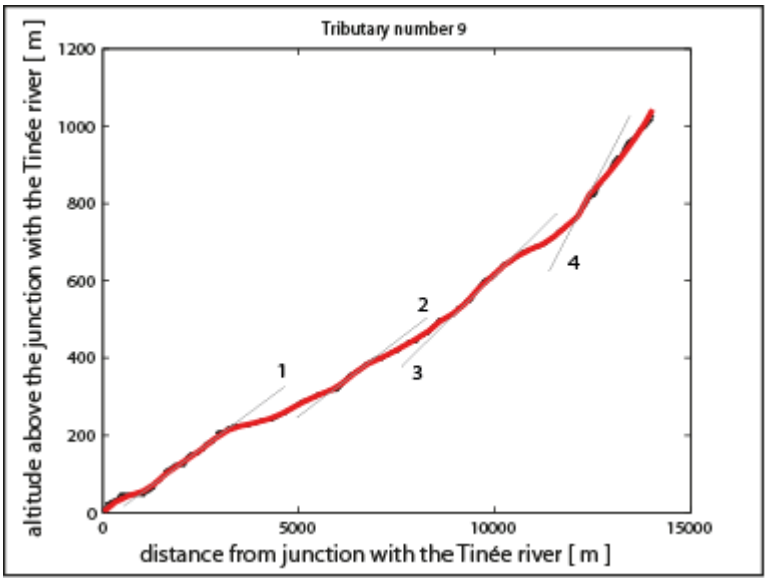


*Figure 28: topographic profile of tributary 2. The tangent segment with relative letter are the changingin slope that have probably been read by the program as the incision peaks.*

| | Gobal min mean [ mm/yr ] | Min mean 1st part [ mm/yr ] | Min mean 2nd part [ mm/yr ] | Min mean 1st – 2nd [ mm/yr ] |
|---|---|---|---|---|
| **Tributary 9** | 5,2 | 3,6 | 6,3 | 2,8 |
| | **Global int. mean [ mm/yr ]** | **Int. Mean 1st part [ mm/yr ]** | **Int. mean 2nd part [ mm/yr ]** | **Int. mean 1st – 2nd [ mm/yr ]** |
| **Tributary 9** | 6,4 | 6,2 | 7,4 | 1,2 |

*Table 10: integral mean and incision-rate mean calculated over the minima of the profile for the whole profile, for the inteval: 140 – 60 kyr B.P (1st part), 60 – 0 kyr B.P. (2nd part). In the last column are reported the difference between the incision rates of the two intervals.*

A punctual mean effectuated on the three river incision-rate profiles, results to be in good synchronization with the Epica curve. It shows a general increase in erosion at the beginning of the MIS5a interstadial. It is interesting to see also, how in the punctual-mean profile the incision peak linked to the MIS5a warming up period, starts around 82 kyr B.P., but reaches his maximum around 71 kyr B.P. (beginning of stadial MIS4).

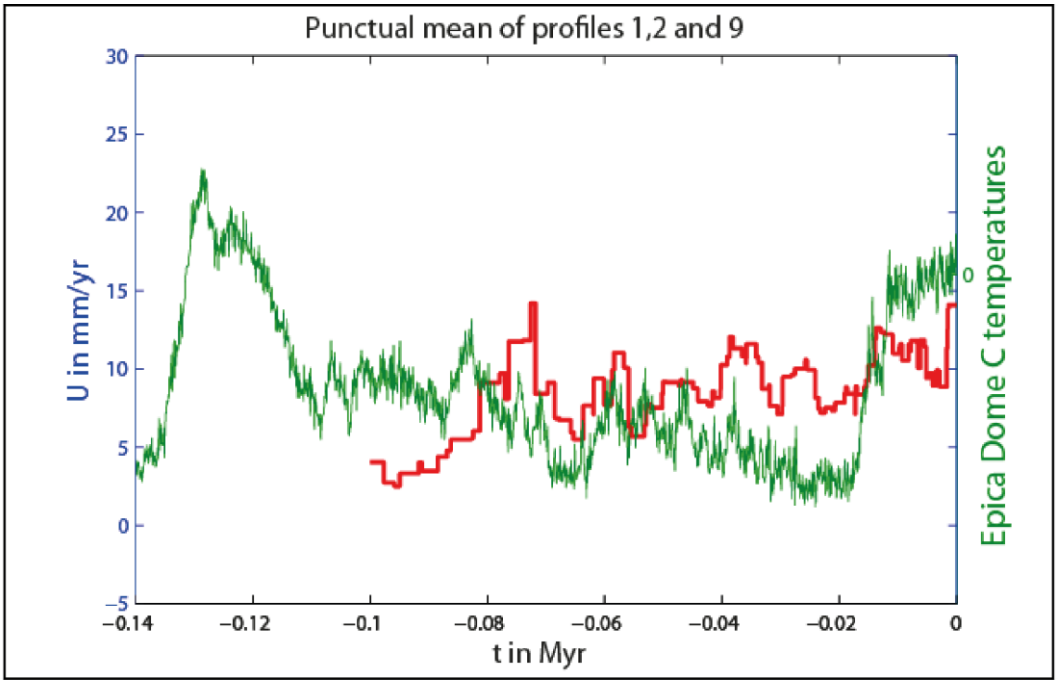


*Figure 29:punctual mean of incision rate of profile 1, 2 and 9 (red line), with the Epica curve (green line).*

III.1.2.2 Group 2, with tributaries 3, 4, 5.

The time – incision-rate profiles of these three rivers show, at the beginning of MIS1 (14000 yr B.P.), an incision maximum clearly above all the other incision peaks. Before this post MIS1 maximum, the profiles do not show large incision rate peaks, especially for Tributary 3 and 4. These three rivers are the three most downstream tributaries of the studied area.

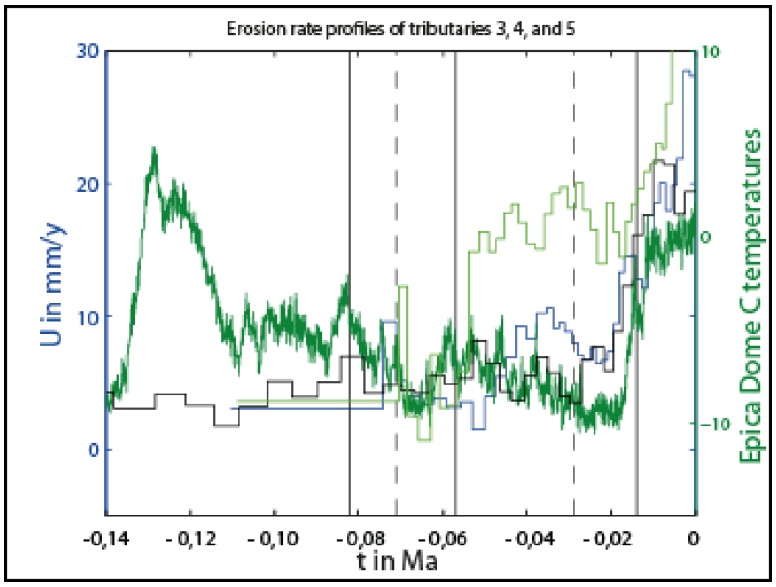


*Figure 30: comparison between the incision rate profiles of Tributary 3 (blue), Tributary 4 (black) and Tributary 5 (green). The green line is the Epica Dome Temperature record for the last 140000 yr. The vertical black continuous line represents the warm MIS (from right: MIS1, MIS3, MIS5a), the black dotted lines the cold MIS (from right: MIS2, MIS4).*

- Tributary 3:

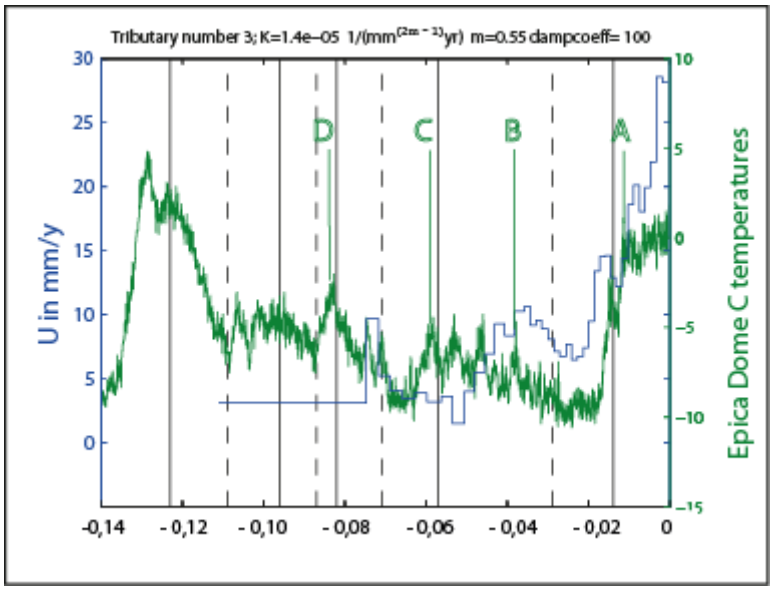


*Figure 31: incision-rate profile of Tributary 3 (blue line), with the Epica curve (green line).The vertical black continuous line represents the warm MIS (from right: MIS1, MIS3, MIS5a), the black dotted lines the cold MIS (from right: MIS2, MIS4).*

The incision-rate profile of Tributary 3 (Auron) shows a very well marked peak A, a local incision maximum in correspondence of peak B, and an incision peak placed in correspondence with a positive fluctuation of the Epica curve, just before the beginning of the MIS4; it could be considered as a right-shifted peak D, but a proper peak D is absent. The peak C is not presents. The calibration of this profile seems difficult: to have an erosion peak A correctly placed, it is necessary to invoke quite old ages (c.a. 80 kyr) while the profile is short (*Table 3*). This would be in agreement with a displacement of the knick point at a much slower rate than in other tributaries of group 1, which seems unlikely. I also had to deal with the incision rate absolute value, that, to respect the position of peak A, has been forced to elevated values because quite elevated values of K ($14 \cdot 10^{-6}$) were used. The possible acceptable alternative, would have anyway needed parameters K and m out of the range from the literature (Saillard et al, 2014) and the analysis

would suggest for this area, or would have generated peak ages too elevated for a profile of neither 7 km. The incision is anyway concentrated in the last 50000 years (*Table 11* for values).

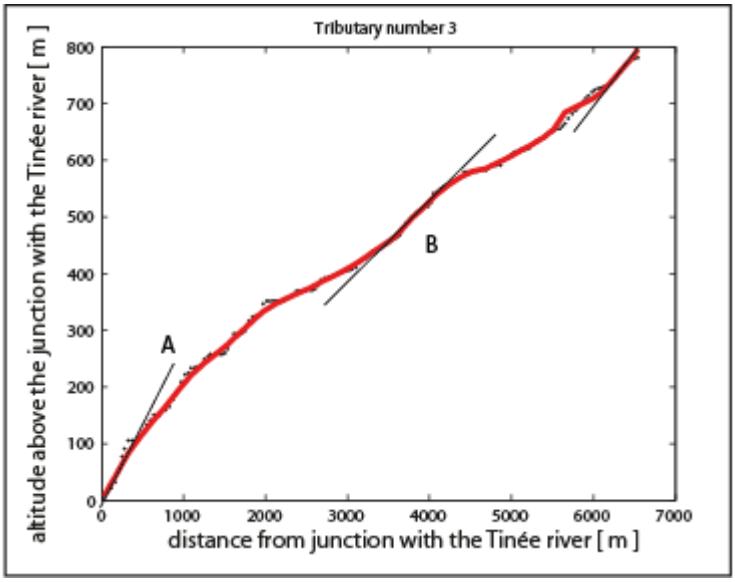


*Figure 32: along the topographic profile of Tributary 3 is possible to see the changes in slope that the code read as erosion peak A, B and, up on the right, the slope increase probably linked to the peak placed at 72 kyr B.P.*

| | Gobal min mean [ mm/yr ] | Min mean 1st part [ mm/yr ] | Min mean 2nd part [ mm/yr ] | Min mean 1st – 2nd [ mm/yr ] |
|---|---|---|---|---|
| **Tributary 3** | 5,9 | 2,5 | 9,1 | 6,7 |
| | **Global int. mean [ mm/yr ]** | **Int. Mean 1st part [ mm/yr ]** | **Int. mean 2nd part [ mm/yr ]** | **Int. mean 1st – 2nd [ mm/yr ]** |
| **Tributary 3** | 6,4 | 4,1 | 8,8 | 4,7 |

*Table 11:integral mean and incision-rate mean calculated over the minima of the profile for the whole profile and for the interval: 80 – 50 kyr B.P (1st part), 50 – 0 kyr B.P. (2nd part). In the last column are reported the difference between the incision rates of the two intervals.*

- Tributary 4:

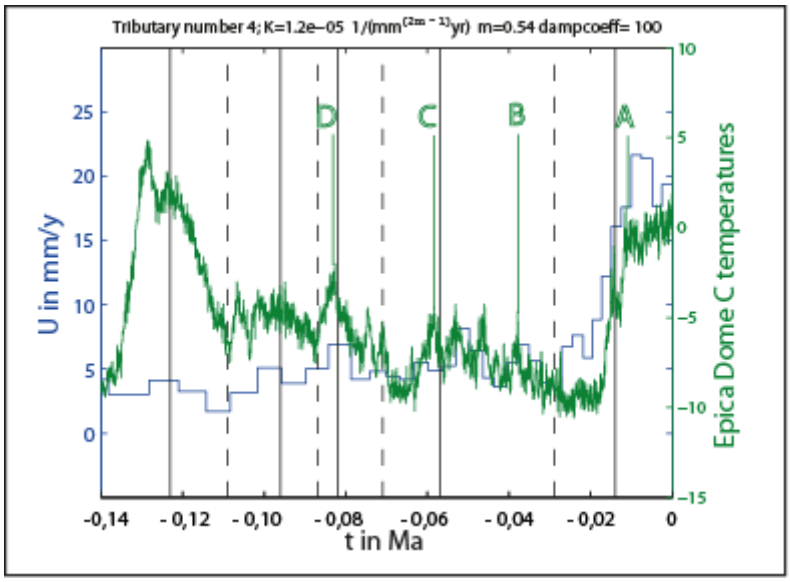


*Figure 33: incision-rate profile of Tributary 4 (blue line), with the Epica curve (green line).The vertical black continuous line represents the warm MIS (from right: MIS1, MIS3, MIS5a), the black dotted lines the cold MIS (from right: MIS2, MIS4).*

In the incision-rate profile of Tributary 4 (Roya), the difference in intensity between the incision-rate of peak A and the precedent peaks, is really marked (*Figure 33*, *Table 12* for values). The profile follows quite well the Epica fluctuations. The peak B and D are present, while peak C is absent or anyway the incision-rate profile registers an augmentation a bit later, in correspondence of the following Epica peak, around 55 kyr B.P.. Due to the low amplitude of the incision-rate peaks, is a quite hard task to spot into the topographic profile their originating slopes. In the model calibration then I focused on the peak A position. Having Tributary 4 the oldest incision-rate profile, but being only few kilometres longer than profile 1, it is reasonable to suppose his knick points to move slower. For this reason, knick points probably linked to the same incision events, appear to be closer to the junction with the Tinée river.

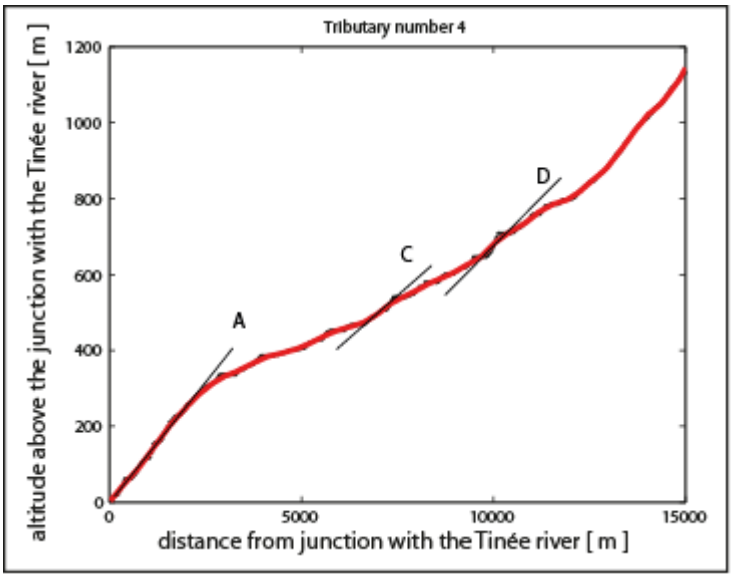


*Figure 34: topographic profile of tributary 4. The tangent segment with relative letter are the changing in slope that have probably been read by the program as the incision peaks.*

| | Min mean 1st part [ mm/yr ] | Int. mean 1st part [ mm/yr ] |
|---|---|---|
| **Tributary 4** | 3,7 | 4,2 |

*Table 12: integral incision rate mean, and incision rate mean calculated over the profile minima in the interval 140 – 14 kyr B.P.*

- Tributary 5:

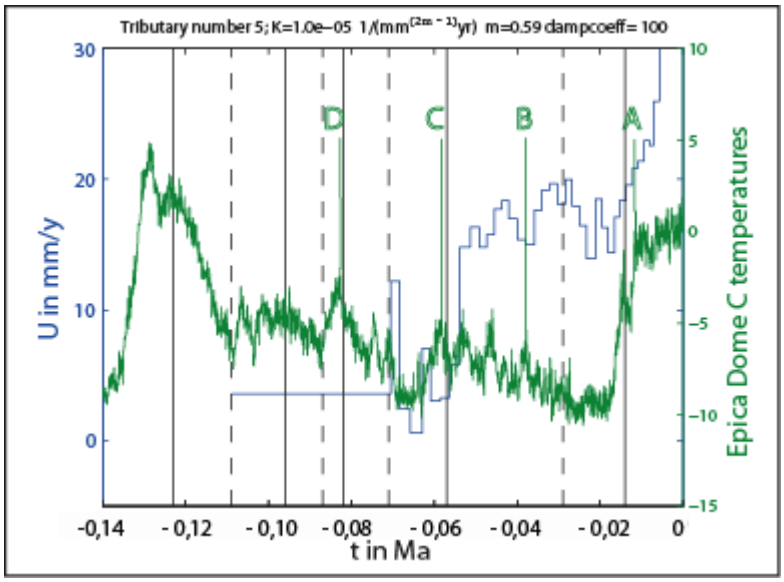


*Figure 35: incision-rate profile of Tributary 5 (blue line), with the Epica curve (green line).The vertical black continuous line represents the warm MIS (from right: MIS1, MIS3, MIS5a), the black dotted lines the cold MIS (from right: MIS2, MIS4).*

Tributary 5 (Douans) incision-rate profile, shows a very high incision rate value as compared to other rivers. This fact is the consequence of the calibration of m and k. The profile, with lower values of m, results into too "old" ages with respect to the length of the river (5300 m). With more elevated values of k, the incision-rate would have also been higher. The peak A is presents, although with an exaggerated value. A very elevated erosion mean characterised the incision-rate profile between 55 and 19 kyr B.P (*Table 13* for values), with fluctuations following, a bit late, the Epica curve. This period of elevated incision rate is well evident in the topographic profile, where a homogeneous and steep slope goes from around1200 m of elevation above the Tinée River bed, to almost 400 m. An older peak is present around 70 kyr B.P, just after the beginning of stadial MIS4. This peak and another of lower intensity are marked in the topographic profile.

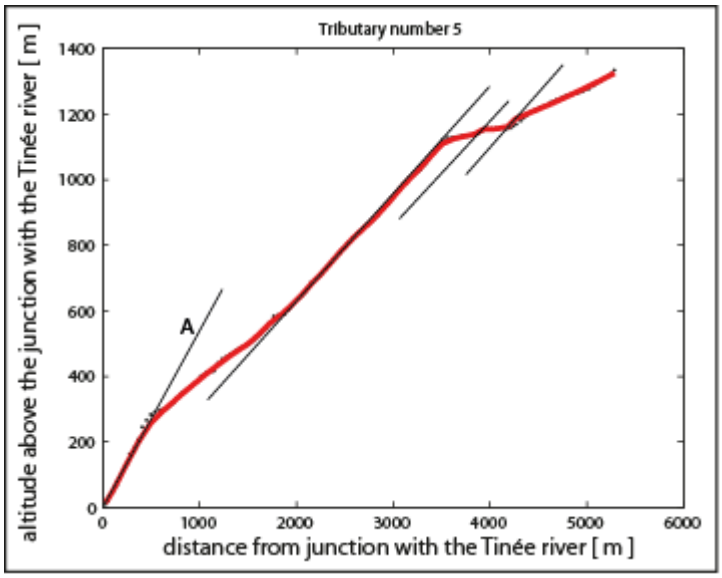


*Figure 36: topographic profile of Tributary 5. After the peak A, there are the tangent segment of the slopes linked to the high incision rate of the interval 55 – 20 yr B.P., and to the following 2 peaks.*

| | Gobal min mean [ mm/yr ] | Min mean 1st part [ mm/yr ] | Min mean 2nd part [ mm/yr ] | Min mean 1st – 2nd [ mm/yr ] |
|---|---|---|---|---|
| **Tributary 5** | 11,4 | 2,0 | 16,0 | 14,0 |
| | **Global int. mean [ mm/yr ]** | **Int. Mean 1st part [ mm/yr ]** | **Int. mean 2nd part [ mm/yr ]** | **Int. mean 1st – 2nd [ mm/yr ]** |
| **Tributary 5** | 13,0 | 6,1 | 17,5 | 11,4 |

*Table 13:integral mean and incision-rate mean calculated over the minima of the profile for the whole profile, for the interval: 80 – 55 kyr B.P (1st part),55 – 14 kyr B.P. (2nd part). In the last column are reported the difference between the incision rates of the two intervals. The global mean has been calculated considering the whole profile, also the peak A. Is than probably over estimated. For the global mean calculated without peak A see Table II. Is important to note that the minima-mean incision rate loose significance in the second part, where the minima are secondary fluctuation along a maximum of higher order.*

The punctual mean effectuated on the three river incision-rate profiles, results to be in correspondence with the Epica curve only for what concerns the post MIS 1 incision peak. It shows a general increase in erosion around 55kyr B.P.

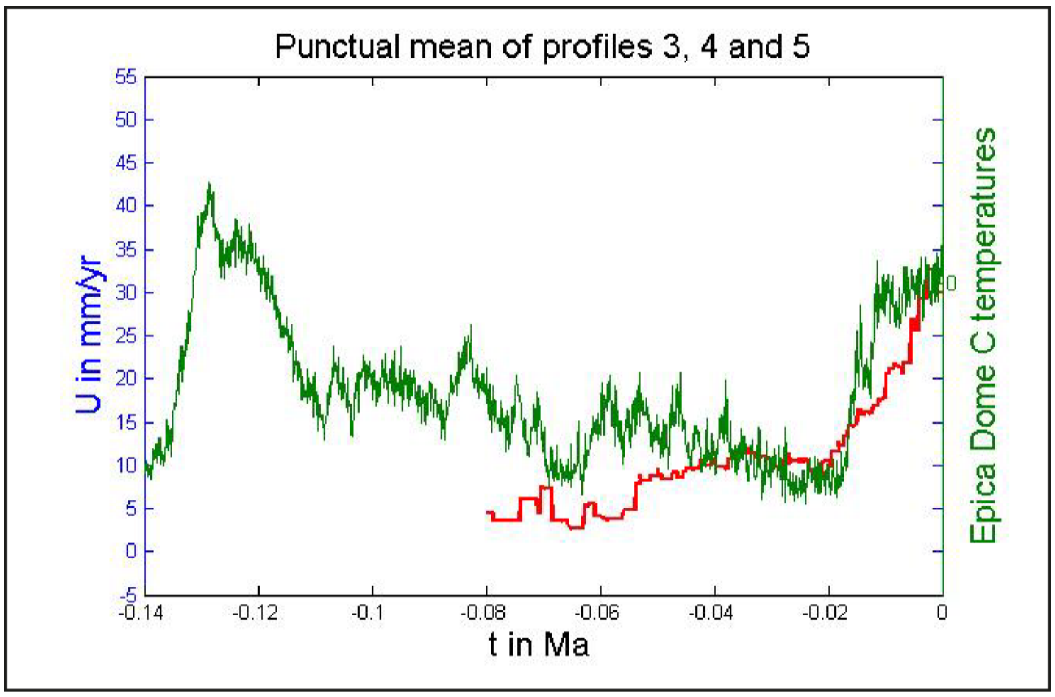


*Illustration 37:incision rate profiles of Tributary 3 (blue), Tributary 4 (black) and Tributary 5 (red thin line). The red thick line report the punctual mean calculated over the three profiles.*

III.1.2.3 Group 3, with tributaries 6, 7 and 8.

These three rivers flow next to one another on the left side of the Tinée (*Figure 20*). With Tributary 5 they represent the shortest and also the steepest rivers studied in the High Tinée catchment area. In the three rivers it is possible to identify the peaks A, B and C, but not the Peak D. In all of them it is also possible to note a sharp decrease in the incision rates after the incision-rate-peak A. It is important to underline that the steepness of these three rivers is around 25%, which is very high as compared to average, and may accelerate the upward migration of the knick points and result in the lost of information regarding oldest incision history (not older than 70 kyr). The tributaries of this group show similar k ($11 \cdot 10^{-6}$ [$mm^{1-2m} yr^{-1}$]) and m (0,56) values.

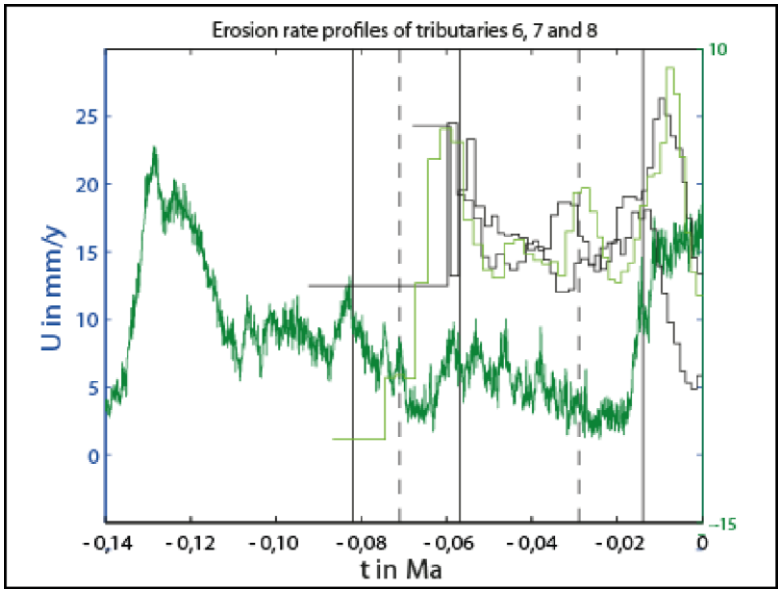


*Figure 38:comparison between incision rate profiles of Tributary 6 (black), Tributary 7 (blue) and Tributary 8 (green). The green line is the Epica Dome Temperature record for the last 140000 yr. The vertical black continuous line represents the warm MIS (from right: MIS1, MIS3, MIS5a), the black dotted lines the cold MIS (from right: MIS2, MIS4).*

- Tributary 6

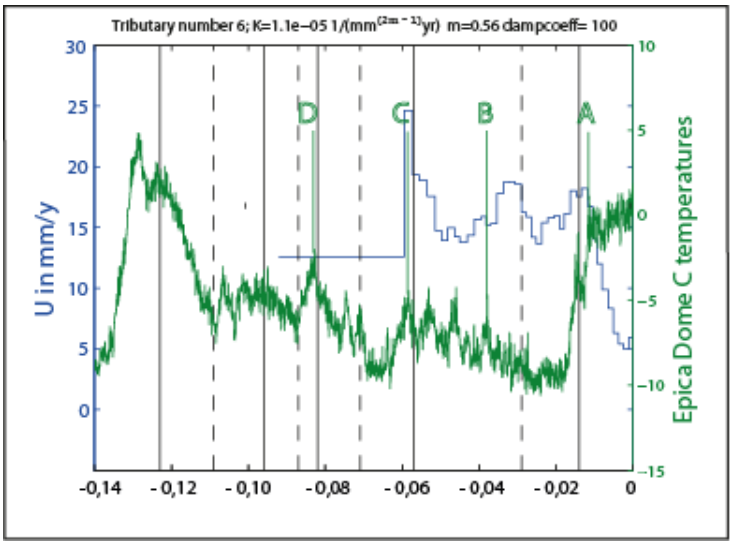


*Figure 39: incision-rate profile of Tributary 6 (blue line), with the Epica curve (green line).The vertical black continuous line represents the warm MIS (from right: MIS1, MIS3, MIS5a), the black dotted lines the cold MIS (from right: MIS2, MIS4).*

Tributary 6 (Asueros) is the shortest studied river and present an incision-rate profile of only 60000 yr. It presents the three peaks A, B and C (*Table 7*), and a sharp decrease in erosion rate after the MIS1. His mean erosion is particularly elevated between 60 and 14 kyr B.P (*Table 6* for values).

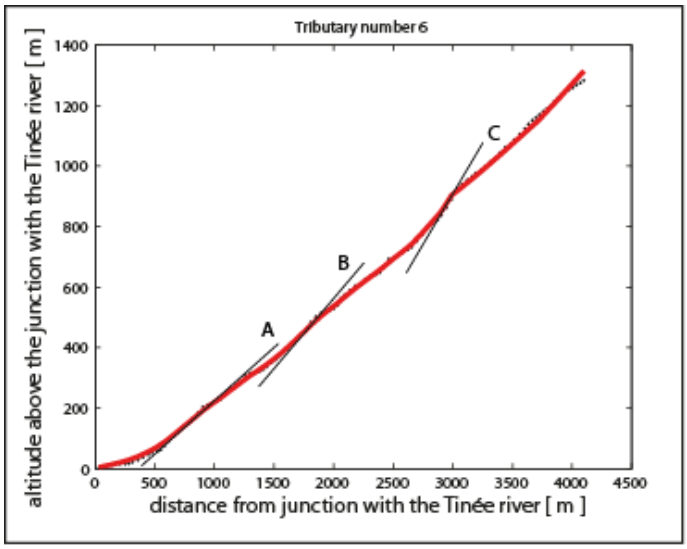


*Figure 40: topographic profile of tributary 6. The tangent segment with relative letter are the changing in slope that have probably been read by the program as the incision peaks.*

- Tributary7:

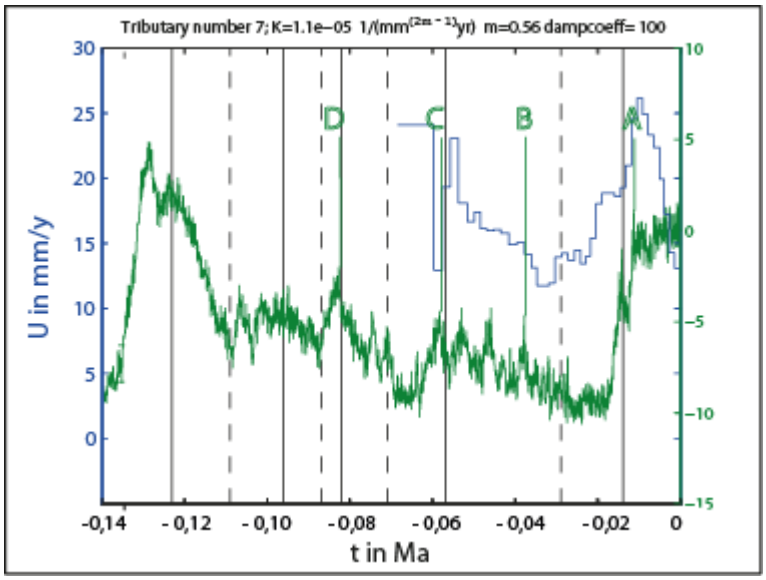


*Figure 41: incision-rate profile of Tributary 6 (blue line), with the Epica curve (green line).The vertical black continuous line represents the warm MIS (from right: MIS1, MIS3, MIS5a), the black dotted lines the cold MIS (from right: MIS2, MIS4).*

Tributary 7 (Rabuons), presents a quite short incision-rate profile (*Figure 22*) with well developed peaks A and C. Peak B is absent. At the beginning of MIS2 there is the incision-rate absolute minimum. In the topographic profile (*Figure 23*) it is possible to see the gradual change in slope that has been interpreted as the change in the incision rate that has brought from the MIS2 minimum to peak C (change in inclination from tangent segment preceding "segment C" and this one). The segment tangent to the topographic profile, further on the right, is probably associated to the oldest peak of *Figure 22*, that is with good probability linked to local factors. Also for this river the average incision-rate is quite elevated (*Table 4*).

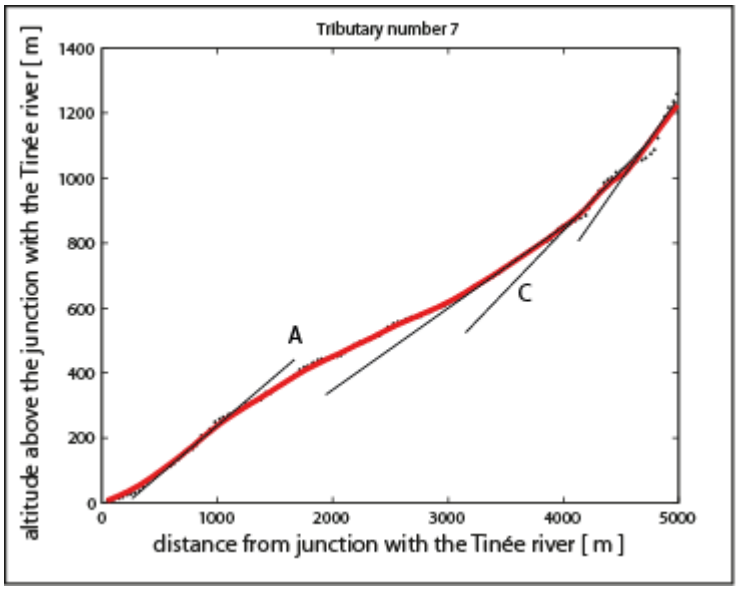


*Figure 42:topographic profile of tributary 7. The tangent segment with relative letter are the changing in slope that have probably been read by the program as the incision peaks.*

- Tributary 8:

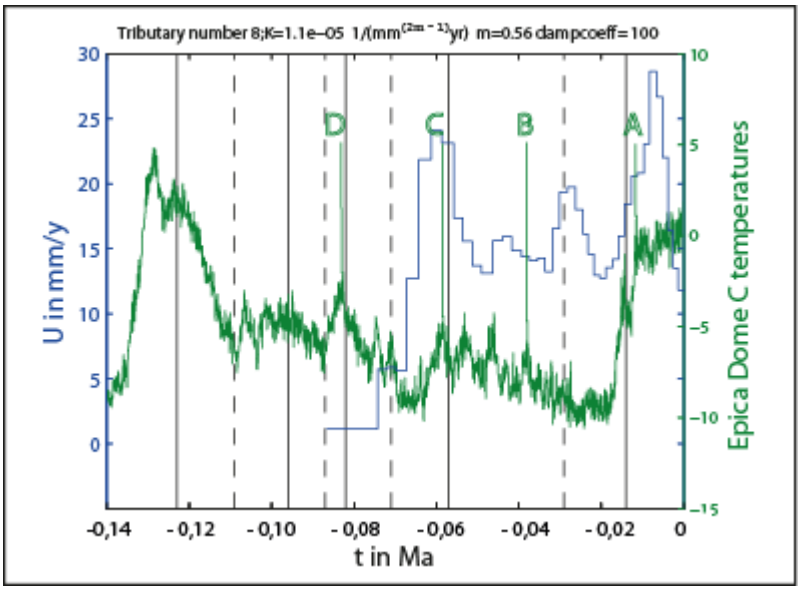


*Figure 43: incision-rate profile of Tributary 8 (blue line), with the Epica curve (green line). The vertical black continuous line represents the warm MIS (from right: MIS1, MIS3, MIS5a), the black dotted lines the cold MIS (from right: MIS2, MIS4).*

Tributary 8 (Ténibres), has an incision-rate profile quite well synchronised with the Epica curve, with only one peak that doesn't correspond to a positive temperature inflection. This peak is attributed to the first part of the MIS2. The incision peak corresponding to Epica Peak A is slightly shifted toward younger ages as compared to MIS1, while peak B and C are well marked. Also in this profile, in the last 10000 yr, there is a drop in the incision-rate.

The erosion mean that has been calculated starting from 70 kyr B.P. is very high along the whole profile (*Table 6* for values), which also reflects the very steep slope of this river.

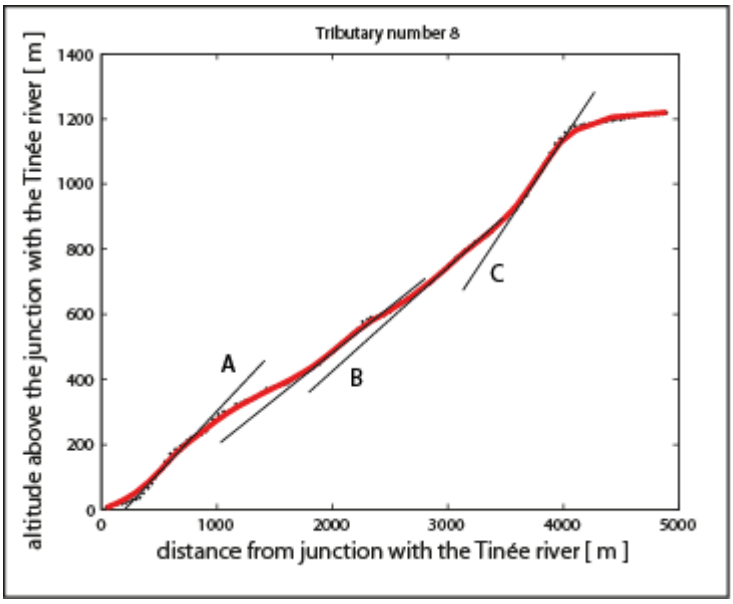


*Figure 44: topographic profile of tributary 7. The tangent segment with relative letter are the changing in slope that have probably been read by the program as the incision peaks.*

The punctual mean of the three river incision-rate profiles, results to have a general trend that follows, with good approximation, the Epica curve. In *Figure 26* is possible to see clearly peak A and peak C. Between the two peaks, anyway, the mean of the three profiles recalls the temperature fluctuations, with peaks slightly shifted toward lower ages.

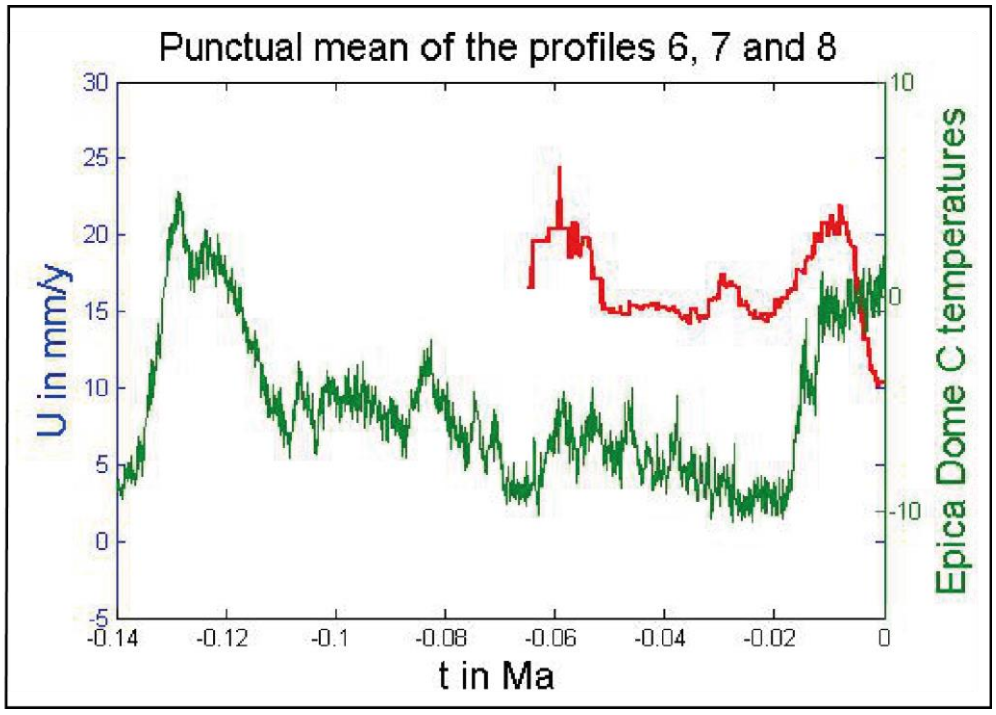


*Figure 45:punctual mean of incision rate of profile 6, 7 and 8 (red line), with the Epica curve (green line).*

*III.1.3 Discussion of modelling results:*

III.13.1 Geomorphological peculiarities of analysed rivers

In order to correctly interpret the incision rate profiles obtained through the numerical modelling, it is important to underline some geomorphological peculiarities characterising the studied rivers.

Tributary 2: A particularity of the Ardon (Tributary 2) Valley, is its lack in hanging glaciers geomorphological evidences. The valley has been cut entirely on a limestone-marls substrate, and shows a pronounced V shape while the neighbouring ones, underneath their delimiting ridges, conserve well preserved glacial cirque. The substrate entirely in marls and limestone could explain partly the elevated values of K (*Table 5*), and the younger ages (10 kyr) reached by the incision rate profile. The absence of glacial cirque may have led to a lower sensibility of this valley to the glacial retreat i.e. to temperature changing, while the profile show a good correlation in time with the Epica curve.

Tributary 3 and 4 display, as seen above (*Figure 33 and 35*), an increased incision in the post LGM period. This fact may be linked to the glacier that those valleys hosted probably until the beginning of MIS1 (Darnault et al. 2012, Darnault et al. submitted). The glaciers hidden from south by elevated mountain ridges, concentrate their melting after the LGM. This fact could have led to a late discharge in water and sediment that engraved deeply and rapidly the river gorges as shown in the profiles.

Tributary 5 has a very steep final reach, that is reflected in the modelling by a very fast change in the incision rate, which becomes very high due to a drop of the Tinée level. The field investigations associated to satellite images studied through Google Earth have revealed that the local steepness is due to a quite anomalous structure very inclined with several outcrops of gneiss. Some of these outcrops

show polished surfaces probably linked to glacial activity (*Photo 3, A – B*). This steep part of the valley east side, may be a local accentuated expression of a slope which extends at the scale of the mountain slope itself, showing, upstream in the valley and at more elevated altitude, glacier polished surfaces dated at 11 kyr (Darnault, 2012). Looking at a topographic profile perpendicular to the Tinée valley it is possible to see a change in slope steepness in both sides of the valley (Photo 2 – B). This changing is located at 1200m on the west side, and at 1250m on the east side (the Tributary 5 flowing side, *Figure 47*).

*Figure 46: Duans river (Tributary 5) cutting through the steep slope above the junction with the Tinée. (photo by Cassol D.)*

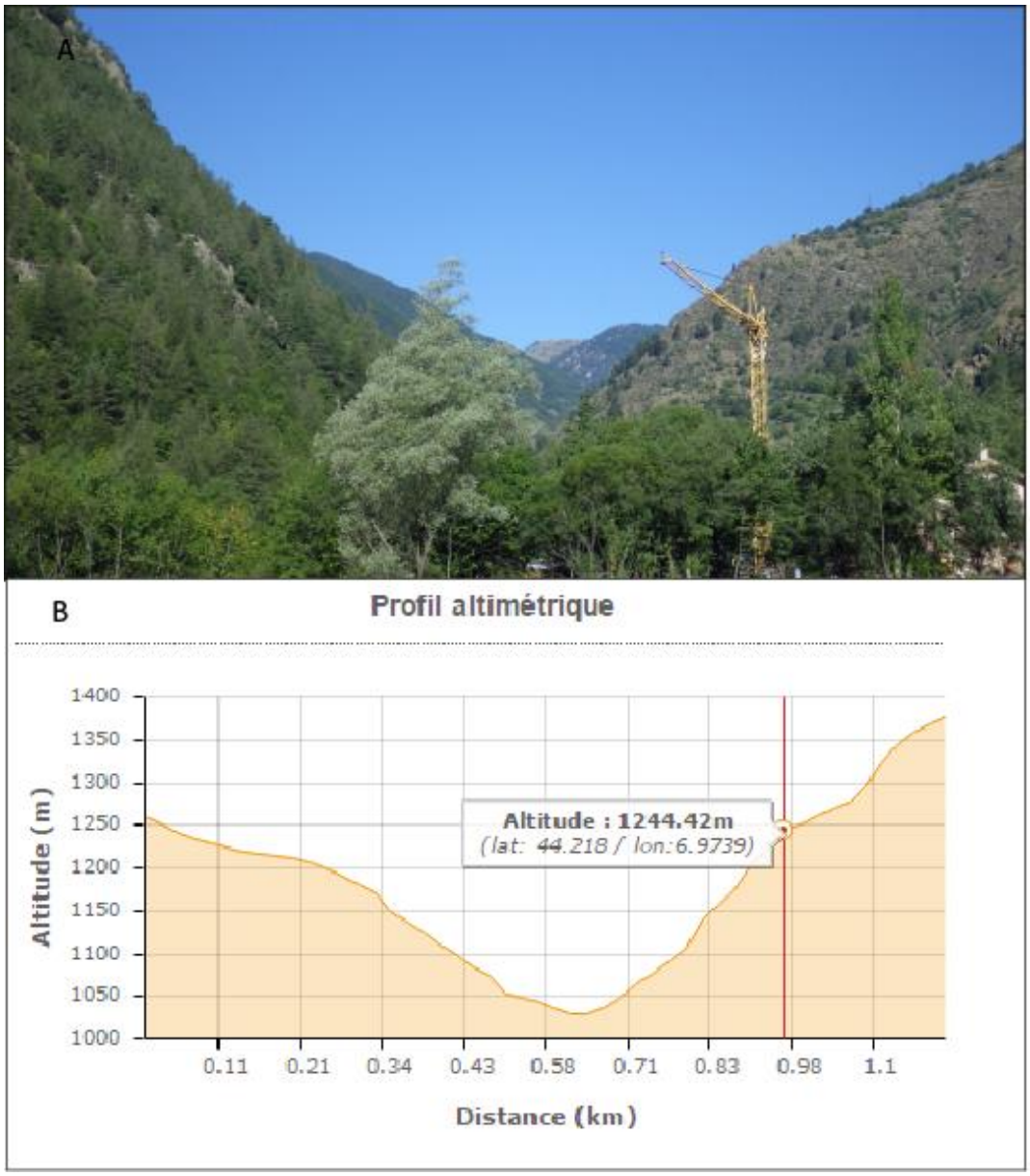


*Figure 47: A) The change in the mountainside inclination on the orographic left of Tinée river. Photo taken from south to north*

*B) Elevation profile with, in the data tip, GPS coordinates and altitude of the slope changing. (profile created with Géoportail; [http://www.geoportail.gouv.fr/](http://www.geoportail.gouv.fr/)). (Photo by Cassol D.)*

Some dating of glacier polished surfaces effectuated upstream in the Tinée valley (Darnault et al. 2012), report three stages of deglaciation after the LGM. A first one around 15 kyr B.P. , a second one around 11kyr B.P. and a third one around 8,5 kyr B.P.. These data could justify the hypothesis of a glacial tongue arriving until the Douans level during the LGM. The steep slopes of *Figure 46* could thus have a glacial origin. During field work I observed a polished surface, which it is preserved on the steep slope just downstream of the Douans valley, while others, better preserved, have been found above the village of Saint Etienne de Tinée, along the Ténibres valley (*Figure 48 and 49*). It is important to note that the steep face cut by Tributary 5, has been affected, and still partially is, by gravitational processes. This unstable situation may be the effect of a post glacial distension, as modelled and dated by Sanchez (2010) and Darnault (2012) at ages between 7 and 2 kyr, which doesn't help to find intact polished surfaces.


*Figure 48:A – B: polished surface in the left side of the Tinée. [ GPS coordinates : N 44°12'55.7'' ; E 6°58'22.8'' Altitude 1107 m a.s.l]. Polished surface orientation parallel to the Tinée valley axis, N/NW – S/SE. Little-notebook and pen for scale.*

*C – D: polished surface above Saint Etienne de Tinée village. [ GPS coordinates : N 44°15'21.5" ; E 6°55'55.1" Altitude 1256 m a.s.l.]. Polished surface orientation parallel to the Tinée valley axis, N/NW – S/SE. Little-notebook and pen for scale.*

*Figure 49:polished surface above Saint Etienne de Tinée village. [ GPS coordinates : N 44°16'18.8" ; E 6°56'26.6" Altitude 1620 m a.s.l.]. Striations orientation N/NE – S/SW. GPS and pen for scale.*

Tributaries 6, 7 and 8 show instead the opposite trend of the incision rate profile: after the MIS1 their incision rates drop down to about a half of previous intensity (*Figure 39, 41, 43*). This sharp change is ascribed to the development of alluvial fans that each of the three tributaries develop out-coming from the gorges. These three rivers are the most steep of those here studied, have the highest mean incision rate, and flow through really narrow valleys that keep the flow energy elevated and doesn't create the conditions for sediment deposition. The energy dispersion caused from the sudden opening of the valley at the junction with the Tinée, induces the stop of the incision and sedimentation processes. This phenomenon is not present in Tributary 5, although it presents the same characteristics, because it runs into the Tinée valley where this one gets narrower. There, due to the flow energy increase, the formation of an alluvial fan is not possible (*Figure 50A-B*).

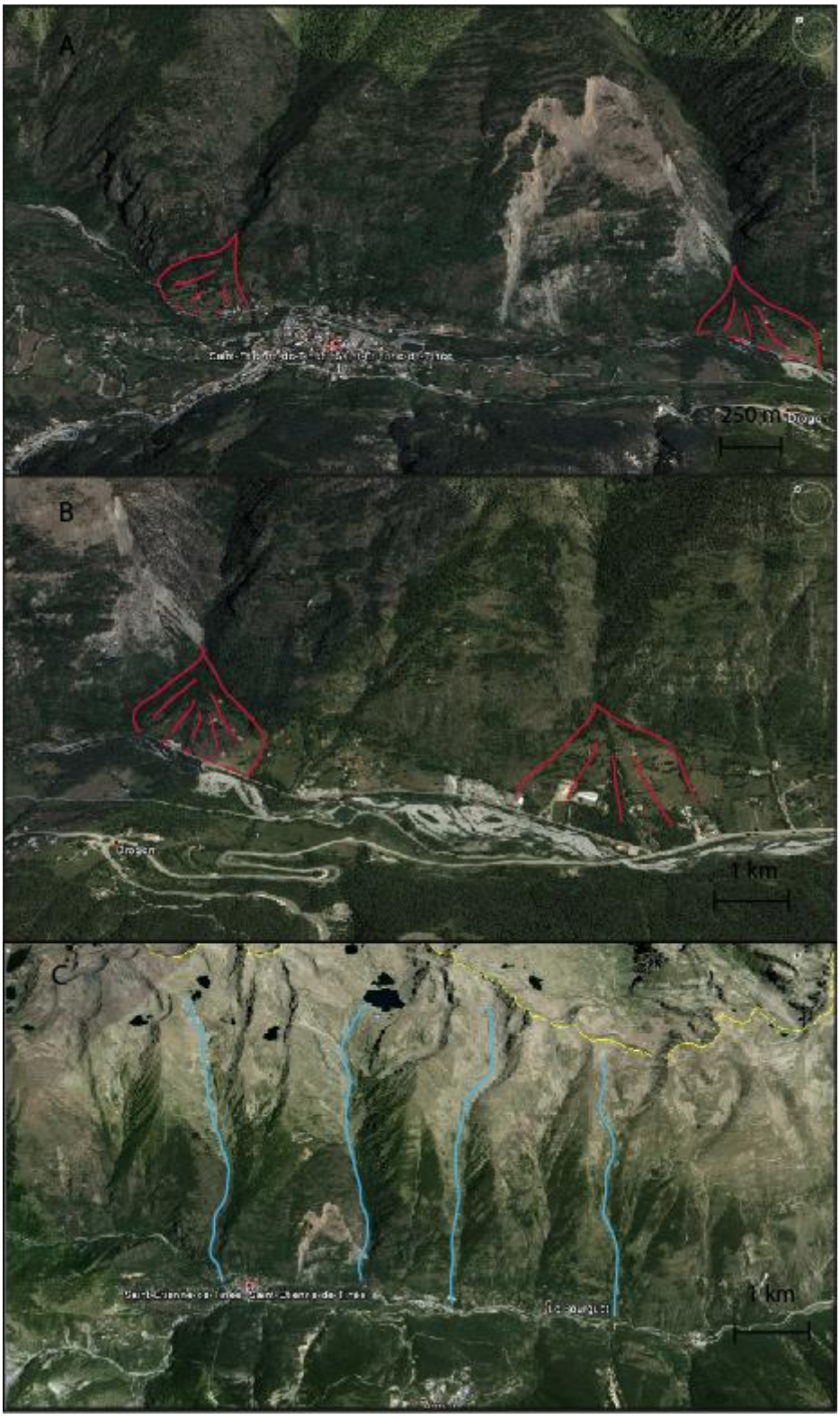


*Figure 50: A)Google earth image of the Tènibres alluvial fan (Tributary 8, left) and of Rabuons alluvial fan (Tributary 7, right). In the photo it is evident the*

*landslide "La Clapiéres", that adds ulterior sediments. B) Google earth image of Rabuons alluvial fan (Tributary 7, left) and of Asueros alluvial fan (Tributary 6, right). C) Google earth image of, from left to right: Tènibres, Rabuons, Asueros and Duans (Tributary 8, 7, 6, 5).*

In alluvial fan formation conditions, there is not incision, while our model estimates an incision rate anyway above 5 mm/yr. The Goren-Willet-Fox code has been conceived for the modelling of bed rock channel and doesn't consider depositional processes and soft sediment conditions. Furthermore the alluvial fans of Tributary 6, 7 and 8, full-fill the gap between the Tinée base level and the altitude at which the rock channels really arrive into the main valley. The alluvial fan, then, not only hide the real signal linked to the base level variations, but also, giving a slope to the bed river, induces the code to attribute a positive incision rate in a depositional area.

### III.1.3.2 Climatic significance of river profiles

The estimated average-profiles, show, for each of the three groups, a relatively good correspondence between incision rates and the change in temperatures. This fact suggests that the shaping of longitudinal river profiles, at least for the studied area, is deeply influenced by climatic factors. Another evidence that leads to consider the climatic signal as the first information brought by studied profiles, is the high value of obtained incision rates. Even without taking into account the Tributaries 3, 5, 6, 7 and 8, that show the most elevated erosion mean of the area, we have a general average of incision rate of 6,7±2 mm/yr. The uplift rate in the area is considered to be around 0,8 mm/yr (Walpersdorf et al, , 2015), but could reach high values of several mm/yr (Serpelloni et al., 2013), that appears to be slightly lower than the estimated incision rates (still considering only Tributary 1, 2, 4, 9). However, the relationship between the regional rate and the river incision rate is not simple, and we do not expect to have similar rates. Further, it seems

logical that river incision is faster than the regional erosion rate, as it corresponds to a focussed erosion. This will be tested by the direct dating of the river polished surfaces which is presented in the second part of this work.

Further, the part of incision which could be attributed to tectonics and isostasy is thought to be reflected in the incision rate minima in the profiles, which may highlight the part of the signal that most probably was influenced by the long-term uplift. From our data, we see a widespread augmentation in the minima incision mean starting between 80 and 55 kyr B.P. and still lasting until today, which is globally not correlated to the climatic signal. An increase in the incision rate minima, based only on climatic factors, would see fluctuations of the same order of the Epica curve temperature variations. It is then possible suppose a link between this changing and the active uplift, which would be driven by tectonics.

## *III. 2 $^{10}$Be Terrestrial Cosmogenic Nuclides dating*

### *III.2.1 Sampling site and criteria*

To quantify Tinée incision rates, we have applied the TCN Be-10 dating method on 11 granite samples. The samples have been taken from a river polished surface situated in the gorges cut by the Tinée into the crystalline basement, 10 km downstream of the Isola settlement (*Figure 51-B*).
The sampled surface is sufficiently compact and vertical to ensure a river-incision origin of the surface thereby ensuring the correspondence between the exposure age and the incision history.
The sampling site has been chosen due to the other following advantages:

- The homogeneity of the lithology, this fact implies that possible changes in incision rates are linked to climatic or tectonic changing and not to variation in rock texture.

- The granite wall surface doesn't show any kind of rock fall.

- The polished surface is nicely preserved and can confidently be attributed to river incision, and span a range of elevation up to 30 m above the river.

- The valley's opposite side has a gentler slope, fact that augment the cliff exposition to cosmic rayon and reduce the shielding factor.

- The sampling site is situated downstream from the lowest glacial evidence present in the valley (Julian, 1980), therefore it should be out of the zone influenced by glacier erosion.

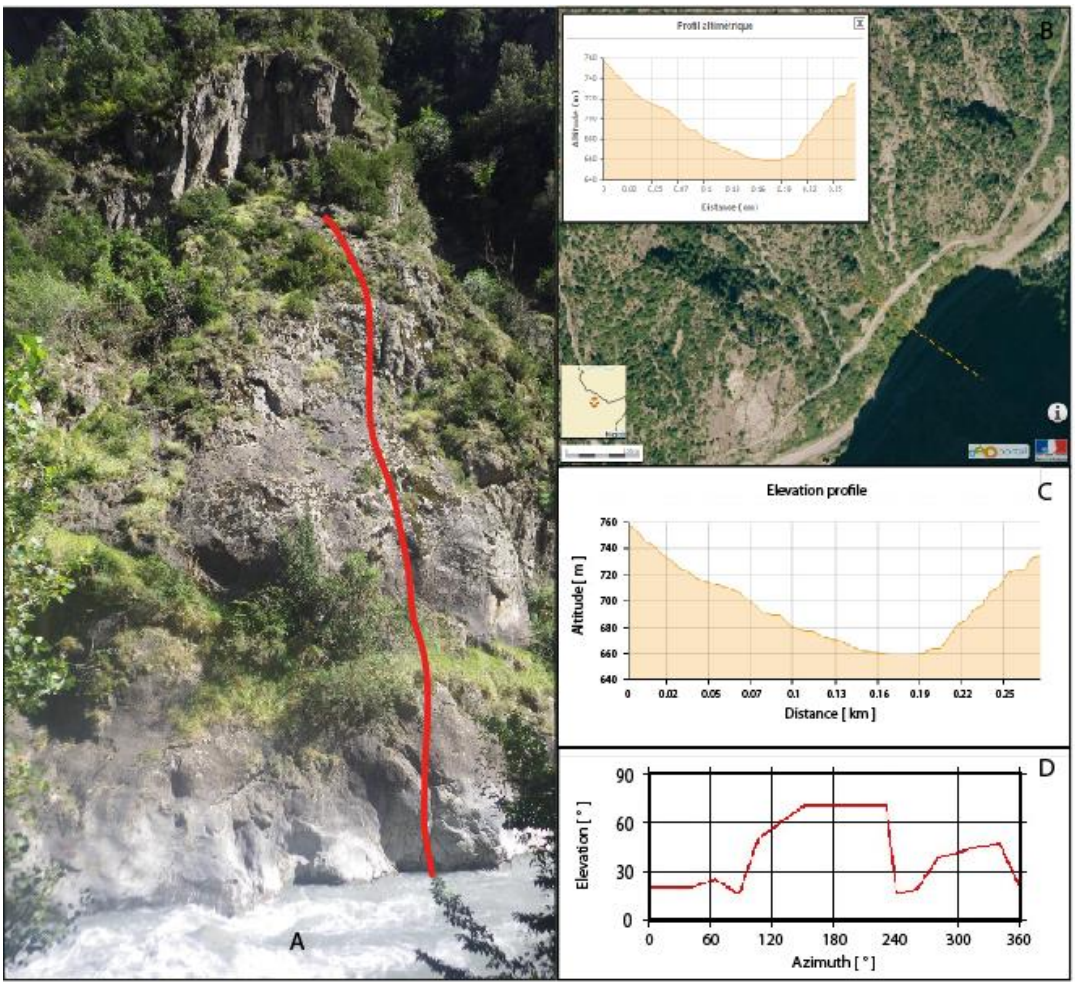


Figure 51: *A) The granite wall where the analysed samples have been collected. The red line indicates the approximate position of the sampled vertical profile.*

*B) Position inside the Tinée valley and elevation profile of the sampled site, perpendicular to the valley axis.*

*C) Elevation profile perpendicular to the valley axis.*

*D) Profile of shielding seen from the sampling site (with the sampling side on the back).Obtained with CRONUS – earth online calculators (http://hess.ess.washington.edu).*

*III.1.2 $^{10}$Be exposure ages presentation and description*

The study of the in-situ-produced cosmogenic nuclides concentration, has given a series of 11 exposure ages going from 18257 to 2332 yr B.P. The obtained ages decrease from Ti – 1 to Ti – 4 with an evidently too elevated age for sample Ti – 3. After the sample Ti – 4, the exposure ages of sample Ti – 5, Ti – 6 and Ti – 7, increase of 422 years despite a deepening inside the gorge of 9,9 m. The sample Ti – 6 shows the oldest exposure age of this group, 15463 yr BP. The increasing trend doesn't stop and samples Ti – 8 and 9 result to have exposure ages above 16 kyr. Starting from Ti – 9 the exposure ages restart to decrease with the altitudes above the river bed (*Figure 52*).

| Samples [-] | Exposure ages [yr] | Altitude above river [m] | External uncertainty [yr] |
|---|---|---|---|
| Ti – 1 | 18257 | 38,5 | 2449 |
| Ti – 2 | 15278 | 35,3 | 1736 |
| Ti – 3 | 25798 | 32,6 | 3366 |
| Ti – 4 | 14934 | 28,7 | 2300 |
| Ti – 5 | 15390 | 26,1 | 1781 |
| Ti – 6 | 15463 | 21,8 | 1687 |
| Ti – 7 | 15356 | 18,8 | 1578 |
| Ti – 8 | 16256 | 15,6 | 1737 |
| Ti – 9 | 16872 | 12,9 | 2070 |
| Ti – 10 | 4501 | 9,5 | 1083 |
| Ti – 11 | 2332 | 0,0 | 468 |

| Samples [-] | %external error [-] | Internal uncertainty [yr] | % internal error [-] |
|---|---|---|---|
| Ti – 1 | 13,4 | 1860 | 10,2 |
| Ti – 2 | 11,4 | 1113 | 7,3 |
| Ti – 3 | 13,0 | 2498 | 9,7 |
| Ti – 4 | 15,4 | 1895 | 12,7 |
| Ti – 5 | 11,6 | 1171 | 7,6 |
| Ti – 6 | 10,9 | 1015 | 6,6 |
| Ti – 7 | 10,3 | 834 | 5,4 |
| Ti – 8 | 10,7 | 1003 | 6,2 |
| Ti – 9 | 12,3 | 1456 | 8,6 |
| Ti – 10 | 24,1 | 1010 | 22,4 |
| Ti – 11 | 20,1 | 421 | 18,1 |

*Table 14: Beryllium - 10 cosmogenic dating obtained applying a constant production rate model, with the Stone (2000 )scaling scheme for spallation and a shielding factor of 0,655.*

The external uncertainties associated to these ages are included in a range with extremes of 468yr and 3366yr. The internal uncertainties instead are comprised between 421 yr and 2498 yr. The percentage error linked to the external uncertainties, goes from a maximum of 24,1% to a minimum of 10,3% with a mean value of 13,9 % ; 5,4%, 22,4% and 10,4% are minimum, maximum and average of percentage errors linked to internal uncertainties (*Table 12*).

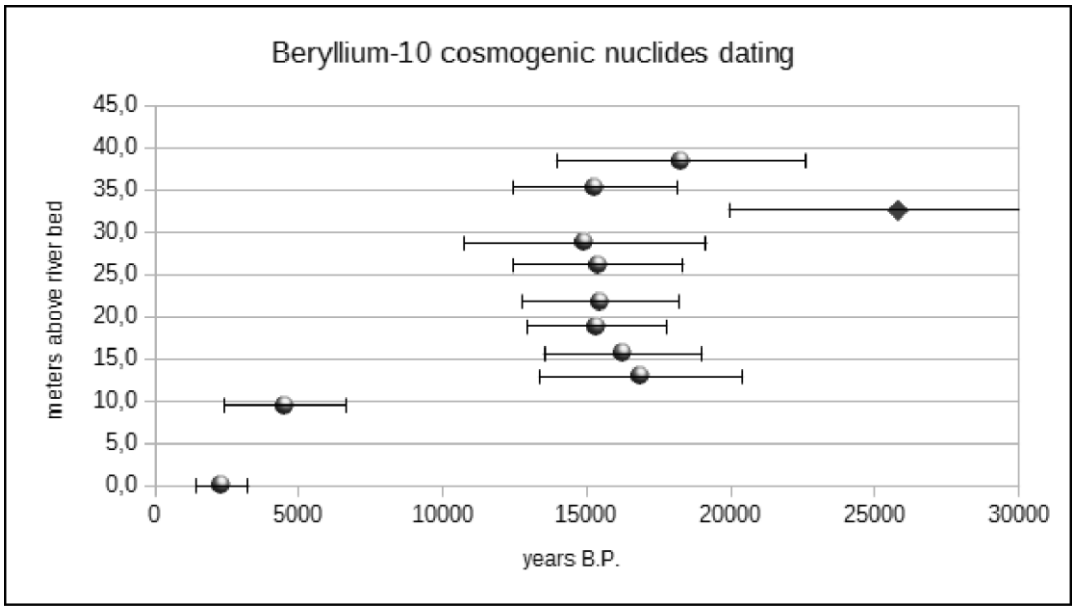


*Figure 52:altitude above the river bed and exposure ages of the eleven samples with associated error considered as the sum of internal and external uncertainties. Sample Ti – 3, marked by a blue has been considered as an outlier.*

| | Erosion rate (mm/yr) |
|---|---|
| **Interval 1 – 2** | 1,1 |
| **Interval 2 – 4** | 19,2 |
| **Interval [2;9];9 – 10** | 0,003 |
| **Interval 10 – 11** | 4,4 |

*Table 15:incision rate calculated for the relative intervals between samples. The intervals [2;9];9 – 10 means that the incision rate has been quantified using the mean exposure age, calculated over samples 2, 4, 5, 6, 7, 8, 9, and the altitude above the river of sample 9.*

As shown in Figure 29, we see that the age repartition is not linear and can be divided into 2 ages groups. We can consider the sample Ti – 3, as an outlier. The incision rate shows a relevant increase between 14 and 20 kyr B.P. that engrave the river bed of 22,4 m. After this high incision event low incisions can be inferred (< 1mm/yr) until the Subboreal period (5200 – 2600 yr B.P.), where, again, the incision rate increases. This new incision pulse starts with the Subboreal and between samples 10 and 11 has been calculated a difference of 2169 yr in 9,5 m, meaning a rate-incision-mean of 4,4 mm/yr.

The overall incision mean, averaged for the whole cliff, has been estimated to 2,4 mm/yr.

### *III.2.3 Discussion of $^{10}$Be TCN dating profile*

The incision rate obtained from the TCN Be – 10 analysis, underline the notable effect of the post LGM deglaciation on the Tinée gorges shaping. Based on surface exposure ages, quantified incision rates are up to 2 cm/yr for that period which extends down to 14 kyr (*Table 15*). After this high incision period, follows a sharp deceleration in the fluvial deepening that starts after 14 kyr B.P. and lasts until 4,5 kyr B.P. During this interval the massif underwent the glacier phase of the Younger Dryas, especially at 12-11 kyr (Darnault et al., 2012) (*Table 15*). The last 4500 yr are marked by a second increase in the incision rate, which coincides with the climatic optimum of the Holocene featured by increased rainfall at 4000 yr (Saillard et al., 2014). Consequently, we see that the river incision profile is not constant, and that pulses of erosion can be attributed to the major climate changes. The incision of 40 meters in only 20 kyr is however of the same order as the GPS rates obtained by Serpelloni et al.(2013), which suggests that, in the long term, the average incision rate could be of the same order as the subsidence-tectonic uplift.

# IV Discussion

## *IV.1 Numerical modelling results discussion*

Numerical modelling allows to test the role of one or several parameters in a given process. In this study I have worked modifying the values of K (erodibility factor) and m (concavity index when n = 1) hypothesising river with profiles in steady state conditions and with a linear ratio between slope and incision rate, i.e. n = 1. With such assumption I've been free to study the influence, above the incision-rate-profiles, of the only parameters K and m, and, aware of the limits that such approach involves, to study tectonic and climatic effects on fluvial incision rate.

The results obtained through the model are, for what concerns the incision rate absolute values (*Table 3*), too high compared to those derived from the direct $^{10}$Be dating method. Considering for example the actual incision-rate-mean estimate for the Tinée River, from the tributaries incision rate (*Figure 21*), and the incision rate estimated with the TCN methodology (*Table 15*), we obtained a 16 mm/yr incision rate in the numerical simulation and a 4,4 mm/yr incision rate from the TCN dating.

The adopted calibration methodology is based on the variation of m and k values (chapter 2). In order to obtain a signal showing "logical" ages with respect to climate fluctuations, we have decided to leave free the incision rate variation in terms of quantitative values. Another explanation for the systematic difference in the results could be found in the n value. For the reasons, explained in chapter II, and for an easier control of the model, the n value has been fixed to 1. This assumption allows to have a linear relation between incision rate and river slope. To assume n = 1 means, among the others consequences, to neglect thresholds effects (i.e. n > 1 in threshold-independent model) on the river slope. This assumption may be erroneous, especially for tributaries 1, 2, 4 and 9 and could generate the not consideration of the fact that an n > 1 would preserve only the erosion peak linked to concave down knick points (*Figure 13*; Perron and Royden,

2013). It would be interesting to conduct a study centred on the effect of the "n" parameter above the incision-rate-profiles of the High Tinée tributaries, to see if it could be the cause of the difference in incision rate estimates.

Another point that would deserve further investigations is the knick point migration rate. Under the same long term tectonic forcing field and with n = 1, the knick points should have all the same horizontal-upstream migration rate (Perron and Royden, 2013). In steep river, then, knick point should move faster than along less steep river, while in our modelling, the knick point, associated to the steeper river, have covered a lower distance (*Table 16*) than those associated to the less steep ones. One of the constraint that have been decided to use in calibrating the model for this study, has been the variation range accepted for "m" and "K" values. This fact has lowered the possibility of incision-rate-profile shortening (increasing of incision rate intensity) and/or extension (decreasing of incision rate intensity). In other words, to keep the correspondence between the Epica curve and the incision-rate-profiles through profiles younger or older than those obtained, I should have used values of K and m out of the prefixed range. However I've preferred to keep the prefixed working strategy, that moved from the idea that in a geographically, geologically and climatically homogeneous area, the erodibility factor should remain relatively constant. The m value has been kept around 0,5 because of the elevated scatter values. This decision could have led to an over estimation of the ages of the "short river" incision rate peaks, and then to an under estimation of their knick point moving rate. Indeed, looking at the topographic profiles of the studied rivers (*Figure 24, 26, 28, 32, 34, 36, 40, 42, 44*) it is possible to see how in T3, T5, T6, T7 and T8 the slope variations linked (probably) to Peak B and C are much closer to the Tinée junction than those of the long tributaries. However, in *Table 16* it is possible to see how the Peaks A are all placed at more or less at the same distance of 150 +/- 50 m from the Tinée with only exceptions of T6, T7, T8. These last tributaries are those forming an alluvial fan at the Tinée junction (*Figure 50*), structure that move upstream the break in slope. Probably the reason of the same "distance"-coordinate for all the Peaks A, is that a 14 kyr time span was not sufficient to highlight the differences between

the migration rates of knick point belonging to different tributaries.

| | Peak A (14kyr) [m] | Peak B (38kyr) [m] | Peak C (57kyr) [m] | Peak D (82kyr) [m] |
|---|---|---|---|---|
| T 1 | 100 | 6500 | 10000 | 11000 |
| T 2 | 200 | 6500 | 10000 | 11000 |
| T 3 | 100 | 4000 | | |
| T 4 | 100-200 | 6000 | 8000 | 10500 |
| T 5 | 100-500 | 2000-3500 | | |
| T 6 | 500-1000 | 2000 | 3000 | |
| T 7 | 1000 | | 3500 | |
| T 8 | 500-1000 | 2500-3500 | 3800-4000 | |
| T 9 | 50-300 | 6500 | 10000 | 11000 |

*Table 16: distance from the junction with the Tinée of the topographic profile slope-breaking for each one of the studied rivers respectively associated to one of the incision rate peaks.*

In the rivers steeper than 20% (*Table 3*) it is important to consider the possible occurrence of debris-flows (Sklar et al., 1998). However in Tinée tributaries we registered an over estimation of incision-rate-peaks widespread all over the rivers, suggesting other causes for this systematic error. Further the debris-flows are phenomena intimately linked to precipitation amount, thus at most they can affect the incision rate value, but certainly won't shift the incision peak away from the climate ones.

Despite the fact that the absolute values of incision are overestimated in the model, it is their relative variations that provide the most valuable information.

The first evidence is that in all the incision-rate-profiles is present a post – Oldest Dryas incision rate increasing, situation underlined also by the TCN dating results. This marked change in incision dynamics around 15kyr B.P. is in agreement with the results of Darnault et al. (2012), that defines a first phase of glacier retreat at, indeed, 15kyr B.P. This glacial retreat, with the consequent water and sediment discharge, could be the reason of the post LGM incision acceleration evidenced by our results. However, as it will be discussed later in this chapter, the obtained incision rates corresponding to this period indicate, maybe, a more long-lasting

process of glaciation of the Tinée valley than previously thought. In all the incision-rate-profiles, indeed, is present a belated increase in the incision rate. For instance, the Roya (Tributary 4) incision-rate-profile shows for almost all its length a limited incision rate, that abruptly increases around 15 kyr B.P.

Besides this main agreement between model and geochemical results, in the incision-rate-profiles obtained from the modelling of Tributaries 1 and 9 is present also the Holocene incision increase, clearly visible in the TCN profile. This incision peak is not visible in the other profiles, which is probably due to: the alluvial fan structure of Tributaries 6, 7 and 8; the over estimation of the incision rate value for what concerns Tributaries 3 and 5; the anthropic structures present in the lowest part of Tributary 2.

Beyond this more recent and temporally localized influence of climate on the incision rates in the High Tinée basin, the model results, show a relatively good agreement with Epica curve over the last 80000 yr. Calculating a punctual mean profile for each one of the three groups defined in chapter 4, we aimed to reduce the local factors showing out for each of the different areas of the High Tinée basin, the common incision fluctuations. In *Figures 29, 37, 45* this global relation between incision rate and climate is clearly shown. However, it is important to note that temperature variations do not necessarily reflect variations in rainfall rate. However, in a restricted area, along a glacial-interglacial period, a significant amount of river discharge is due to glaciers melting, fact that instead is directly depending on temperature. These profiles-punctual-mean lead to infer that the incision of the Tinée and its tributaries, is dominated by the climate influence. This climatic control above river behaviour is confirmed by the frequency of incision rate fluctuation, that is too elevated to be caused by changes in the tectonic behaviour. Changing in uplift rates would have led to variations in incision rates over a much longer time scale.

With the purpose of analysing the uplift signal present in the obtained incision-rate-profiles, I have tried to isolate the periods with lowest climatic influence. To do that I have calculated a mean over the incision rate minima. Considering indeed the active tectonics as a background noise, this one will be directly

detected only when the climatic activity becomes of second order. This kind of approach entails the risk of an under estimation of the tectonic uplift. It is indeed sufficient that the incision is concentrate only along the high discharge period, linked to the favourable climatic phases. These intensive erosive phases would allow to regain a steady state. However, along the not-climate-influenced periods, is convincing that the little accumulated incision is generated by tectonic or isostatic uplift.

Although also in this case the values obtained from the model are too elevated, they bring anyway interesting information. Among the incision-rate-means two groups appear to be distinguishable: (i) a first one with values above 10mm/yr and (ii) a second one with values around 5mm/yr.

(i) The rivers with the high incision rate means, are the Tinée east Tributaries, which are also the shortest and steepest ones. A possible explanation linked to tectonic reasons could be found in the strike-slip fault lying along the valley bottom (*Figure 7*). This interpretation seems however to be invalidated from the fact that also the highest stem of the Tinée (here called improperly Tributary 9) is located in the east side of the fault, but has a minima mean incision of 5,2 mm/yr. It is thus reasonable to think that the much more elevated incision rates of the east Tinée tributaries, is due to their steepness that cause a faster upstream migration of knick points. The incision means minima for these "shorts river" thus probably feature secondary fluctuations of the climatic effects on the incision rate, and probably do not give any information on the tectonic activity.

Among the Tinée tributaries belonging to the "low incision rate" group (T1,T2, T3, T4, T9), it is interesting to note how their "background" incision-noise is always around 5mm/yr (what is worth is not the value itself but its stability). This stability could indicate a common constraint, that may be individuated as a 'whole block uplift'. From the punctual-profile-mean of *Figure 29* and *37* it is also possible to note an increase in the incision rate around 80 and 55 kyr B.P. Of course this result is associated to many uncertainties, but still it would be interesting to lead further research on this question.

### *IV.2 10Be Terrestrial Cosmogenic Nuclides dating results discussion*

As seen above, the modelling results have been partly confirmed by the Terrestrial Cosmogenic Nuclides dating. The TCN profile obtained, shows two sharp increases in incision rates respectively at 15 and 4,5 kyr B.P.

The oldest one is the most evident in both the TCN and modelling results. This result matches well the main glacier retreat phase documented at 15 kyr in the valley (Darnault et al., 2012) as well as for the rest of the Alps (Ivy-Ochs, 2015). In Darnault et al. (2012) are reported the exposure ages of some polished surfaces placed at 2500m in the High Tinée valley. Dating 14.9 +/- 0.8 kyr, these data constrain the Oldest Dryas deglaciation at those altitudes. Our ages relative to the first incision-rate increase, are probably linked to the deglaciation period that followed the Oldest Dryas. However, for a better knowledge of the glacial retreat dynamic, would be interesting to date the polished surfaces found above the Tinée – Roya junction and at the level of the settlement of Saint Etienne de Tinée (*Figure 48 and 49*). The valley bottom at the Tinée – Roya junction level, has an elevation of 1020 m a.s.l., while the found polished surface (*Figure 48* – A) is located at 1107m a.s.l. If we assume a mean erosion rate of 2 mm/yr (chapter III) for the last 18 kyr, and a valley bottom 36 m higher than now, the thickness of the hypothetical glacier would be of about 50 m. The rapid deglaciation at the end of the Oldest Dryas stadial, of the glacial front, would be perfectly fit by the results obtained from the $^{10}$Be nuclides dating.

The end of this high incision period dates approximately at 14500 yr, and could be explained by the Older Dryas stadial. Starting with this cold period the TCN profile highlights a low incision period that lasted until 4,5 kyr B.P. The incision rate doesn't seem to have been affected by the MIS1 warming phase and the related deglaciation (Darnault et al. 2012), as instead is clearly visible in the Vesubie river record (Saillard et al., 2014). An explanation for the low incision rate of this period could be found in the stabilization of river slopes by vegetation, that developed rapidly during the Holocene climatic optimum (Ortu et al., 2008; Mourier et al., 2010). Furthermore it is important to note that not

necessary all the incision events get registered by the river. Several factors as, for instance, sediment deposition and channel temporary damming, can affect the dating hiding incision events.

The younger incision rate increase (4-5 kyr B.P.) corresponds in time to the middle-late Holocene transition at 4,2 kyr B.P., a period of increased runoff (Walker et al., 2012). Fluvial sequences of Holocene period show, in the French Riviera, a transition from fine to coarse sediment, which reflects a change in hydrological regime. From 8 to 5 kyr B.P. energy of rivers was likely low, while, starting around 4,5 kyr B.P. it probably increased, with a relative more abundant and coarser sediment transport, likely related to a major incision phase in the upstream part of the catchments (Dubar and Anthony, 1995). In this period a sedimentological change in the Alpine lakes has also been documented, and, after some authors (e.g. Brisset et al., 2013), may represent an augmentation in the anthropic activity. The increase in agriculture pastoralism and other human activities, may have reduced the forest cover in the Tinée catchment, causing more slope instability and increase of sediment supply to river channels. A further indirect confirmation of a climatic change with relatively high hydrological pulses in this period and in this region, is given by the elevated landslide activity during the time period from 5,1 to 3,3 kyr B.P. (Sanchez et al., 2010a; Zerathe et al., 2013, 2014). Finally, an enhancement in incision rates for the same period has been estimated also for the neighbouring Vesubie Valley (Saillard et al., 2014).

Such elevated and fluctuating values of incision rates are then to be ascribed to climatic variability and to the concentration of the river energy inside narrow gorges.

In the Tinée basin, beyond the TCN dating presented here, there exist four additional dating profiles carried out on river polished surface using the Terrestrial Cosmogenic Nuclides methodology. The dated surfaces are located (*Figure 54*): in the very north side of the Tinée catchment area in the gorge of Salso Moreno river, just upstream of the Isola settlement (Darnault et al., 2012), in the lower part of the Vesubie valley (Saillard et al., 2014), in the lowest part of the Tinée valley not far from the junction with the Var river (still unpublished data).

The comparison between the different datings suggests some questions. Looking at the two TCN profiles dating the incision rate of the Tinée (Tin Be, Tin Cl), is evident that the period of more intense incision activity of the $^{36}Cl$ profile is younger than the peak of incision activity found in this study. It is also interesting that this increase of incision is located at the end of the Younger Dryas stadial, roughly at the same time of the one found for the Vesubie (profile VES, Saillard et al., 2014). These profiles are the lowest ones, and the youngest Dryas deglaciation seems to have had more influence on the incision of this part of the river network.
What instead is clear, it is the transient character of the incision process, that alternate in all the 4 profiles, periods of very low incision to others reaching incision rates up to 20 mm/yr (*Table* 15). This erosion trend is another confirmation of the climate control over the incision processes of the Tinée basin. However, while the climatic control on the phases of increased incision can clearly be put forward, our data show that the rivers did not reach an equilibrium after the long-lasting glacial phases of the Quaternary. In this context of disequilibrium, it could be hypothesized that the peaks in river erosion allow to accommodate the long-term tectonic uplift. Thus, there could be a more complex interaction between tectonics and climate in the shaping of mountain valleys.

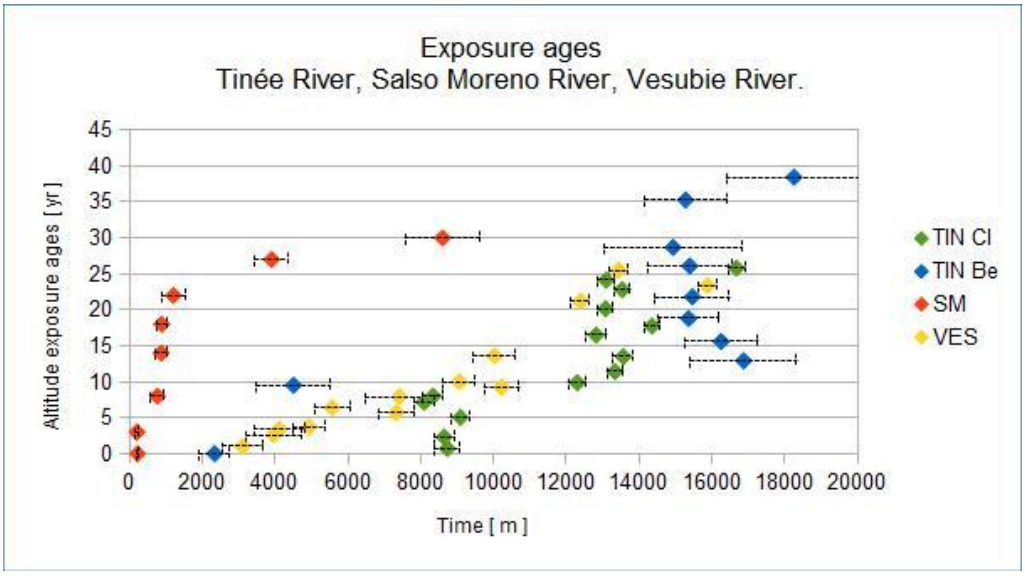


*Figure 54: TCN dating profiles effectuated in the Tinée valley: TIN Cl (N43°56'14.30 E7°10'02.77, 275 m, unpublished article) and TIN Be (N 44°07'22,5" E 07°05'42,5"), in the Salso Moreno valley. SM (N 44°19,8'21,1" E 6°52,2'24,3", Darnault et al., 2012), and in the Vesubie valley, VES (N43°56'06.7" E7°15'54.8". Saillard et al., 2014).*

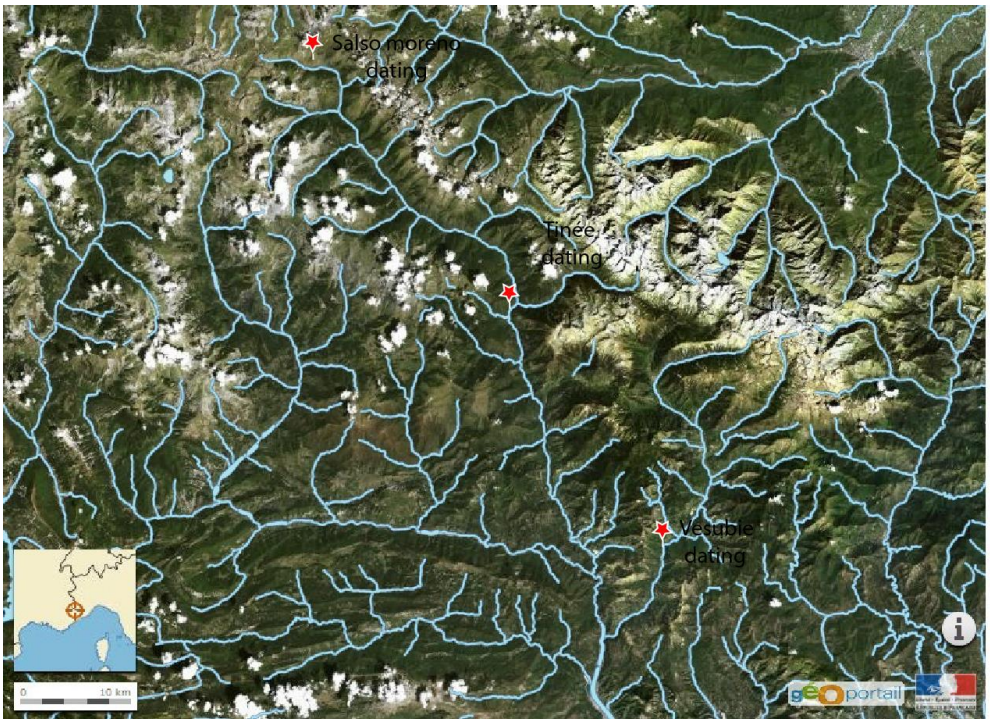


*Figure 53: Satellite image of the High Tinée basin showing the sampling sites. The sampled site giving the TIN Cl data, and located in the lowest Tinée valley is visible only in the less-zoomed pictures on the right.*

# V Conclusions

Both the numerical and the geochemical approaches lead to the conclusion that the climate is the factor driving the fluvial incision processes, at least for what concerns the Tinée catchment area.

The application of the Goren model suggests that climate is the parameter leading the Tinée incision process highlighting the remarkable effects of the post LGM deglaciation on the incision dynamic. However the model also shows a constant background noise, partly hidden by the high incision rate linked to the climatic erosion-favourable conditions. The model results are not reliable in what concern the absolute values of the incision rate. Anyway, with the help of the TCN profile (*Figure 52* and *Table 15*), is not unreasonable to associate the long term incision rate value (2,0+/-0,5 mm/yr) estimated over the whole period covered by the 10Be dating (last 18 kyr), to the uplift influence upon the river incision rate. Incision rate is of the same order of magnitude of the vertical moving rate, derived by GPS measurements and proposed by Serpelloni et al. (2013).

The successfully performed analysis of the in-situ produced $^{10}$Be Terrestrial Cosmogenic Nuclides has confirmed that climate is the most important factor in the Tinée valley incision. It has allowed to quantify the incision rate fluctuation over the last 18 kyr with a good resolution (int+ext uncertainties mean, of 3139 yr). For the study period, the dating has provided a mean incision rate of 2mm/yr with two evident period of rapid incision around 15 and 4,5 kyr B.P. This periods correspond to climate changes causing, respectively, a rapid post LGM deglaciation and more abundant rainfall. Overall, this study confirms the results obtained by Darnault et al. (2012), with incision rate values clearly higher than the uplift rates measured for the area (Walpersdorf et al., 2015). Several open questions still remain. The Tinée valley deglaciation dynamics and timing is indubitably still waiting for a more detailed description. Other interesting topic is the calibration of the model, specifically of the n parameter. It would be interesting, also, to apply the model to the area considering uplift varying within the catchment. In this way it would be possible to detect eventual difference in the

uplift rate between the two sides of the strike fault cutting the west tributaries of the High Tinée (*Figure 7*). Finally, an application of the model to rivers far away from tectonic areas could help to know and decipher the climatic effects on the Goren-Willet-Fox model signal.

**References**

Adams J., 1985, Large-scale tectonic geomorphology the Southern Alps, New Zealand, in Tectonic Geomorphology, edited by M. Morisawa and J.T. Hack, pp. 105-128, Allen and Unwin,Winchester Mass.

Anderson R, .S., 1994, The growth and decay of the Santa Cruz Mountains. J, . Geophys R. es., 99, 20,161-20,180.

Baotian, P., H. Xiaofei, G. Hongshan, H. Zhenbo, C. Bo, G. Haopeng, and L. Qingyang, 2013, Late Quaternary river incision rates and rock uplift pattern of the eastern Qilian Shan Mountain, China, Geomorphology, 184, 84–97, doi:10.1016/j.geomorph.2012.11.020.

Baroux E., Béthoux N., and Bellier O., 2001, Analyses of the stress field in southeastern France from earthquake focal mechanisms. *Geophysical Journal International* **145**, 336-348.

Béthoux N., Fréchet J., Guyoton F., Thouvenot F., Cattaneo M., Eva C., Feignier B., Nicolas M., and Granet M., 1992, A closing Ligurian sea ? *Pure and Applied Geophysics* **139(2)**, 179- 194.

Béthoux N., Sue C., Paul A., Virieux J., Fréchet J., Thouvenot F., and Cattaneo M. ,2007, Local tomography and focal mechanisms in the south-western Alps: Comparison of methods and tectonic implications. *Tectonophysics* **432**(1-4), 1-19.

Bigot-Cormier F., Braucher R., Bourles D., Guglielmi Y., Dubar M., Stephan J.F., 2005. Chronological constraints on processes leading to large active landslides. Earth and Planetary Science Letters 235, 141- 150.

Brisset, E., et al., 2013, Non-reversible geosystem destabilisation at 4200 cal. BP: Sedimentological, geochemical and botanical markers of
soil erosion recorded in a Mediterranean alpine lake, Holocene, 23, 1863–1874.

Bogdanoff S., 1986. Evolution de la partie Occidentale du massif de l'Argentera.

Place dans l’arc Alpin : Geol. Fr., v. 4, p. 433--- 453.

Böhlert, R., M. Egli,M.Maisch, D. Brandovà, S. Ivy-Ochs, P. W. Kubik, andW. Haeberli, 2011, Application of a combination of dating techniques to reconstruct the late glacial and early Holocene landscape history of the Albula region (eastern Switzerland), Geomorphology, 127, 1–13.

Borgatti, L., Soldati, M., 2002. In: Rybar, J., Stemberk, J., Wagner, P., Landslides, A.A. (Eds.), The Influence of Holocene Climatic Changes on Landslide Occurrence in Europe. Balkema Publishers, Lisse, pp. 111- 116.

Bouissou S., Darnault R., Chemenda A., Rolland Y., 2012. Evolution of gravity--- driven rock slope failure and associated fracturing: geological analysis and numerical modelling. Tectonophysics 526--- 529, 157- 166.

Campredon, R., M. Franco, G. Giannerini, P. Gigot, F. Irr, M. Lanteaume, H. Spini, and J.-F. Tapoul, 1977, Les déformations de conglomérats pliocènes de l’arc de Nice (chaînes subalpines méridionales), C. R. Somm. Soc. Géol. Fr., 2, 75–77.

Campy M., 1982. Le Quaternaire franc--- comtois : Essai chronologique et paleoclimatique. These d’Etat, Universite de Franche- conte, 575 p.

Corsini, M., Ruffet, G. & Caby, R., 2004. Alpine and late hercynian geochronological constraints in the Argentera Massif (Western Alps). Eclogae Geologicae Helvetiae, 97, 3- 15.

Cossart E., Braucher R., Fort M., Bourles D. L., Carcaillet J., 2008. Slope instability in relation to glacial debuttressing in alpine areas (Upper Durance catchment,southeastern France) : Evidence from field data and 10Be cosmic ray exposure ages. Geomorphology 95, 3--- 26.

Cossart E., Fort M., Bourles D., Carcaillet J. Perrier R., Siame L., Braucher R., 2010. Climatic significance of glacier retreat and rockglacier re--- assessed in the

light of cosmogenic dating and weathering rind thickness in Claree valley (Brianconnais, French Alps). Catena 80, 204--- 219.

Coutterand S., 2010. Etude geomorphologique des flux glaciaires dans les Alpes Nord- Occidentales au Pleistocene recent. Du maximum de la derniere glaciation aux premieres etapes de la deglaciation. Manuscrit de these, 471 pages.

Darnault R., Rolland Y., Revel M., Bourles D., Braucher R., Bouissou S. Submitted in Boreas in april 2012. New TCN 10Be evidence for progressive high- altitude glacier retreat from 11 ka to 8 ka following the Younger Dryas in SW Alps, insights for potential rejuvenation of ages.

Darnault R., Rolland Y., Braucher R., Bourles D., Revel M., Sanchez G., Bouissou S., 2012. Timing of the last deglaciation revealed by receding glaciers at the Alpine- scale: impact on mountain geomorphology. Quaternary Science Reviews 31, 127- 142.

Delacou B., Sue C., Champagnac J.-D., and Burkhard M., 2004, Present-day geodynamics in the bend of the western and central Alps as constrained by earthquake analysis. *Geophysical Journal International* **158**(2), 753-774.

Dunai, T., and F. M. Stuart, 2009, Reporting of cosmogenic nuclide data for exposure age and erosion rate determinations, Quat. Geochronol., 4, 437–440.

Dunai,T., 2010, Cosmogenic Nuclides: principles, concepts and applications in the Earth Surface Sciences, edited by Cambridge, www.cambridge.org/978052187380

El Bedoui S., Guglielmi Y., Lebourg T., Perez J. L., 2009. Deep--- seated failure propagation in a fractured rock slope over 10000 years: the La Clapiere slope, the South--- Eastern French Alps. Geomorphology 105, 232- 238.

El Bedoui S., Bois T., Jomard H., Sanchez G., Lebourg T., Tric E., Guglielmi Y., Bouissou S., Chemenda A., Rolland Y., Corsini M., Perez J. L., 2011. Paraglacial gravitational deformations in the SW Alps: a review of field investigations, 10Be

cosmogenic dating and physical modelling. Geological Society, London, Special Publications 351, 11--- 25.

Eva E. and Solarino S.,1998, Variations of stress directions in the western Alpine arc. *Geophysical Journal International* **135**, 438-448.

Faure- Muret A.,1955. Etudes geologiques sur le massif de l'Argentera--- Mercantour et ses enveloppes sedimentaires. Memoire de la Societe Geologique de France, 336.

Federici, P.R., Granger, D.E., Pappalardo, M., Ribolini, A., Spagnolo, M., Cyr, A.J., 2008. Exposure age dating and equilibrium line altitude reconstruction of an Egesen moraine in the Maritime Alps, Italy. Boreas 37, 245- 253.

Ferrier, K. L., K. L. Huppert, and J. T. Perron, 2013, Climatic control of bedrock river incision, Nature, 496, 206–209, doi:10.1038/nature11982.

Giardini D., Grunthal G., Shedlock K. M., and Zhang P. Z., 1999, The GSHAP Global Seismic Hazard Map. *Annali Di Geofisica* **42(6)**, 1225-1230.

Goldrick, G., and P. Bishop, 1996, Stream long profile analyses and the reconstruction of landscape evolution with examples from the Lachlan Valley, south eastern Australia, in Bedrock Channel, *Conference* edited by E.E.Wohl and K . Tinklerp, p.2 3, Colorado State Univ., Fort Collins.

Goren, L., M. Fox, and S. D. Willett, 2014, Tectonics from fluvial topography using formal linear inversion: Theory and applications to the Inyo Mountains, California, *J. Geophys. Res. Earth Surf., 119,* 1651–1681, doi:10.1002/2014JF003079.

Guiot J., Pons A., De Beaulieu J. L., Reille M., 1989. A 140 000 year continental climate reconstruction from two European pollen records. Nature 338. P. 309- 313.

Heuberger H., 1966. Gletschergeschichtliche Untersuchungen in den zentral alpen

zwischen Sellrain und otztal. Wissenschaftliche Alpen vereinshefte 20, 126.

Heuberger, H., 1968. Die Alpengletsherim Spat--- und Postglazial. Eiszeitalter und Gegenwart 19, 270- 275.

Heisinger, B., Lal, D., Jull, A. J. T., Kubik, P., Ivy-Ochs, S., Knie, K. and Nolte, E., 2002a. Production of selected cosmogenic radionuclides by muons: 2. Capture of negative muons, Earth Planet. Sci. Lett. 200 357–369.

Howard A., D., and G. Kerby, 1983, Channel changes in badlands Geol. Soc. Am. Bulletin, 94, 739-752.

Howard A.D., 1994, M.A. Seidl and W. E. Dietrich, Modeling fluvial erosion on regional to continental scales J. Geophys Res., 9 9, 13,971-13,986.

Isacks B.L.. 1992, 'Long-term' land surface processes: Erosion, tectonics and climathe history in mountain belts in Terra 1: Understanding the terrestrial enviroment, edited byP.M. Mather, pp. 2 1-36, T aylor and Francis, Bristol, Pa.

Ivy- Ochs, S., Kerschner, H., Kubik, P.W., Schlüchter, C., 2006. Glacier response in the European Alps to Heinrich event 1 cooling: the Gschnitz stadial. Journal of Quaternary Science 21, 115-130.

Ivy- Ochs, S., Kerschner, H., Reuther, A., Preusser, F., Heine, K., Maisch, M., Kubik, P.W., Schlüchter, C., 2008. Chronology of the last glacial cycle in the European Alps. Journal of Quaternary Science 23, 559- 573.

Ivy- Ochs, S., Kerschner, H., Maisch, M., Christl, M., Kubik, P.W., Schlüchter, C., 2009. Latest Pleistocene and Holocene glacier variations in the European Alps. Quaternary Science Reviews 28, 2137e2149.

Ivy-Ochs, S., 2015, Glacier variations in the eureopean Alps at the end of the last glaciation, Cuadernos de Investigatigacion Geografica, N°41, p.p 295-315, ISSN 0211-6820

Jomard H., 2006. Analyse multi- echelle des deformations gravitaires du Massif de l'Argentera Mercantour. PhD thesis, 268 p. Jorda et al., 2000 Jorda M., Rosique T., Evin J., 2000. Donnees nouvelles sur l'age du dernier maximum glaciaire dans les Alpes meridionales francaises. C. R. acad. Sc. Paris 331, 187- 193

Jorda, M., and T. Rosique, 1994, Le Tardiglaciaire des Alpes françaises du Sud: Rythme et modalités des changements bio-morphoclimatiques,

Quaternaire, 5, 141–149.

Jorda, M., T. Rosique, and J. Évin, 2000, Données nouvelles sur l'âge du dernier maximum glaciaire dans les Alpes méridionales françaises, C.R. Acad. Sci., Ser. IIA: Earth Planet. Sci., 331, 187–193, doi:10.1016/S1251-8050(00)01408-7.

Jourdon, A., et al., 2014, Style of Alpine tectonic deformation in the Castellane fold-and-thrust belt (SW-Alps, France): Insights from balanced cross-section. Tectonophysics, http://dx.doi.org/10.1016/j.tecto.2014.06.022

Julian,M.,1980. Les AlpesMaritimes Franco- Italiennes :Etude geomorphologique. These d'etat, Aix- Marseille II, p. 836

Kelly, M.A., Kubik, P.W., Von Blanckendurg, F., Schlüchter, C., 2004. Surface exposure dating of the Great Aletsch Glacier Egesen moraine system, western Swiss Alps, using the cosmogenic nuclide 10Be. Journal of Quaternary Science 19, 431e441.

Kelly, M.A., Ivy--- Ochs, S., Kubik, P.W., Von Blanckenburg, F., Schlüchter, C., 2006. Chronology of deglaciation based on 10Be dates of glacial erosional features in the Grimsel Pass region, central Swiss Alps. Boreas.

Kerschner, H., 1986. Zum Sendersstadiumim Spätglazial der nördliche Stubaier Alpen, Tirol. Zeit schrift für Geomorphologie Supplement Band 61, 65--- 76.

Kohl, C. P. and Nishiizumi, K., 1992. Chemical isolation of quartz for

measurementof in-situ- produced cosmogenic nuclides, Geochim. Cosmochim. Acta 56 3583–3587.

Kirby, E., and K. Whipple, 2001, Quantifying differential rock-uplift rates via stream profile analysis, *Geology*, *29*(5), 415–418, doi:10.1130/0091-7613(2001)029<0415:QDRURV>2.0.CO;2.

Kirby, E., and K. X. Whipple, 2012, Expression of active tectonics in erosional landscapes, J. Struct. Geol., 44, 54–75.

Kooi H., and C. Beaumont, 1994, Escarpement evolution on high-elevation rifted margins: Insights derived from a surface processes model that combines dffusion, advection and reaction, J. Geophys Res., 9 9, 12,191-12,209.

Koppes M. N., Montgomery D. R., 2009. The relative efficacy of fluvial and glacial erosion over modern to orogenic timescales. Nature geosciences 2, 644- 647.

Larroque C., Béthoux N., Calais E., Courboulex F., Deschamps A., Déverchère J., Stéphan J.-F., Ritz J.-F., and Gilli E., 2001, Active and recent deformation at the southern Alps-Ligurian bassin junction. *Netherland Journal of Geosciences/Geologie en Mijnbouw* **80**, 255-272.

Larroque C., Delouis B., Godel B., and Nocquet J.-M., 2009, Active deformation at the southwestern Alps- igurian basin junction (France-Italy boundary): Evidence for recent change from compression to extension in the Argentera massif. *Tectonophysics* **467**(1- 4), 22-34.

Leith, K., M. Fox, J.R. Moore. Submitted article. 700'000 years of fluvial incision in the European Alps.

Maisch, 1992. Die GletscherGraubundens. Rekonstruktion und Auswertung der Gletscher und deren Veranderungenseit dem Hochstand von 1850 im Gebiet der ostlichen Schweizer Alpen (Bundnerland und angrenzende Regionen). Physische

Geographie 331.

Maisch M., Wipf, A., Denneler, B., Battaglia, J., Benz, C., 1999. Die Gletscher der Schweizer Alpen. Gletscherhochstand 1850, Aktuelle Vergletsherung, Gletscherschwund--- Szenarien Schlussbericht NFP 31, Zürich.

Mangerud, J., Andersen, S.T., Bergland, B.E., Donner, J.J.,1974. Quaternary stratigraphy of Norden, a proposal for terminology and classification. Boreas 3, 109- 126.

Masarik, J. and Beer, J., 1999. Simulation of particle fluxes and cosmogenic nuclide production in the Earth's atmosphere, J. Geophys. Res. 104D 12099–12111.

Molnar, P. and P . England, 1990, Late Cenozoic uplift of mountain ranges and global climate change: Chicken or egg?, Nature, 346, 29-34.

Ortu, E., Peyron, O., Bordon, A., de Beaulieu, J.L., Siniscalco, C., Caramiello, R., 2008. Lateglacial and Holocene climate oscillations in the South- Western Alps: an attempt at 234 quantitative reconstruction. Quaternary Stratigraphy and Evolution of the Alpine Region and the Mediterranean Area in the European and Global Framework 190, 71e88.

Patzelt, G., 1972. Die spatglazialenSchwankungen von Ostalpengletschern. Bericht der deutschen Botanische Gesellshaft 85, 47- 57.

Perron, J. T., and L. Royden (2013), An integral approach to bedrock river profile analysis, Earth Surf. Processes Landforms, 38, 570–576, doi:10.1002/esp.3302.

Raymo, M.E. and W.F. Ruddiman, 1992, Tectonic forcing of late Cenozoic climate, Nature, 359, 117-122.

Rosenbloom, N.A. and R.S. Anderson, 1994, Evolution of the marine terraced landscape, Santa Cruz, California, J. Geophys, Res. 99,14,013-14,030.

Rothé J. P., 1941, Les séismes des Alpes françaises en 1938 et la sismicité des Alpes occidentales. *Annales de l'Institut de Physique du Globe de Strasbourg* **3**, 1-105.

Saillard, M., C. Petit, Y. Rolland, R. Braucher, D. L. Bourlès, S. Zerathe, M. Revel, and A. Jourdon, 2014, Late Quaternary incision rates in the Vésubie catchment area (Southern French Alps) from in situ-produced 36Cl cosmogenic nuclide dating: Tectonic and climatic implications, J. Geophys. Res. Earth Surf., 119, 1121–1135, doi:10.1002/ 2013JF002985.

Sanchez G., Rolland Y., Corsini M., Braucher R., Bourlès D., Arnold M., and Aumaître G., 2010a, Relationships between tectonics, slope instability and climate change: Cosmic ray exposure dating of active faults, landslides and glacial surfaces in the SW Alps. *Geomorphology* **117**, 1-13.

Sanchez G., Rolland Y., Schreiber D., Giannerini G., Corsini M., and Lardeaux J.-M., 2010b, The active fault system of SW Alps. *Journal of Geodynamics* **49**, 296-302.

Seidl, M.A., and W.E. Dietrich, 1992, The problem of channel erosion into bedrock, Catena Suppl., 23, 101-124.

Seidl, M.A., W.E. Dietrich, and J.W. Kirchner, 1994, Longitudinal profile development into bedrock: An analysis of Hawaiian channels J. Geol., I02, 457-474.

Serpelloni, E., C. Faccenna, G. Spada, D. Dong, and S. D. P. Williams, 2013, Vertical GPS ground motion rates in the Euro-Mediterranean region: New evidence of velocity gradients at different spatial scales along the Nubia-Eurasia plate boundary, J. Geophys. Res. Solid Earth, 118, 6003–6024, doi:10.1002/2013JB010102.

Sklar, L., and W.E. Dietrich, 1998, River longitudinal profiles and bedrock incision models: Stream power and the influence of sediment supply, in Rivers Over Rock: Fluvial P rocesses in Bedrock Channels, Geosphys Monogr. Ser.,vol.

107, edited by K.J. Tinkler and E.E. Wohl, pp. 237-260, AGU, Washington, D.C.

Snyder, N. P., K. X. Whipple, G. E. Tucker, and D. J. Merritts, 2000, Landscape response to tectonic forcing: Digital elevation model analysis of stream profiles in the Mendocino triple junction region, northern California, *Geol. Soc. Am. Bull.*, *112*(8), 1250–1263.

Snyder, N. P., K. X. Whipple, G. E. Tucker, and D. J. Merritts, 2003, Importance of a stochastic distribution of floods and erosion thresholds in the bedrock river incision problem, *J. Geophys. Res.*, *108*(B2), 2117, doi:10.1029/2001JB001655.

Soldati M., Corsini A., and Pasuto A., 2004, Landslides and climate change in the Italian Dolomites since the Late glacial. *CATENA. Geomorphic Impacts of Rapid Environmental Change* **55**(2), 141-161.

Stock, J. D. & Montgomery, D. R., 1999, Geologic constraints on bedrock river incision using the streampower law. J. Geophys. Res. Solid Earth 104, 4983–4993.

Stock, J. D. and D. R. Montgomery, 1999, Geologic constraints on bedrock river incision using the stream power law, *J. Geophys. Res.*, *104*(B3), 4983–4994.

Stone, J. O., 2000, Air pressure and cosmogenic isotope production, J. Geophys. Res., 105, 23,753–23,759.

Sue C., 1998, Dynamique actuelle et récente des Alpes occidentales internes. Approche structurale et sismologique. *Thèse de 3ème cycle UJF Grenoble*.

Sue C. and Tricart P., 1999, Late Alpine brittle extension above the Frontal Pennine Thrust near
Briançon, Western Alps. *Eclogae Geol Helvet* **92**, 171-181.
Sue C. and Tricart P., 2002, Widespread post-nappe normal faulting in the internal Western

Sue C., Martinod J., Tricart P., Thouvenot F., Gamond J. F., Fréchet J., Marinier

D., Glot J. P., and Grasso J. R., 2000, Active déformation in the inner westernn Alps inferred from comparison between 1972-classical and 1996- GPS geodetic surveys. *Tectonophysics* **320**, 17-29.

Thouvenot F., Paul A., Senechal G., Hirn A., and Nicolich R., 1990, Ecors-Crop wide-angle reflexion seismics: contraints on deep interfaces beneath the Alps. *Mémoires de la Société géologique de France* **156**, 97-106.

Tucker, G.E., and R. Slingerland, 1996, Predicting sediment flux from fold and thrust belts, Basin Res., 8, 329-349.

Walpersdorf. A., C. Sue, N. Cotte, P. Bascou, C. Beauval, P. Collard, G. Daniel, H. Dyrer, J.-R. Grasso, O. Hautecoeur, A. Helmstetter, S. Holk, M. Langlais, G. Menard, Z. Mousavi, F. Ponton, M. Rizza, L. Rizza, L. Rolland, D. Souami, L. Thirard, P. Vaudey, C. Voisin, J. Martinod, 2015, Coherence between geodetic and seismic deformation in a context of slow tectonic activity (S.W. Alps, France). Journal of Geodynamics, 85, 58 – 65. http:// www.elsevier.com/locate/jog.

Whipple, K. X., and G. E. Tucker, 1999, Dynamics of the stream-power river incision model: Implications for height limits of mountain ranges, landscape response timescales, and research needs, J. Geophys. Res., 104, 17,661–17,674.

Whipple, K. X., 2001, Fluvial landscape response time: how plausible is steady-state denudation? *American Journal of Science*, *301*(4/5), 313–325.

Whittaker A.C, Boulton SJ., 2012. Tectonic and climatic controls on knickpoint retreat rates and landscape response times. Journal of Geophysical Research 117: F02024. DOI.10.1029/2011JF002157

Wobus, C., K. X. Whipple, E. Kirby, N. Snyder, J. Johnson, K. Spyropolou, B. Crosby, and D. Sheehan, 2006, Tectonics from topography: Procedures, promise, and pitfalls, in Tectonics, Climate, and Landscape Evolution, Spec. Paper, vol. 398, edited by S. D. Willett et al., pp. 55–74, Geol. Soc. Am., Penrose Conference Series.

Zerathe S., Lebourg S., 2012. Evolution stages of large deep--- seated landslides at the front of a subalpine meridional chain (Maritime--- Alps, France). Geomorphology 138, 390- 403.

Zerathe S., Braucher R., ebourg T., Bourles D., Manetti M., Leanni L., 2014 Dating chert using in- situ produced 10Be: Possible complications revealed through the comparison with 36Cl applied on coexisting limestone.

**Appendix:**

***Appendix 1:*** *the four Matlab script developed by Lirian Goren and employed during this study*

*Code 1: Receives the topography ASCII grid as input, reproducing the river topographic profiles*

```
%%% extracts data from Whitebox files
%%% once the latter converted into ARCGIS ASCII files
%%% (it's not necessary to remove the 6-lines header)
%%% exports at the format needed by Calctau
%%% x:y:z:flow dir:flow length:basin:order:area:slope

close all;
clear all;


%% CHANGE FOR EACH DEM
ncols = 908;
nligs = 694; %
xll =  6.782638888888889;
yll = 44.15513888888889;
cellsize = 2.7777777777777794E-4; %cell size in degrees

pixelsize=30*22;

%%%

slop = zeros(nligs,ncols);

%%% INPUT FILES
%%% 1 is the DEM topo file
input_1 = dlmread ('C:\Users\Davide\Desktop\Codici_Matlab_WB_mod2\02-06-
2015\ASCIITinee\tin_topo.txt',' ',6,0);
%%% 2 is the flow direction file
input_2 = dlmread ('C:\Users\Davide\Desktop\Codici_Matlab_WB_mod2\02-06-
2015\ASCIITinee\tin_pointer.txt',' ',6,0);
%%% 3 is the flow length file
input_3 = dlmread ('C:\Users\Davide\Desktop\Codici_Matlab_WB_mod2\02-06-
2015\ASCIITinee\tin_dist.txt',' ',6,0); %HO USATO IL FILE FLOWPATH
APPLICATO ALL'INTARO BACINO
%%% 4 is the basin file (selects a watershed)%%TINEE
%VESUBIE
input_4 = dlmread ('C:\Users\Davide\Desktop\Codici_Matlab_WB_mod2\02-06-
2015\ASCIITinee\tin_watersheds.txt',' ',6,0);
```

```
%%% 5 is the flow order file
input_5 = dlmread ('C:\Users\Davide\Desktop\Codici_Matlab_WB_mod2\02-06-2015\ASCIITinee\tin_HS.txt',' ',6,0); %usato di nuovo file generale
%%% 6 is the drainage area in pixels
input_6 = dlmread ('C:\Users\Davide\Desktop\Codici_Matlab_WB_mod2\02-06-2015\ASCIITinee\tin_accumPIX.txt',' ',6,0); %????
%%% 7 is the stream file
%input_7 = dlmread ('D:\VESUBIE\DEMS\tineezoommain.txt',' ',6,0);
input_7 = dlmread ('C:\Users\Davide\Desktop\Codici_Matlab_WB_mod2\02-06-2015\ASCIITinee\tin_mains.txt',' ',6,0); %MS


%% Makes a lat/lon grid coordinate
latcoor = repmat((nligs:-1:1)',1,ncols)*cellsize+yll;
loncoor = repmat (1:ncols,nligs,1)*cellsize+xll;

%makes a km grid coordinate
deglat = 40e6/360; % one degree of latitude in m
deg2m = 90000;% one degree of longitude in m
ycoor = (latcoor-yll)*deglat;
coslat = cos(latcoor*pi/180);
xcoor = (loncoor-xll)*deglat.*coslat;
new_dir=ones(nligs,ncols);

npts=1;

%%% In this step we compute the along channel slope which is not properly
%%% done in whitebox

step_calc = 'computing along-channel slope '
for i=2:nligs-1
   for j=2:ncols-1
      % checks only for points within a channel
      if input_7(i,j)>0

         %% finds the flow direction and computes local slope
   switch input_2(i,j)
            case 1
               dist = sqrt((xcoor(i-1,j+1)-xcoor(i,j))^2 + (ycoor(i-1,j+1)-ycoor(i,j))^2);
               slop(i,j) = -(input_1(i-1,j+1) - input_1(i,j))/dist;
               new_dir(i,j)=128;
            case 2
               dist = sqrt((xcoor(i,j+1)-xcoor(i,j))^2 + (ycoor(i,j+1)-ycoor(i,j))^2);
               slop(i,j) = -(input_1(i,j+1) - input_1(i,j))/dist;
               new_dir(i,j)=64;
```

```
            case 4
               dist = sqrt((xcoor(i+1,j+1)-xcoor(i,j))^2 + (ycoor(i+1,j+1)-
ycoor(i,j))^2);
               slop(i,j) = -(input_1(i+1,j+1) - input_1(i,j))/dist;
               new_dir(i,j)=32;
            case 8
               dist = sqrt((xcoor(i+1,j)-xcoor(i,j))^2 + (ycoor(i+1,j)-ycoor(i,j))^2);
               slop(i,j) = -(input_1(i+1,j) - input_1(i,j+1))/dist;
               new_dir(i,j)=16;
            case 16
               dist = sqrt((xcoor(i+1,j-1)-xcoor(i,j))^2 + (ycoor(i+1,j-1)-
ycoor(i,j))^2);
               slop(i,j) = -(input_1(i+1,j-1) - input_1(i,j))/dist;
               new_dir(i,j)=8;
            case 32
               dist = sqrt((xcoor(i,j-1)-xcoor(i,j))^2 + (ycoor(i,j-1)-ycoor(i,j))^2);
               slop(i,j) = -(input_1(i,j-1) - input_1(i,j+1))/dist;
               new_dir(i,j)=4;
            case 64
               dist = sqrt((xcoor(i-1,j-1)-xcoor(i,j))^2 + (ycoor(i-1,j-1)-
ycoor(i,j))^2);
               slop(i,j) = -(input_1(i-1,j-1) - input_1(i,j))/dist;
               new_dir(i,j)=2;
            case 128
               dist = sqrt((xcoor(i-1,j)-xcoor(i,j))^2 + (ycoor(i-1,j)-ycoor(i,j))^2);
               slop(i,j) = -(input_1(i-1,j) - input_1(i,j+1))/dist;
               new_dir(i,j)=1;
         end
       else
         slop(i,j)=0;
      end
    end
end

step_calc = 'writing table '
new_dir(nligs,:)=new_dir(nligs-1,:);
 for i=1:nligs
   for j=1:ncols
      % checks only for points within a channel
      if input_4(i,j)>-9999 && input_5(i,j)>-9999 && input_7(i,j)>0 &&
input_1(i,j)<2350  % selectionne en fonction de l'altitude

      % writes a table for calctau with the following data
      % x:y:z:flow direction:flow length:watershed number: stream order:
      % :area:slope
```

```
        table1(npts,:)=[latcoor(i,j) loncoor(i,j) round(input_1(i,j)) new_dir(i,j)...
      input_3(i,j)*deg2m input_4(i,j) input_5(i,j) input_6(i,j) slop(i,j)];
            npts=npts+1;
        end
    end
end

% outlet = min(table1(:,5));
table1(:,3)=table1(:,3)-min(table1(:,3));
table2 = sortrows(table1, [-3 -1]);
table3 = sortrows(table1, 6);

%%% Sorts stream for Inversion (for each individual basin))
number_basins = max(table3(:,6));
prefix = input ('enter files prefix ' ,'s')
% delete allrivers.txt

%%% The outlet of the basin must have a x=0 coordinate
for k=1:number_basins
%k=1;
nodes=find(table3(:,6)==k);
    mintop = min(table3(nodes(1):nodes(size(nodes,1)),3));
    minlen = min(table3(nodes(1):nodes(size(nodes,1)),5));

    filename=[prefix num2str(k) '.dat']
    ElevationTau2=table3(nodes(1):nodes(size(nodes,1)),:);
    ElevationTau2(:,3)=ElevationTau2(:,3)-mintop;
    ElevationTau2(:,5)=ElevationTau2(:,5)-minlen;
    dlmwrite (filename,ElevationTau2,'delimiter',' ','newline','pc','precision',12)
    dlmwrite                    ('allrivers_new.txt',ElevationTau2,'-append','delimiter','
','newline','pc','precision',12)

end

% dlmwrite ('tineezoomdat.txt',table3,'delimiter',' ','newline','pc','precision',12)
%%% plots topo

figure (1);
scatter(table1(:,1),table1(:,2),20,table1(:,3),'o','filled');
colorbar;title('altitude');

 %% plots flow length
figure (2);
scatter(table1(:,1),table1(:,2),20,table1(:,5),'o','filled');
colorbar;title('flow length');
```

```
%% plots flow order
figure (3);
scatter(table1(:,1),table1(:,2),20,table1(:,7),'o','filled');
colorbar;title('flow order');

%
%
% %%% plots ks
% figure (5);
% m=0.6;
% ks =table3(:,9)./table3(:,8).^m ;
% scatter(table3(:,2),table3(:,1),30,ks,'o','filled');colorbar;
% title('ks')
```

*Code 2: calculates the various scatter linked to all the m values ranging between 0 and 1*

```
%function res = CalcScatterForM

%The function calculates tau for different values of m and presents the
%scatter in tau-z plots

all_data=load('MyDataAllData');
all_data = all_data(:,1:6);
[r,c] = size(all_data);
sort_data2 = sortrows(all_data,4); %sort by elevation
sort_data=sort_data2(1:80,:);
[r,c] = size(sort_data);
rec_list=load('MyData_river_network');

%%% vector of tested m values
m_vec = (0.2:0.01:1);

scatter_vec = zeros(1,length(m_vec));

bins = 20;
outlets = find(all_data(:,5)==0); %no flow length

figure(1);
hold off;
for q = 1:length(m_vec)
   tau_vec = zeros(1,r);
   m= m_vec(q);
   %calculate tau:
```

```
    for i=1:r
        j=rec_list(i); % i and j are ids
        if j~=0
            ii = find(sort_data(:,1)==i);
            jj = find(sort_data(:,1)==j);
            %my tau = tau of my receiver + dx/A^m (for n=1)
            tau_vec(ii) = tau_vec(jj) +...
            sort_data(ii,5)/sort_data(ii,6)^m;

%               tau_vec(ii) = tau_vec(jj) +...
%               sort_data(ii,5)/sort_data(ii,6)^m/K;

            plot([tau_vec(ii),tau_vec(jj)],[sort_data(ii,4),sort_data(jj,4)])
            hold on;
        end
    end
    max_tau = max(tau_vec);
    bin_size = max_tau/bins;
    bin_std = zeros(1,bins);
    for k = 1:bins
        index = find(tau_vec >= (k-1)*bin_size & tau_vec < k*bin_size);
        bin_z = sort_data(index,4);
        bin_std(k) = std(bin_z);
    end
    scatter_vec(q) = mean(bin_std);
    %hold off;
end
figure(2);
plot(m_vec,scatter_vec);

[a,b]=min(scatter_vec);
mmin = m_vec(b)
```

*Code 3: chosen the m value for the river, calculate the chi-profile*

```
%function res=CalcTauFromTable
clear all;
close all;
%pixelsize=88.7820251907; %area of pixel, depends on the DEM
pixelsize=30;
%pixeltoarea=pixelsize^2; %m^2
m_of_concavity=0.57;
pixelLatLon = 0.0002777777777;
pixeltoarea=30*22; % approximate pixel area in m2 at this latitude
```

```
%this function expect an input ascii file
%each row is one pixel and
%the columns corresponds to
%|x|y|z|flow direction|flow length|basin|order|area in pixel|slope
% 1 2 3     4            5            6    7      8            9
k= input('entrez numero bassin ')
basin_index=k;
%fileinput = ['tineeall' num2str(k) '.dat'];

fileinput=['socchi',num2str(k),'.dat'];
AllData=load(fileinput);%
[r,c]=size(AllData);

SortData=sortrows(AllData,[6 5]);

% converts pixels into square meters (drainage area)
SortData(:,8)=SortData(:,8)*pixeltoarea;

% find receiver relations
% go basin by basin.
% find all 0 is flow length - this is the outlet of a basin

%IMPORTANT - the script assumes lat-lon for x and y.
outlets=find(SortData(:,5)==0);
receiver_array=zeros(r,1);

for i=1:length(outlets)
   if i==length(outlets)
      top=r;
   else
      top=outlets(i+1) - 1;
   end
   bottom=outlets(i);
   receiver_array(bottom)=0;
   for j=bottom+1:top
      xlook=SortData(j,1)
      ylook=SortData(j,2)
      check_range=[(bottom:j-1) , (j+1:top-1)];
      distmin=1.e-5;
      switch SortData(j,4)
         case 1
            test = 'case 1'
            xlook=xlook+pixelLatLon;
            ind=find(abs(SortData(check_range,1)- xlook) < distmin & ...
               SortData(check_range,2) == ylook,1);
         case 2
```

```
            test = 'case 2'
            xlook=xlook+pixelLatLon;
            ylook=ylook-pixelLatLon;
            ind=find(abs(SortData(check_range,1)- xlook) < distmin & ...
                abs(SortData(check_range,2) - ylook)<distmin,1);
        case 4
            test = 'case 4'
            ylook=ylook-pixelLatLon;
            ind=find(SortData(check_range,1)== xlook & ...
                abs(SortData(check_range,2) - ylook)<distmin,1);
        case 8
            test = 'case 8'
            xlook=xlook-pixelLatLon;
            ylook=ylook-pixelLatLon;
            ind=find(abs(SortData(check_range,1)- xlook) < distmin & ...
                abs(SortData(check_range,2) - ylook)<distmin,1);
        case 16
            test = 'case 16'
            xlook=xlook-pixelLatLon;
            ind=find(abs(SortData(check_range,1)- xlook) < distmin & ...
                SortData(check_range,2) == ylook,1);
        case 32
            test = 'case 32'
            xlook=xlook-pixelLatLon;
            ylook=ylook+pixelLatLon;
            ind=find(abs(SortData(check_range,1)- xlook) < distmin & ...
                abs(SortData(check_range,2) - ylook)<distmin,1);
        case 64
            test = 'case 64'
            ylook=ylook+pixelLatLon;
            ind=find(SortData(check_range,1)== xlook & ...
                abs(SortData(check_range,2) - ylook)<distmin,1);
        case 128
            test = 'case 128'
            xlook=xlook+pixelLatLon;
            ylook=ylook+pixelLatLon;
            ind=find(abs(SortData(check_range,1)- xlook) < distmin & ...
                abs(SortData(check_range,2) - ylook)<distmin,1);
    end
            receiver_array(j)=ind+bottom-1;
  end
end

%At this point we should have a donor-receiver relationships stored in
%receiver_array. To check for mistakes we plot the network using these
%relationships.
```

```
figure;
hold on;
for i=1:r
      l_rec=receiver_array(i);
      if l_rec~=0
         plot([SortData(i,1),SortData(l_rec,1)],...
            [SortData(i,2),SortData(l_rec,2)]);
      end
end
axis equal

%prepare the results matrix
%column 1: pixel id
%column 2: lon
%column 3: lat
%column 4: z
%column 5: distance to receiver
%column 6: upstream drainage area
%column 7: basin id
%column 8: stream order
%column 9: distance along river from base level
%column 10: tau* value (==chi)

DataTauMat=zeros(r,10); % 10 colums matrix
DataTauMat(:,1)=(1:r);
DataTauMat(:,2:4)=SortData(:,1:3); % xyz
DataTauMat(:,6)=SortData(:,8); % drainage area
DataTauMat(:,7:8)=SortData(:,6:7); % basin number and stream order

%distance between donor-receiver
for i =1:r
   j=receiver_array(i);
   if j~=0
     DataTauMat(i,5)= pos2dist(SortData(i,2),SortData(i,1),...
        SortData(j,2),SortData(j,1),1)*1000;
   end
end

%calculate tau
DataTauMat(outlets,10)=0; % at the outlets tau=0;
for i=1:r
   j=receiver_array(i);
   if j~=0
      DataTauMat(i,10) = DataTauMat(j,10) +...
         DataTauMat(i,5)/DataTauMat(i,6)^m_of_concavity;  %update the tau
      DataTauMat(i,9)  =  DataTauMat(j,9)  +  DataTauMat(i,5);  %commulative
```

```
distance from base level

   end
end

A_0 = 1e7;

% figure;
% scatter(DataTauMat(:,3),DataTauMat(:,2),20,DataTauMat(:,10));colorbar
% %scatter(DataTauMat(:,2),DataTauMat(:,3),20,tau_real);colorbar
% axis equal

% plots response time depending on K in Ma
figure;
K_err=8e-6;
scatter(DataTauMat(:,3),DataTauMat(:,2),20,DataTauMat(:,10)/K_err/1e6);colorb
ar

%Saves individual basins

number_basins = max(DataTauMat(:,7));
%for k=1:number_basins
k=basin_index;
clear ElevationTau2
   nodes=find(DataTauMat(:,7)==k);
   filename=['MyDataElevationTau' num2str(k)]
   ElevationTau2(:,1)=DataTauMat(nodes(1):nodes(size(nodes,1)),4);
   ElevationTau2(:,2)=DataTauMat(nodes(1):nodes(size(nodes,1)),10);
   ElevationTau2(:,3)=DataTauMat(nodes(1):nodes(size(nodes,1)),9);
   save(filename,'ElevationTau2','-ascii');
%end

%  ElevationTau(:,1)=DataTauMat(:,4);
%  ElevationTau(:,2)=DataTauMat(:,210);
% save('MyDataElevationTau','ElevationTau','-ascii');
save('MyDataAllData','DataTauMat','-ascii');
save('MyData_river_network','receiver_array','-ascii');

% filename=['MyDataElevationTau' num2str(k)]
%     save(filename,'ElevationTau','-ascii');
%

%save('vesubiem08','DataTauMat','-ascii');
```

*Code 4: starting from the chi-profile, calculate the adimensional uplift rate and recalibrate it following the local characteristics and the parameters K and m chosen by the user*

```
%function
[Ks_res,time_vec,ks_new,time_vec_n]=InvertKSWithRegularizationVardt(file,time
_interval_i,damp_coeff,K,color)
%function
[Ks_res,time_vec,ks_new,time_vec_n]=InvertKSWithRegularizationVardt(MyDat
aElevationTau,10,1,9e-6,jet)
%file: a string with a file name. The file should have 2 columns. The
%first column contains elevations and the second tau values. Such a file
%is one of the outputs of CalcTauFromTable
%time_interval: an integer value of how many time intervals should be
%resolved. if 0, then the script loops over a predefined vector of time
%intervals.
%K: the erodibiility. If still unknown use 1.
%color: a matlab color for the inversion results graph.

clear all;
close all;

knum = input ('numero du bassin versant ');
file=['MyDataElevationTau' num2str(knum)];
my_data=load(file);

%%% K is the erodibility (assumed)
%%% Time interval is the number of time intervals you wan to consider
%%% damp_coeff will avoid too large U changes with time

time_interval_i=40;
damp_coeff=100;
K = 13e-6;
m_prime = 0.57;

%K=1;
color='jet';

%all_data = load('Inyo030AllData');
[r,c]=size(my_data);
%an arbitrary choice
A0 = 1e6;
%A0 = 1;
%IMPORTANT! m_prime has to be equal to the m used for the generation of the
%z-tau data.
```

```
j=1;
dataerr=10; % m vertical error of 30 m SRTM
for i=1:r
   if my_data(i,1)~=0 && my_data(i,2)~=0
      my_data_no_zero(j,:)=my_data(i,:);
      %all_data_no_zero(j,:)=all_data(i,:);
      j=j+1;
   end
end
r=j-1;
sorted_data=sortrows(my_data_no_zero,2);
%sorted_all_data = sortrows(all_data_no_zero,7);
z=sorted_data(:,1);
chi=sorted_data(:,2)*A0^m_prime;
x=sorted_data(:,3);

chi_max=max(chi);
if time_interval_i~=0
   time_interval=(time_interval_i);
else
   time_interval=(2:1:40);
   %time_interval=[11,20,40];
end

for p=1:length(time_interval)
   data_per_interval=floor(r/time_interval(p));
   time_vec=zeros(1,time_interval(p));
   for i=1:time_interval(p)
      time_vec(i)=chi(i*data_per_interval);
   end
   time_vec(end)=chi_max;
   dt_vec=[time_vec(1),diff(time_vec)];
   G=zeros(r,time_interval(p));

   for i=1:r-1
      chi_i=chi(i);
      ind=find(time_vec>chi_i,1);
      if ind>1
         G(i,(1:ind-1))=dt_vec(1:ind-1);
         reminder=chi_i - time_vec(ind-1);
         if reminder>0
            G(i,ind)=reminder;
         end
      else
         G(i,1)=chi_i;
      end
```

```
    end
    G(r,:)=dt_vec;
    ks_pri=mean(z./sum(G')')*ones(time_interval(p),1);
    z_pri=G*ks_pri;
    R=damp_coeff*eye(time_interval(p));
    denom=G'*G + R'*R ;
    nom2=G'*(z-z_pri);
    nom=G'*z;

    ks=ks_pri + denom\nom2;
    %ks=denom\nom;
    Ks_res=ks;
    j=1;
    for i=1:time_interval(p)
        if i-1==0
            time_vec_n(j)=0;
        else
            time_vec_n(j)=time_vec(i-1);
        end
        time_vec_n(j+1)=time_vec(i);
        ks_new(j)=ks(i);
        ks_new(j+1)=ks(i);
        j=j+2;
    end
    figure(1);

    col=strcat('-',color);
    col_vec = ['r','g','b'];
    if K==1
       % plot(time_vec_n'/K,ks_new*K,'r-','Linewidth',2)
        %plot(time_vec_n'/1e-5/1e6,ks_new*1e-5*1e3,'r-','Linewidth',2)
        %axis ([0 100 10 42]);
    else
        %plot(time_vec_n'/K/1e6,ks_new*K*1e3,col,'Linewidth',2)
%       plot(time_vec_n'/K/1e6/A0^m_prime,ks_new*K*1e3*A0^m_prime,...
%           'Color','g');

        %                   hl1                   =                   line(-
time_vec_n'/K/1e6/A0^m_prime,ks_new*K*1e3*A0^m_prime,...
        %   'Color','g');

        time_up=-time_vec_n'/K/1e6/A0^m_prime;
        uprate=ks_new*K*1e3*A0^m_prime;
        %hold on;
        %plot (Age_incis, Rate_incis, 'ko'); hold off
      %  hl1 = line(time_vec_n'/K/1e6,ks_new*K*1e3,...
```

```
    %    'Color','g');
%       ax1 = gca;
%       set(ax1,'XColor','k','YColor','k')
%       set(ax1,'XLim',([0 5]))
%       set(ax1,'YLim',([0.01 1.5]))

%       ax2 = axes('Position',get(ax1,'Position'),...
%         'XAxisLocation','top',...
%         'YAxisLocation','right',...
%         'Color','none',...
%         'XColor','b','YColor','b');
%
%       hl2 = line(time_vec_n',ks_new,'Color','b','Parent',ax2);
%       xlimits = get(ax1,'XLim');
%       ylimits = get(ax1,'YLim');
%       %xinc = (xlimits(2)-xlimits(1))/5;
%       %yinc = (ylimits(2)-ylimits(1))/5;
%       set(ax2,'XLim',xlimits*K*A0^m_prime*1e6);
%       set(ax2,'YLim',ylimits/K/A0^m_prime/1e3);
      %set(ax2,'XTick',[xlimits(1):xinc:xlimits(2)],...
      %'YTick',[ylimits(1):yinc:ylimits(2)])

   end

   filenam = ['uplift_hist_' num2str(knum)]
   time_hist = time_vec_n'/K/1e6/A0^m_prime;
   up_hist =ks_new*K*1e3*A0^m_prime;
   dlmwrite (filenam, [time_hist up_hist']);

    save('uplift_hist.mat' , 'time_hist' , 'up_hist' );

   %calculate the resolution matrix
   Resolution=(denom\G')*G;
   figure(2)
   image(Resolution,'CDataMapping','scaled')
   %pause
   nn=length(z);
   misfit(p)=sqrt(sum((G*ks - z).^2))/(nn - time_interval(p));
   %misfit(p)=sqrt(sum((G*ks - z).^2))/(nn);
   figure(3);
   plot(sum(G'),G*ks,'k-','LineWidth',2)
   lnL = -(log(2*pi)/2*nn + log(dataerr)*nn + 0.5*sum(((G*ks-z)./dataerr).^2));
   BIC(p)=-2*lnL+time_interval(p)*log(nn);
  % pause
end
% if time_interval_i==0
```

```
%     figure(3)
%     plot(time_interval,misfit)
% end

tempdat = dlmread('Epica-tpt-co2b.txt');
agebp = tempdat(:,1);
temp = tempdat(:,2);

U_over_K = ks_new*A0^m_prime;
toto = time_vec_n'/K/1e6/A0^m_prime;

ymax = 30 %max(ks_new*K*1e3*A0^m_prime);
% ymax=20;
ymin=-5; %min(ks_new*K*1e3*A0^m_prime);

figure(1)
%plot (time_up,up_hist);
[ax,p1,p2] = plotyy(time_up,up_hist,agebp/1e6,temp) %U_over_K da sostituire a
up_hist per plottare U/K
axis(ax(1),[-0.14 0 -5 30]) % axe y correspondant a U/K
axis(ax(2),[-0.14 0 -15 10]) % axe y correspondant aux temperatures

% axis([-0.14 0 -5 30]);
% xlabel('t in Ma','Fontsize',16);
% ylabel('U in mm/y','Fontsize',16);

ylabel(ax(1),'U in mm/y','Fontsize',16)
ylabel(ax(2),'Epica Dome C temperatures','Fontsize',16)
title      (['K=',num2str(K),'      ','      m=',num2str(m_prime),'      ','dampcoeff      =
',num2str(damp_coeff) ]);%, '  ', 'n° of T.I.=',num2str(time_interval_i) ])
set(gca,'FontSize',12)
res=0;
hold on

plot ([-0.014 -0.014], [ymin ymax], 'k');
plot ([-0.029 -0.029], [ymin ymax], '--k');
plot ([-0.057 -0.057], [ymin ymax], 'k');
plot ([-0.071 -0.071], [ymin ymax], '--k');
plot ([-0.082 -0.082], [ymin ymax], 'k');
plot ([-0.087 -0.087], [ymin ymax], '--k');
plot ([-0.096 -0.096], [ymin ymax], 'k');
plot ([-0.109 -0.109], [ymin ymax], '--k');
plot ([-0.123 -0.123], [ymin ymax], 'k');


 figure(4)
```

```
%plot(sum(G'),z,'k.');hold on
%plot(sum(G'),G*ks,'r','LineWidth',2);hold off
plot(x,z,'k.');hold on
plot(x,G*ks,'r','LineWidth',2);hold off
title (['Tributary number ', num2str(knum)])

U_over_K = ks_new*A0^m_prime;
toto = time_vec_n'/K/1e6/A0^m_prime;

save (['hist' num2str(knum),'.mat'],'U_over_K','toto')
```

***Appendix 2:*** *mathematical passages to linearise the stream power law for a river in steady state conditions. For a more comprehensive formal explication, please refer to Goren at al. 2014.*

Starting from the stream power law written in function of slope,

$$S(x) = \left(\frac{E}{K}\right)^{1/n} A(x)^{-m/n}$$

and the variation of the river bed elevation, for a river in stable state conditions,

$$\frac{dz}{dt}(t,x) = U(t,x) - E(t,x) \rightarrow \; U(t,x) = E(t,x)$$

is possible to write the river slope in function of the uplift rate,

$$S(x) = \frac{dz}{dx} = \left(\frac{U}{K}\right)^{1/n} A(x)^{-m/n}$$

and then, integrating,

$$z(x) = z_b + \left(\frac{U}{K}\right)^{1/n} \int_{xb}^{x} \frac{dx}{A(x)^{m/n}}$$

and defining the integral part as a new variable $\chi$ [-],

$$\chi = \int_{xb}^{x} \left(\frac{A_0}{A(x)}\right)^{m/n} dx$$

we obtain the equation of a straight line in a $\chi$ – z space: $z(x) = z_b + \left(\frac{U}{KA_0^m}\right)^{1/n} \chi$

With : U [L/T] : uplift rate.

E [L/T] : river incision rate.

K [$L^{1-2m}T^{-1}$] : erodibility coefficient.

S [-]: river slope.

A [$L^2$] : catchment area.

$z_b$ : altitude of river bed at initial time.

z [L]: altitude.

$A_0$ [$L^2$] : fix area chosen by the user.

n [-] : slope exponent, erosion rule.

m [-] : area exponent, erosion rule.

***Appendix 3:*** *Table taken from "Cosmogenic Nuclides: principles, concepts and applications in the Earth surface sciences" (Tibor J. Dunai, 2010)*

| Isotope (half-life) | Main target minerals | Predominant target elements | Reaction pathways (SLHL) |
|---|---|---|---|
| $^{3}$He (stable) | Olivine, Pyroxene, other He-retentive minerals | All major elements and Li | Spallation: 100% Muons: negligible Thermal neutrons produce $^{3}$He on Li, via precursor $^{3}$H ($T_{½}$ = 12.3 a) |
| $^{10}$Be (1.36 ± .07 Ma) | Quartz (rarely Pyroxene and Olivine) | O, Si (Mg) | Spallation: 96.4% Muons: 3.6% |
| $^{14}$C (5730 ± 30 a) | Quartz | O, Si | Spallation: 82% Muons: 18% |
| $^{21}$Ne, $^{22}$Ne (stable) | Quartz, Pyroxene, Olivine | Mg, Al, Si | Spallation: >96.4% Muons: ≤3.6% |
| $^{26}$Al (708 ± 17 ka) | Quartz | Si | Spallation: 95.4% Muons: 4.6% |
| $^{36}$Cl (301 ± 2 ka) | Carbonates, Feldspar, Whole rock | K, Ca, Cl (Fe, Ti) | K: spallation 95.4%; muons 4.6% Ca: spallation 86.6%; muons 13.4% Fe, Ti: spallation presumed 100% Thermal neutrons produce $^{36}$Cl from Cl and K. |
| $^{36}$Ar, $^{38}$Ar (stable) | Feldspar, Amphibole, Pyroxene | K, Ca, | Spallation: up to 100% Muons: not determined Thermal neutrons produce $^{36}$Ar from Cl and K, via precursor $^{36}$Cl ($T_{½}$ = 301 ka). |
| $^{41}$Ca (104 ± 4 ka) | Fe–Ti oxides | Fe, Ti, (Ca) | Fe, Ti: spallation 100% Thermal neutrons produce $^{41}$Ca on $^{40}$Ca |
| $^{53}$Mn (3.7 ± .4 Ma) | Fe-bearing minerals | Fe, Mn | Fe: spallogenic 90.2%; muons 9.8% Mn: not determined. |

***Appendix 4:*** *Geological map of Saint Etienne de Tinée*

Faure-Muret, A. and Fallot, P. , 2012, Sheet 920, Saint Etienne de Tinée.

http://infoterre.brgm.fr/viewer/MainTileForward.do#

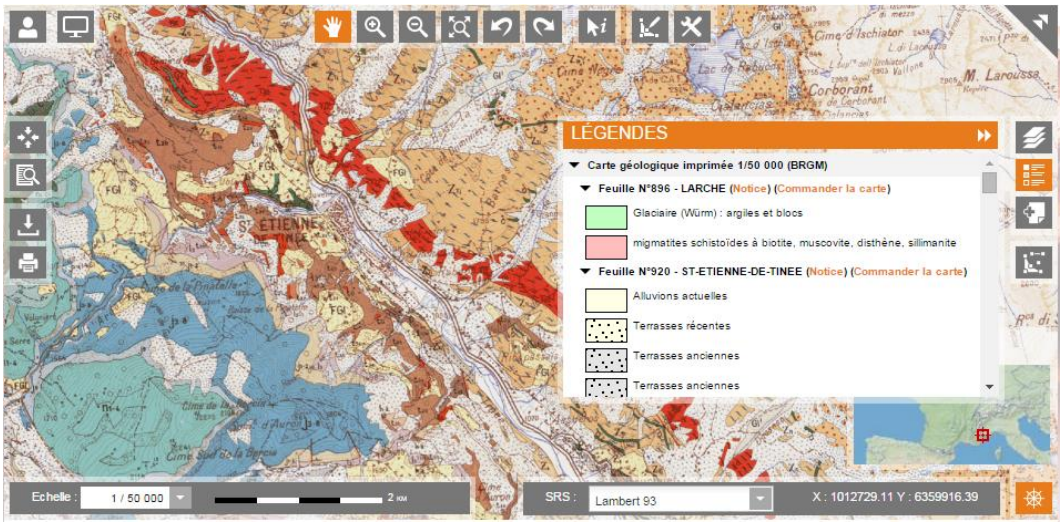

***Appendix 5:*** *Table 17 of data used for the samples age estimation, by Cronus-Earth online calculators (http://hess.ess.washington.edu/).*

| Samples [ - ] | Latitude [ decimal degrees ] | Longitude [ decimal degrees ] | Altitude a.s.l. [ m ] | Thickness [ cm ] |
|---|---|---|---|---|
| Ti – 1 | 44,12 | 7,10 | 728,45 | 6,00 |
| Ti – 2 | 44,12 | 7,10 | 725,30 | 3,00 |
| Ti – 3 | 44,12 | 7,10 | 722,60 | 5,00 |
| Ti – 4 | 44,12 | 7,10 | 718,70 | 2,00 |
| Ti – 5 | 44,12 | 7,10 | 716,10 | 3,00 |
| Ti – 6 | 44,12 | 7,10 | 711,80 | 2,00 |
| Ti – 7 | 44,12 | 7,10 | 708,80 | 2,00 |
| Ti – 8 | 44,12 | 7,10 | 705,60 | 5,00 |
| Ti – 9 | 44,12 | 7,10 | 702,90 | 3,00 |
| Ti – 10 | 44,12 | 7,10 | 699,50 | 13,00 |
| Ti – 11 | 44,12 | 7,10 | 690,00 | 1,50 |

| Samples [ - ] | Densité [ g/cm³ ] | Shielding factor [ - ] | Erosion rate [ mm/yr ] | (Atoms10Be)/(g qtz) [ atoms/g ] |
|---|---|---|---|---|
| Ti – 1 | 2,70 | 0,65 | 0,00 | 96842,80 |
| Ti – 2 | 2,70 | 0,65 | 0,00 | 82872,14 |
| Ti – 3 | 2,70 | 0,65 | 0,00 | 137037,05 |
| Ti – 4 | 2,70 | 0,65 | 0,00 | 81235,10 |
| Ti – 5 | 2,70 | 0,65 | 0,00 | 82852,08 |
| Ti – 6 | 2,70 | 0,65 | 0,00 | 83629,62 |
| Ti – 7 | 2,70 | 0,65 | 0,00 | 82848,50 |
| Ti – 8 | 2,70 | 0,65 | 0,00 | 85367,17 |
| Ti – 9 | 2,70 | 0,65 | 0,00 | 89826,33 |
| Ti – 10 | 2,70 | 0,65 | 0,00 | 22139,41 |
| Ti – 11 | 2,70 | 0,65 | 0,00 | 12480,94 |

| Samples [ - ] | Error in Atoms10Be/g qtz | Prod. Rate (muons) [ Atoms/g/yr ] | Prod. Rate (spallation) [atoms/g/yr] |
|---|---|---|---|
| Ti – 1 | 9823,68 | 0,228 | 5,10 |
| Ti – 2 | 6016,75 | 0,229 | 5,22 |
| Ti – 3 | 13185,07 | 0,228 | 5,12 |
| Ti – 4 | 10272,11 | 0,229 | 5,23 |
| Ti – 5 | 6277,66 | 0,228 | 5,18 |
| Ti – 6 | 5465,62 | 0,229 | 5,20 |
| Ti – 7 | 4484,83 | 0,228 | 5,19 |
| Ti – 8 | 5246,75 | 0,227 | 5,05 |
| Ti – 9 | 7720,56 | 0,227 | 5,12 |
| Ti – 10 | 4963,91 | 0,224 | 4,70 |
| Ti – 11 | 2254,50 | 0,227 | 5,13 |

**Acknowledgement**

I would like to express my sincere gratitude to all those people who have made this work possible.
I'm particularly grateful to Professors Yann Rolland, Carole Petit and Marianne Saillard, of Nice University, who followed and suggested me along the last six months.
I would like to thank also Professor Nicola Surian, who accepted to be my thesis supervisor and helped me to conclude my work as best as possible.
Many thanks also go to Professor Giorgio Pennacchioni who helped me to get in contact with the Géoazur Laboratory and to Lara Maritan, who gave me precious information about the Erasmus Traineeship Program.
Finally I can not fail to thank all the PHD and master students of Géoazur Laboratory with whom I've shared six great months.

*Dedicated to*
*Agostino, Grazia, Jacopo and Veronica,*
*my family,*
*to whom I owe everything.*